The Oxidative Modification of Mitochondrial Proteins in 1,3-Dinitrobenzene Induced Neurotoxicity

by

Stephen R. Steiner

A dissertation submitted in partial fulfillment
of the requirements for the degree of
Doctor of Philosophy
(Toxicology)
in The University of Michigan
2009

Doctoral Committee:

Professor Martin A. Philbert, Chair
Professor Yoichi Osawa
Professor Michael J. Welsh
Associate Professor Peter Mancuso

To my family and friends

Acknowledgments

In many ways, the acknowledgments section is the most difficult part of the dissertation to put down on paper. There are no words that can accurately describe the gratitude I have for everyone who supported me during my doctoral training. I would first like to thank the members of my committee. I thank my mentor and friend, Dr. Martin Philbert, for all of his support and allowing me the honor of working in his laboratory. Thank you for everything, Martin. I will always treasure the years of learning and laughing that I spent as a member of the Philbert laboratory. I thank Dr. Peter Mancuso, Dr. Michael Welsh, and Dr. Yoichi Osawa for participating in my committee and their guidance during critical moments over the course of my training.

I would like thank past and present members of the Philbert/"G.T.T.B" crew including Dr. James Miller, Stephanie Runkle, Dr. Hao "B" Xu, Dr. Ed Park, Dr. Gwangseong Kim, Yipei "Mao Bao" Wang, Brad Martin, Evan Milton, Jen Fernandez and Tracy Crew. My interest and appreciation for the toxicological sciences is the reason I chose to pursue a Ph.D. I could not predict that becoming friends with such an amazing group of people would be an integral part of my learning experience. I cannot imagine laughing or eating as much Chinese buffet (or Korean food) will be an almost vital part of my future endeavors as it was during the past few years. We were made comrades-at-arms through

shared experiences like the nervous anticipation of guessing who Martin would choose to give the next impromptu “Go To The Board” chalkboard lecture. Amidst all of the humor and “merry-making,” I can truly say with pride that I worked with an amazingly talented, industrious, and intelligent group of eclectic personalities. I learned so much about science and friendship from each of you, that I will be forever indebted to you.

In addition to the past and present members of my own lab, I would like to thank past and present members of the EHS department and the other laboratories who enriched my experience during my training. I would like to mention a few names: Dr. Craig Harris, Dr. Loch Caruso, Dr. Rudy Richardson, Dr. Ted Zellers, Dr. John Phipps, Dr. Jason Cannon, Dr. Kelly Brant, Nichole Hein, Ali Kamal, Mark Miller, Lauren Tetz, Becki Veeneman, Margaret Cabaj, Sue Crawford, Patrice Sommerville, the rest of the administrative staff....there are truly too many names to list. I would like to thank all of these people. Our experiences brought us together as friends and as colleagues and to not mention how much each of you means to me would be unjust.

Finally, I would like to thank my family and friends (outside of SPH). Mom, Dad, Grandma, Grandpa, mis tios, mis primos, and Vally….I simply could not have made it this far without any of you.

Table of Contents

List of Figures

Figure

List of Abbreviations

1,3-DNB	1,3-dinitrobenzene
2,4-DNP	2,4-dinitrophenol
3-CPD	3-chloropropanediol
3-NPA	3-nitropropionic acid
BkA	Bongkrekic acid
CsA	Cyclosporin A
DIC	Differential interference contrast
DMSO	Dimethyl sulfoxide
DNPH	Dinitrophenylhydrazine
DTT	Dithiothreitol
ER	Endoplasmic reticulum
GSSG	Glutathione disulfide
LAU	Linear arbitrary units
mPTP	Mitochondrial permeability transition pore
MPT	Mitochondrial permeability transition
ROS	Reactive oxygen species
SOD	Superoxide dismutase

Chapter I

Introduction

Industrialized countries throughout the world have used toxic compounds during the manufacturing process of various goods for decades. Heightened awareness and concern for anthropogenic sources of environmental contamination has led some governments to establish regulatory parameters detailing how industry should handle toxic chemicals and waste byproducts during and after the manufacturing process. One such chemical is the nitroaromatic compound 1,3-dinitrobenzene (1,3-DNB). 1,3-DNB is a multi-organ toxicant used as a chemical intermediate during the manufacture of various plastics, explosives, and dyes. Industrial and military facilities that conduct improper methods of production or disposal of 1,3-DNB-containing compounds are known to be responsible for the contamination of local soil and groundwater sources [1]. Environmental disposition and fate of chemicals such as DNB may place residents in adjacent neighborhoods at a risk of exposure similar to, or less than workers who directly handle 1,3-DNB during manufacturing processes. Nevertheless, the best characterized exposures are in workers who either inhale, touch, or ingest 1,3-DNB and go on to exhibit various symptoms of acute toxicity

including methemoglobinemia, cyanosis, anemia, and decreased sperm count [1]. Neurologic symptoms of toxicity include headache, confusion, vertigo, nausea, loss of cognition, hyperalgesia, and paresthesias [2]. 1,3-DNB associated toxicity in humans provided the necessary impetus for establishing toxicologic analyses of 1,3-DNB pathogenesis in susceptible animal models. Histopathologic examination of rat brain slices isolated from animals dosed with 1,3-DNB revealed the formation of region-specific gliovascular lesions within the periaqueductal gray matter of the 4th ventricle, inferior colliculi, vestibular and cerebellar roof nuclei, in the absence of any significant neuronal pathology [3]. Closer examination of the lesions revealed that the type 1 astrocyte located within these affected brainstem sites are the primary target of 1,3-DNB mediated neurotoxicity.

Astrocytes have an important role in maintaining metabolism by providing the connections through which metabolic substrates can selectively travel between the blood and neurons. The blood-brain barrier is a protective boundary established by astrocyte end-feet processes that ensheath the microvasculature of the central nervous system. Within susceptible brainstem nuclei, 1,3-DNB exposure induces swelling of the perivascular foot processes of the astrocytes while apparently causing no overt morphological changes in the perineuronal foot processes [3]. Swelling of the perivascular connections leads to vascular leakage and the formation of edematous lesions with each specific group of nuclei, with any neuronal changes occurring as secondary effects. The histopathological changes involving astrocytic injury in brainstem nuclei are

thought to disrupt neurological function of these specific regions and are likely the cause of the neurologic deficits, such as ataxia, associated with 1,3-DNB neurotoxicity. Why this pathology is observed only in the brainstem and not in type 1 astrocytes of cortical nuclei remains a mystery that may be solved through in depth biochemical and molecular analysis of the mechanisms leading to 1,3-DNB neurotoxicity.

The regio-selective gliotoxicity resultant from 1,3-DNB exposure resembles the pathology observed in a group of neurological disorders known as energy deprivation syndromes, or mitochondrial encephalopathies [3,4]. The topography of the lesions in 1,3-DNB intoxication are similar, though not identical, to lesions present in other models of chemical-induced energy deprivation syndromes caused by other compounds including misonidazole, metronidazole, and the chlorosugar, α-chlorohydrin [3,4]. The lesions produced by 1,3-DNB intoxication accompanied by significant metabolic impairment, a characteristic shared between the other aforementioned toxicants. Significant increases in glucose consumption and lactic acid production have been observed in F344 rat astrocyte cultures 24 hours after exposure to a 0.5 mM dose of 1,3-DNB, both occurring before the development of cytotoxicity [5]. In terms of *in vivo* metabolic perturbation, Romero *et al*. (1995) demonstrated increased local cerebral utilization of glucose in several brain regions before development of pathology.

Oxidative stress is implicated as a contributing factor in 1,3-DNB induced neurotoxicity *in vivo*, though it is not yet clear whether loss of any homeostasis as

a function of oxidative stress is a primary cause of 1,3-DNB-induced neurotoxicity. Using primary cultures of type I hippocampal astrocytes, Romero *et al.*, 1995 showed an eightfold increase in nitroblue tetrazolium reduction upon exposure to 1,3-DNB compared to the DMSO vehicle control and a significant increase in the level of oxidized glutathione (GSSG) [5]. Nitroblue tetrazolium reduction was partially inhibited by the presence of superoxide dismutase (SOD) which suggests that 1,3-DNB exposure induces the production of superoxide radicals, altering the homeostatic redox balance within vulnerable cells. More evidence supporting 1,3-DNB involvement in metabolic perturbation and generation of oxidative stress within susceptible cell types comes from a series of experiments performed by Tjalkens *et al.*, (2000) [6]. This study demonstrated significant increases in the levels of reactive oxygen species (ROS) in SY5Y neuroblastoma and C6 glioma cell types exposed to 1,3-DNB. Tjalkens *et al*. (2000) also provided evidence linking increased ROS production with opening of the mitochondrial permeability transition (MPT). Onset of the MPT is an important cellular event, the occurrence of which initiates potentially catastrophic cellular injury through an apoptotic or necrotic signaling cascade [6]. 1,3-DNB exposure led to both onset of the MPT and loss of the mitochondrial membrane potential ($\Delta\Psi_m$) in C6 and SY5Y cells, although the concentration of 1,3-DNB required to induce MPT in SY5Y cells was 10-fold lower than in C6 cells. Use of the antioxidants deferoxamine or α-tocopherol inhibited onset of MPT, which suggests that 1,3-DNB-induced ROS production stimulates opening of the MPT. Since both C6 and SY5Y cells underwent DNB-induced MPT and antioxidants

were capable of preventing onset of MPT in both cell types, it is logical to suggest that 1,3-DNB-induced oxidative stress may alter the cellular redox environment in such a manner that predisposes susceptible mitochondria to onset of MPT and subsequent cellular damage.

The mechanism by which 1,3-DNB produces oxidative stress in susceptible cellular populations is as of yet undetermined, but there is evidence that 1,3-DNB undergoes a nitroreductive metabolism (Fig 1.1.). Reeve *et al.*, (2002) published a study focused on the testicular toxicity caused by 1,3-DNB metabolites and how the presence of these metabolites leads to mitochondrial GSH depletion [7]. The first step in this process is a single-electron reduction that results in the generation of a nitroxyl anion radical. Under aerobic conditions, molecular oxygen is able to abstract an electron from the nitroxyl anion radical, regenerating the parent 1,3-DNB compound and forming superoxide anion in a process known as redox cycling. This chemical process is capable of repeating itself in a manner that produces more and more superoxide anion radical, propagating GSH depletion and GSSG formation. Previous work studying nitrocompound metabolism confirmed the enzymatic generation of superoxide anion radical during metronidazole reduction, a drug known to induce energy deprivation [8]. 1,3-DNB-induced disruption of cellular redox state can lead to redox cycling which consumes molecular oxygen such that the affected cell becomes hypoxic [9]. As a result, the cell can no longer adequately produce ATP via oxidative phosphorylation, metabolically shifting energy production through glycolysis. The hydrolytic function of F_1F_0-ATP synthase is activated

during this phase in a futile attempt to restore cellular energy depletion by consuming ATP generated from glycolysis.

One puzzling aspect of 1,3-DNB pathology concerns the apparent time differential that occurs between the initial appearance of molecular pathology and observed cytopathology in susceptible cell types. Tjalkens et al., (2003) showed that ROS production, loss of $\Delta\Psi_m$, and onset of MPT occurred in brainstem astrocytes exposed to 30µM 1,3-DNB after approximately 10 minutes, when compared to resistant cortical astrocyte cultures that retained a viable $\Delta\Psi_m$ after exposure to 100uM 1,3-DNB for over 1 hour [10]. Loss of mitochondrial membrane potential was prevented by bongkrekic acid in both astrocyte populations. Although 1,3-DNB exposure led to morphological alterations in both astrocyte populations (i.e. stress fiber formation, plasma membrane blebbing), unpublished data from our laboratory shows that cells do not actually succumb to 1,3-DNB intoxication until roughly 48 hours after the initial exposure to toxic concentrations of 1,3-DNB. This implies that the molecular pathologic events observed early after 1,3-DNB exposure are not the final endpoints of toxicity, but they may in fact initiate a cascade of events that lead to downstream pathology and ultimately cell death.

It has been established that 1,3-DNB-induced early mitochondrial stress consists of an initial increase in the generation of ROS, loss of the $\Delta\Psi_m$, and subsequent onset of MPT. One of the main objectives of this study is to confirm that 1,3-DNB-induced oxidative stress occurs before mitochondrial dysfunction, which may indicate that pathological mechanism of neurotoxicity initially develops

through a molecular pathway mediated by oxidative stress. Tjalkens et al., (2000) showed that generation of significant amounts of oxidative stress occurred concurrently with mitochondrial dysfunction in SY5Y neuroblastoma cells exposed to 1,3-DNB [6]. Miller et al., (2003) showed that SY5Y cells exposed to the nitroimidazole radiosensitizer CI-1010 led to a loss of the $\Delta\Psi_m$ followed by a significant increase in ROS [11]. In the previous two studies, loss of the $\Delta\Psi_m$ was prevented by the addition of the MPT inhibitor, cyclosporin A (CsA), and the antioxidant, α-tocopherol. Zorov et al., (2000) describes a process they termed "ROS-induced ROS release" in which an initial slow accumulation of photoexcitation-induced ROS led to a burst of ROS that occurred simultaneously with loss of the $\Delta\Psi_m$ and onset of MPT [12]. This temporal relationship between loss of the $\Delta\Psi_m$ and burst of ROS was measured using a combination of TMRM and DCF fluorescence versus time. TMRM is a cationic fluorescent probe used to monitor $\Delta\Psi_m$ and DCF is a fluorescent probe used to measure ROS production. The results suggest that mitochondrial dysfunction and concurrent burst of mitochondrial ROS could originate from a mechanism of mitochondrial sensitization that occurs through an initial increase of ROS production.

The issue now revolves around how 1,3-DNB-induced early increases in ROS production sensitize mitochondria in a way that leads to dysfunction (i.e. loss of the $\Delta\Psi_m$ and onset of MPT) followed by another, larger, burst of ROS. Mitochondrial sensitization may manifest as a result of oxidative damage specifically in the form of mitochondrial protein modification. Amino acid side chains of proteins are particularly susceptible to the effects of altered cellular

redox states. Proteins contain various amino acid residues such as lysine, arginine, proline, and threonine that are reactive and can become oxidized upon contact with ROS. Oxidative stress can lead to various forms of oxidative modification including protein carbonylation, cross-linked thiol groups, as in the case of oxidized vicinal thiol groups, and thio-bonded adducts, as in the case of S-nitrosylated proteins. It has been shown that S-thiolation of proteins can occur within minutes after a burst of oxidative stress [13]. The mechanism of S-thiolation starts with the formation of partially oxidized sulfhydryl groups, thiyl radical or sulfenic acids, and without adequate glutathione reserves, can lead to the development irreversibly oxidized sulfinic and sulfonic acid groups. Modifying a critical sulfhydryl in this oxidative manner can alter the function of the protein(s) in question. For example, the redox state of vicinal thiol groups in mitochondrial permeability transition pore (mPTP) proteins affects the probability of whether or not the permeability transition pore exists in an open or closed state. Petronilli et al., (1994) showed that oxidized vicinal thiols within cysteinyl residues, alters the voltage sensing capability of the mPTP such that the gating potential of the pore increases, increasing the likelihood of pore opening [14]. This study also showed that pretreatment of mitochondria with low concentrations of the reducing agent, dithiothreitol (DTT), inhibits pore opening in the presence of the oxidizing agent, menadione. This evidence suggests that mPTP proteins contain critical sulfhydryls whose oxidation states dictate the open or closed state of the mPTP. By triggering premature opening of the mPTP, oxidation of these critical protein residues can predispose other mitochondria to onset of the MPT through a

positive feedback mechanism that exacerbates MPT-induced ROS production, leading to downstream oxidative damage of these otherwise unaffected mitochondria [12]. For example, increased protein carbonylation is known to occur in conjunction with increased mitochondrial ROS production [15,16].

Superoxide anion production is a recurrent theme in 1,3-DNB neurotoxicity because of how exogenous sources of superoxide anion can disrupt the cellular redox balance and lead to the formation of more potent oxidizing species. Mitochondria are considered the most important, endogenous source of oxidative stress, produced through aerobic respiration. Mitochondria contain an abundance of transition metals packaged within macromolecules found throughout the mitochondrial matrix and genome, including iron-sulfur clusters [17, 18]. Superoxide anion has a relatively long half-life which allows it to migrate from its site of production and interact with other molecules [17]. Though superoxide anion is not a potent oxidizing ROS, it can react with iron-sulfur clusters causing destabilization of the bonds holding Fe^{2+} in place resulting in release and increasing Fe^{2+} availability for metal-catalyzed oxidation reactions [17, 18, 19]. Three reactions that use superoxide anion as a reactant in the formation of increasingly potent oxidizing species include: dismutation, the Fenton reaction, and the Haber-Weiss reaction [17, 19]. Dismutation of superoxide anion leads to the formation hydrogen peroxide and molecular oxygen. The Fenton reaction involves the reduction of hydrogen peroxide by Fe^{2+}, which results in the formation of highly reactive hydroxyl ion radicals. Additional toxic hydroxyl radical production can occur through the Haber-Weiss

reaction, in which superoxide anion radicals react with hydrogen peroxide to form hydroxyl radicals [17]. The formation of oxidative stress through transition metal chemistry is an important mechanism by which 1,3-DNB-induced production of relatively non-reactive superoxide anion can stimulate the generation of stronger oxidizing species, increasing the likelihood that 1,3-DNB neurotoxicity is mediated through oxidative protein modification.

Identifying patterns of protein oxidation may help elucidate the specific molecular mechanism underlying the development of 1,3-DNB neurotoxicity. A portion of this study was performed using other well-established mitochondrial and metabolic toxicants, known to induce ROS production and protein oxidation, in a comparative analysis of mitochondrial dysfunction and the identification of oxidized proteins. A portion of the overall analysis presented in this dissertation was specifically conducted in order to determine: 1) whether or not specific proteins are uniquely susceptible to DNB-induced oxidative stress and 2) if common or similar cellular mechanisms of mitochondrial toxicity occur also share molecular mechanisms of toxicity. The other toxicants included in this study are 3-chloropropanediol (3-CPD), 2,4-dinitrophenol (2,4-DNP), and 3-nitropropionic acid (3-NPA). 3-CPD is the active metabolite of α-chlorohydrin and, similar to 1,3-DNB, has been used as a model of chemical-induced energy deprivation syndromes [20, 21]. 3-CPD targets Type 1 brainstem astrocytes and disrupts metabolic function through inhibition of glyceraldehyde-3-phosphate dehydrogenase [22]. 2,4-DNP inhibits mitochondrial respiration by uncoupling proton transport down the inner mitochondrial membrane, resulting in increased

ROS production and loss of the $\Delta\Psi_m$ [23, 24]. 3-NPA disrupts oxidative phosphorylation through suicide inhibition of succinate dehydogenase and has been shown to induce protein carbonylation *in vivo* [25, 26]. Throughout the course of this *in vitro* study, confocal microscopy and proteomic analysis were used to analyze time- and concentration-dependent measurements of cellular metabolic activity, ROS production, mitochondrial dysfunction, and protein oxidation in an attempt to identify ROS-sensitive mitochondrial proteins (i.e permeability transition pore proteins), the oxidation of which could define a mechanism that explains how early indicators of molecular pathology predispose vulnerable cell types to downstream injury during 1,3-DNB neurotoxicity.

Hypothesis

Modification of PTP proteins is dependent upon MPT-linked induction of oxidative stress

Specific Aim 1) Confirmation of MPT-linked induction of oxidative stress

Specific Aim 2) Determine whether or not 1,3-DNB induced increases in ROS lead to oxidative modification of mPTP proteins

Specific Aim 3) Determine whether or not 1,3-DNB-induced pattern of protein oxidation is unique to 1,3-DNB exposure

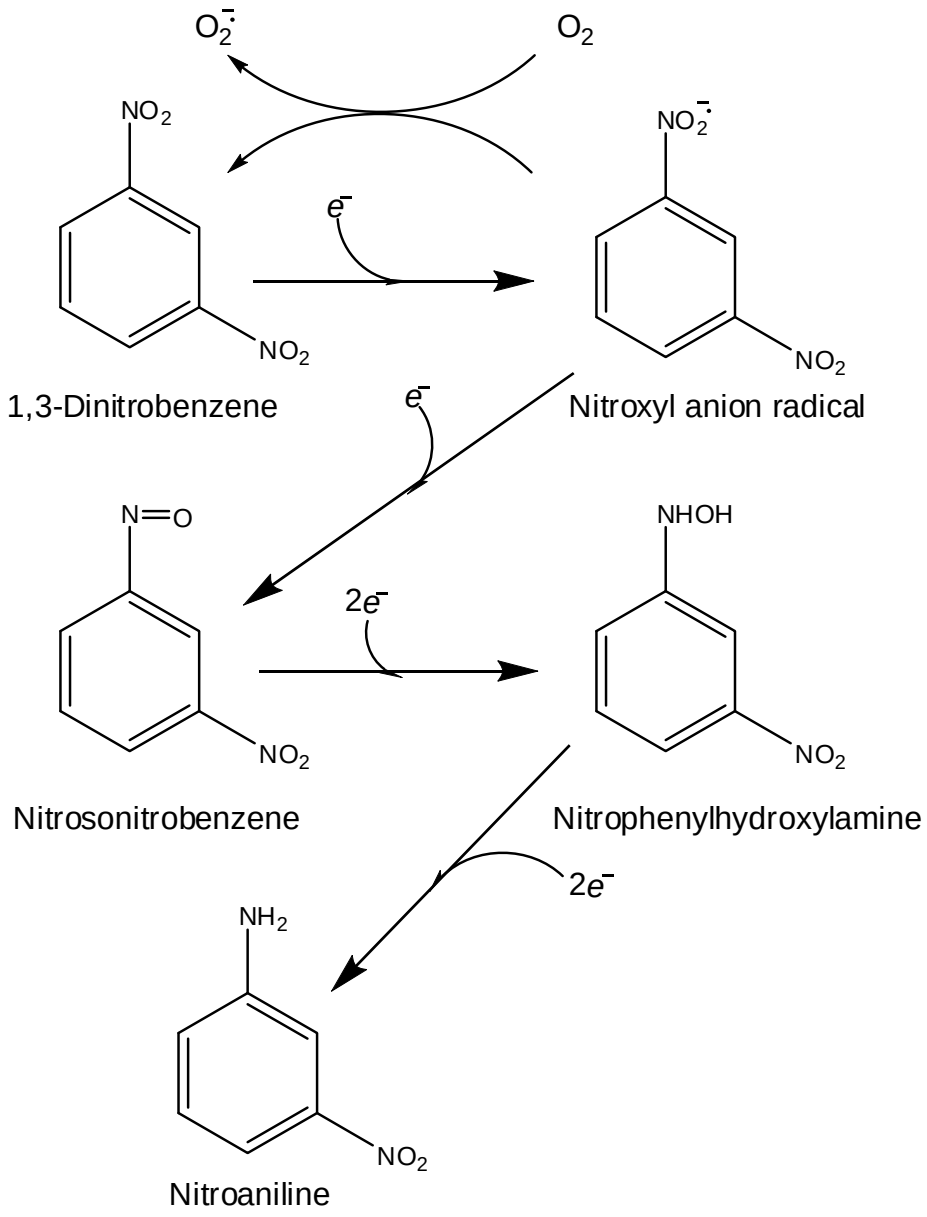

Figure 1.1. The stepwise nitroreductive metabolism of 1,3-DNB that results in the formation of nitroaniline. Redox cycling of nitroxyl anion radical is at least partially responsible for the induction of oxidative stress during 1,3-DNB exposure (initially proposed by Reeve et al., 2002).

References

1. ATSDR. 1995. Toxicological profile for 1,3-dinitrobenzene and 1,3,5-trinitrobenzene. Agency for Toxic Substances and Disease Registry, Division of Toxicology, Atlanta, GA.

2. Von Burg, R. Toxicology update. Dinitrobenzene. *J. Appl. Toxicol.* **9**: 199-202; 1989.

3. Philbert, M. A.; Nolan, C. C.; Cremer, J. E.; Tucker. D.; Brown, A. W. 1,3-dinitrobenzene-induced encephalopathy in rats. *Neuropathol. Appl. Neurobiol.* **13**: 371-389; 1987.

4. Cavanagh, J. B. Methyl bromide intoxication and acute energy deprivation syndromes. *Neuropathol. Appl. Neurobiol.* **18**: 575-578; 1992.

5. Romero, I. A.; Lister, T.; Richards, H. K.; Seville, M. P.; Wylie, S. P.; Ray, D. E. Early metabolic changes during *m*-dinitrobenzene neurotoxicity and the possible role of oxidative stress. *Free. Radic. Biol. Med.* **18**: 311-319; 1995.

6. Tjalkens, R. B.; Ewing, M. M.; Philbert, M. A. Differential cellular regulation of the mitochondrial permeability transition in an *in vitro* model of 1,3-dinitrobenzene-induced encephalopathy. *Brain Res.* **874**: 165-177; 2000.

7. Reeve, I. T.; Voss, J. C.; Miller, M. G. 1,3-dinitrobenzene metabolism and GSH depletion. *Chem. Res. Toxicol.* **15**: 361-366; 2002.

8. Mason, R. P.; Josephy, P. D. An electron spin resonance investigation of the iron-catalyzed reaction of metronidazole with cysteine. *J. Inorg. Biochem.* **24**: 161-165; 1985.

9. Di Lisa, F.; Bernardi, P. Mitochondrial function as a determinant of recovery or death in cell response to injury. *Mol. Cell Biochem.* **184**: 379-391; 1998.

10. Tjalkens, R. B.; Phelka, A. D.; Philbert, M. A. Regional variation in the activation threshold for 1,3-DNB-induced mitochondrial permeability transition in brainstem and cortical astrocytes. *Neurotoxicology* **24**: 391-401; 2003.

11. Miller, T. J.; Phelka, A. D.; Tjalkens, R. B.; Dethloff, L. A.; Philbert, M. A. Cl-1010 induced opening of the mitochondrial permeability transition pore precedes oxidative stress and apoptosis in SY5Y neuroblastoma cells. *Brain Res.* **14**: 43-56; 2003.

12. Zorov, D. B.; Juhasova, M.; Sollott, S. J. Mitochondrial ROS-induced ROS release: An update and review. *Biochim. Biophys. Acta* **1757**: 509-517; 2006.

13. Biswas, S.; Chida, A. S.; Rahman, I. Redox modifications of protein-thiols: emerging roles in cell signaling. *Biochem. Pharmacol.* **71**: 551-564; 2005.

14. Petronilli, V.; Constantini, P.; Scorrano, L.; Colonna, R.; Passamonti, S.; Bernardi, P. The voltage sensor of the mitochondrial permeability transition pore is tuned by the oxidation-reduction state of vicinal thiols. Increase of the gating potential by oxidants and its reversal by reducing agents. *J. Biol. Chem.* **269**: 16638-16642; 1994.

15. Nyström, T. Role of oxidative carbonylation in protein quality control and senescence. *Embo J.* **24**: 1311-1317; 2005.

16. Dalle-Donne, I.; Aldini, G.; Carini, M.; Colombo. R.; Rossi, R.; Milzani, A. Protein carbonylation, cellular dysfunction, and disease progression. *J. Cell. Mol. Med.* **10**: 389-406; 2006.

17. Kohen, R.; Nyska, A. Oxidation of biological systems: oxidative stress phenomena, antioxidants, redox reactions, and methods for their quantification. *Toxicol. Pathol.* **30**: 620-650; 2002.

18. Tangeras, A.; Flatmark, T.; Backstrom, D.; Ehrenberg, A. Mitochondrial iron not bound in heme and iron-sulfur clusters. Estimation, compartmentation, and redox state. *Biophys. Acta* **589**: 162-175; 1980.

19. Stadtman, E. R.; Berlett, B. S. Fenton chemistry. Amino acid oxidation. *J. Biol. Chem.* **266**: 17201-17211; 1991.

20. Cavanagh, J.B.; Nolan, C.C. The neurotoxicity of alpha-chlorohydrin in rats and mice: II. Lesion topography and factors in selective vulnerability in acute energy deprivation syndromes. *Neuropathol Appl Neurobiol.* **19**: 471-479; 1993.

21. Willis, C.L.; Nolan, C. C.; Reith, S. N.; Lister, T.; Prior, M. J. W.; Guerin, C. J.; Mavroudis, G.; Ray, D. E. Focal astrocyte loss is followed by microvascular damage, with subsequent repair of the blood-brain barrier in the apparent absence of direct astrocyte contact. *Glia* **45**: 325-337; 2004.

22. Skamarauskas, J.; Carter, W.; Fowler, M.; Madjd, A.; Lister, T.; Mavroudis, G.; Ray, D. E. The selective neurotoxicity produced by 3-chloropropanediol in the rat is not a result of energy deprivation. *Toxicology* **232**: 268-276; 2007.

23. Han, Y. H.; Kim, S. W.; Kim, S. H.; Kim, S. Z.; Park, W. H. 2,4-dinitrophenol induces G1 phase arrest and apoptosis in human pulmonary adenocarcinoma Calu-6 cells. *Toxicol. In Vitro* **22**: 659-670; 2008.

24. Futakawa, N.; Kondoh, M.; Ueda, S.; Higashimoto, M.; Takiguchi, M.; Suzuki, S.; Sato, M. Involvement of oxidative stress in the synthesis of metallothionein induced by mitochondrial inhibitors. *Biol. Pharm Bull.* **29**: 2016-2020; 2006.

25. Huang, L.; Sun, G.; Cobessi, D.; Wang, A. C.; Shen, J. T.; Tung, E. Y.; Anderson, V. E.; Berry, E. A. 3-nitropropionic acid is a suicide inhibitor of mitochondrial respiration that, upon oxidation by complex II, forms a covalent adduct with a catalytic base arginine in the active site of the enzyme. *J. Biol. Chem.* **281**: 5965-5972; 2006.

26. La Fontaine, M. A.; Geddes, J. W.; Banks, A.; Butterfield, D. A. 3-nitropropionic acid induced in vivo protein oxidation in striatal and cortical synaptosomes: insights into Huntington's disease. *Brain Res.* **858**: 356-362; 2000.

Chapter II

Confirmation of MPT-linked induction of oxidative stress

Introduction

It has been established that 1,3-DNB-induced early mitochondrial stress consists of an initial increase in the generation of ROS, onset of MPT, and loss of the $\Delta\Psi_m$. However, this portion of the study is designed to test whether 1,3-DNB-induced onset of MPT is followed by another significant burst of MPT-induced oxidative stress in a susceptible cellular model. Tjalkens et al., (2000) showed that generation of significant oxidative stress occurred concurrently with the loss of the mitochondrial membrane potential in SY5Y neuroblastoma cells exposed to 1,3-DNB [1]. Miller et al., (2003) showed that SY5Y cells exposed to the nitroimidazole radiosensitizer CI-1010 led to a loss of the $\Delta\Psi_m$ followed by a significant increase in ROS [2]. In both studies, loss of the mitochondrial membrane potential was prevented by the addition of the MPT inhibitor, cyclosporin A (CsA), and the antioxidant, α-tocopherol. Zorov et al., (2000) describes a process they termed “ROS-induced ROS release” in which an initial slow accumulation of photoexcitation-induced ROS led to a burst of ROS that

occurred simultaneously with loss of the mitochondrial membrane potential [3]]. This temporal relationship between loss of the mitochondrial membrane potential and burst of ROS was measured using laser-scanning confocal microscopic analysis of TMRM and DCF fluorescence versus time. The results show that the ROS burst occurred during MPT induction. This implies that the second burst of ROS could originate from the mitochondria, possibly as a result of the decoupling of oxidative phosphorylation.

1,3-Dinitrobenzene (1,3-DNB) is a model neurotoxicant that produces a symmetrical, bilateral lesion similar to the most sensitive regions affected in several mitochondrial encephalopathies. The primary targets are brainstem type 1 astrocytes with secondary involvement of oligodendroctyes and neurons [4]. 1,3-DNB-induces significant perturbations in metabolic function and the generation of ROS within susceptible brainstem [1, 5, 6, 7]. In *in vitro* models of 1,3-DNB neurotoxicity, significant increases in the levels of ROS, loss of $\Delta\Psi_m$, ATP depletion, and onset of the MPT are detected in SY5Y neuroblastoma and C6 glioma cell types. Decreased reduced glutathione content and increased production of superoxide anion in primary rat astrocyte cultures are early indications of disturbances in redox potential that precede later signs of metabolic imbalance, including increased glucose consumption and lactic acid production [5]. The exact mechanism by which 1,3-DNB produces oxidative stress and whether or not early, relatively small increases in oxidative stress are causally linked to cellular damage in susceptible astrocyte populations is unknown. Similar to other nitroaromatic chemicals, 1,3-DNB undergoes

nitroreduction that, in the presence of oxygen, produces superoxide anion [8]. 1, 3-DNB is reduced through single-electron reduction of at least one nitro-group, mediated by NADPH thereby producing the nitroxyl anion radical. Redox cycling in the presence of molecular oxygen converts the nitroxyl anion radical back to the parent compound with simultaneous liberation of superoxide anion. If left unchecked, superoxide anion formation can act as a prelude to the formation of stronger oxidizing species.

The work of these aforementioned studies provides an experimental basis for confirming whether or not 1,3-DNB causes a significant increase in ROS after onset of MPT. In order to show that mitochondrial proteins are susceptible to oxidative modifications during 1,3-DNB toxicity, the objective of this study was to demonstrate that 1,3-DNB causes a significant increase of ROS and mitochondrial dysfunction in DI TNC1 astrocytes using mitochondria-specific fluorescent probes and confocal microscopy.

Materials and Methods

Chemicals

Tissue culture media and materials were obtained from Gibco (Invitrogen, Carlsbad, CA). Fluorescent probes were obtained from Molecular Probes (Invitrogen Eugene, OR). CellTiter 96 MTS assay solution was obtained from Promega (Madison, WI). All other reagents were of analytical grade and were obtained from Sigma-Aldrich (St. Louis, MO).

Cell Culture

DI TNC1 astrocytes, obtained from the American Type Culture Collection, were maintained in a humidified incubator at 37°C in an atmosphere of 5% CO_2 (13). Cells were grown in DMEM containing 4.5g/L D-glucose, L-glutamine, 10% fetal bovine serum, and 1% penicillin-streptomycin-glutamine mixture. Cells grown between passages 5 through 25 were used for all experiments.

MTS assay

The CellTiter 96 cell proliferation assay was used to measure concentration-dependent deficits in metabolic activity of DI TNC1 cells exposed to multiple concentrations of 1,3-DNB within a 24 hr period. The CellTiter 96 solution contains a tetrazolium salt that is converted into formazan by cellular dehydrogenases within metabolically active cells. DI TNC1 cells were subcultured at a density of 5000 cells/well in a 96-well tissue culture plate. Cultures were allowed to proliferate for 24 hrs before addition of 1µM, 10µM, 100µM, 500µM, and 1mM concentrations of 1,3-DNB in DMEM containing 10% FBS and 1% PSG. After 24 hrs of exposure, the dosing media from each well was removed and replaced with serum-free, phenol-free DMEM containing 20µL MTS/PMS solution/well. After 1.5 hrs of incubation, MTS reduction to the formazan product was measured at an absorbance of 490nm in a Gemini SpectraMax spectrophotometer (Molecular Devices, Sunnyvale, CA). Mean

absorbance values from 4 independent experiments for each exposure group were graphed as percentages ± SEM of the DMSO control.

Laser Scanning Confocal Microscopy

Differential interference contrast (DIC) images depicting time-dependent cytoxicity of DI TNC1 astrocytes exposed to 1mM 1,3-DNB. Images were captured using an Olympus Fluoview/FV300 combined with an inverted Olympus IX-70 microscope. Confocal microscopy was used to study the effect of 1,3-DNB on mitochondrial function and the production of superoxide anion ($O_2^{\cdot -}$) in DITNC1 cells. Cells were plated on 22 mm round, glass coverslips and treated with 1,3-DNB for 45 minutes, 5 hrs, 12 hrs, and 24 hrs using 0.14% DMSO (v/v) as a vehicle control. Following each exposure, mitochondrial membrane potential ($\Delta\Psi_m$) was monitored by incubating the cells in 20mM HBSS/HEPES buffer containing 500 nM tetramethyl rhodamine methyl ester (TMRM) for 15 min at 37°C. To determine whether limiting oxidative stress could inhibit 1,3-DNB-induced loss of $\Delta\Psi_m$, cells were pre-treated with 600 µM deferoxamine or 100 µM Trolox for 20 min before incubation with 1mM 1,3-DNB. Mitochondrial-derived ROS was analyzed using the fluorescent superoxide indicator, MitoSOX Red. Cells were plated on 22 mm round, glass coverslips and treated with 1,3-DNB for 45 minutes, 3 hrs, 5 hrs, 8 hrs, 12 hrs, and 24 hrs using 0.14% DMSO (v/v) as a vehicle control. Bongkrekic acid (5µM BkA) was used to determine if blocking the permeability transition pore would inhibit production of superoxide anion. Following each exposure, cells were loaded with 5µM MitoSOX Red in 20

mM HBSS/HEPES buffer for 30 min at 37°C. After individual groups of treated cells were incubated in buffer solution containing each respective dye, the coverslips were placed in a heated stage for live-cell imaging analysis. Confocal analysis was conducted on using an Olympus Fluoview/FV300 combined with an inverted Olympus IX-70 microscope. The confocal microscope was equipped with a system of Argon and HeNe lasers (Melles Griot, Carlsbad, CA) with emission parameters for TMRM and MitoSOX Red, each set at 543 nm. Images were obtained using a 60x oil immersion lens at an exposure rate of 2.41 s/scan in order to limit photobleaching of the dyes. About 2% of the maximum laser intensity was used for analyzing TMRM fluorescence, while about 10% of the maximum laser intensity was used for analyzing MitoSOX Red fluorescence. Mean fluorescence intensities from 3 or 4 independent experiments, ~7-10 cells per experiment, were measured using Adobe Photoshop and graphed using Microsoft Excel.

Statistical Analysis

MTS reduction data from 4 independent experiments were graphed as percentages ± SEM of the DMSO control and compared using two-tailed Student's t-test, with $p < 0.05$ considered a significant difference between the means. Confocal microscopy data was expressed as the mean of the observed fluorescence intensity ± SEM. Data from fluorescent images was compared using a two-tailed Student's t-test, with $p < 0.001$ considered a significant difference between the means.

Results

Cytotoxicity and metabolic activity in DI TNC1 astrocytes exposed to 1,3-DNB

1,3-DNB-induced time-dependent cytotoxicity is shown in Figure 2.1. Widespread vacuolization and formation of dark, punctuate bodies are present 5 hrs and 12 hrs after the initial 1mM 1,3-DNB exposure. Arrows indicate decreased cellular confluence, retracted processes, and membrane blebbing 24 hrs after exposure. Concentration-response data depicting 1,3-DNB-induced deficits in MTS reduction is shown in Figure 2.2. The reductive capacity of DI TNC1 cells exposed to 1,3-DNB diminishes slightly at 1µM 1,3-DNB, but the difference is not significant. Decreased MTS reduction follows a concentration-dependent pattern, although the first statistically significant drop in metabolic activity (~45%) in 1,3-DNB-induced MTS reduction within 24 hrs is observed at 1mM 1,3-DNB.

Mitochondrial function and ROS production in DI TNC1 astrocytes exposed to 1,3-DNB

Superoxide anion production was measured using the fluorescent indicator probe, MitoSOX Red, to determine whether or not 1,3-DNB induces a time-dependent increase in ROS production. MitoSOX Red requires selective migration of the probe to the mitochondrial matrix where oxidation of the

fluorophore by superoxide anion triggers fluorescence. Exposure to 1mM 1,3-DNB led to time-dependent increases in production of superoxide anion in DI TNC1 cells throughout the duration of the experiment (Figure 2.3). 1,3-DNB induced superoxide production reached a 25-fold peak level at 5 hrs (Figure 2.4), which occurred in conjunction with subsequent loss of the $\Delta\Psi_m$ as observed by loss of TMRM-induced fluorescence. MitoSOX Red fluorescence decreases after 5 hrs, but remains significantly higher than the DMSO control at the same time. Pretreatment with the MPT inhibitor, BkA, had no attenuating effect on superoxide production in cells exposed to 1,3-DNB when compared to DMSO controls. However, the levels of superoxide anion in cell cultures pretreated with 5μM BkA were significantly lower during the 45 min, 5 hrs, and 24 hrs 1,3-DNB exposure periods compared to cells treated solely with 1,3-DNB.

Maintenance of the $\Delta\Psi_m$ was assessed with the TMRM, a cationic fluorescent probe that selectively migrates to mitochondria sustaining membrane potentials (Figure 2.5). Robust TMRM fluorescence in healthy cells indicates the presence of an intact mitochondrial membrane potential ($\Delta\Psi_m$). Previous studies using different *in vitro* neural cell culture models show that antioxidants protect cells from loss of the $\Delta\Psi_m$ at 40 min and onset of MPT following exposure to 1,3-DNB at concentrations as low as 50 μM [8]. Significant loss of TMRM fluorescence was initially observed in DI TNC1 astrocyte cultures exposed to 1,3-DNB for 5 hrs (Figure 2.6), coinciding with peak MitoSOX Red fluorescence. Little TMRM fluorescence was observed after 24 hrs of continuous exposure to 1 mM 1,3-DNB, suggesting that 1,3-DNB exposure induces a time-

dependent loss of the $\Delta\Psi_m$. Exposure to DMSO alone had no effect on TMRM fluorescence. Pretreatment with 600μM deferoxamine before exposing the DI TNC1 cells to 1,3-DNB delayed loss of the $\Delta\Psi_m$ until 24 hr after initial exposure. Pretreatment with 100μM Trolox also delayed 1,3-DNB-induced loss of the $\Delta\Psi_m$. However, unlike cells pretreated with deferoxamine, cells pretreated with Trolox exhibited significant loss of TMRM fluorescence as early as 12 hrs after initial 1,3-DNB exposure.

Discussion

The data demonstrate that DI TNC1 astrocytes exposed to 1,3-DNB exhibit time-dependent morphological indices of cytotoxicity and concentration-dependent deficits in metabolic activity. The data indicate that the time course of superoxide anion production reaches maximal levels after 5 hrs of exposure of DI TNC1 astrocytes to 1,3-DNB. Significant levels of superoxide anion production are detected as early as 45 min after the commencement of exposure and occur prior to the loss of $\Delta\Psi_m$. Similarly, 1,3-DNB produces a time-dependent decay of $\Delta\Psi_m$ that starts approximately 5 hrs after initial exposure and coincides with peak production of superoxide anion. However, the production of superoxide anion continues after onset of mitochondrial depolarization suggesting that while uncoupling of mitochondrial electron transport may contribute significantly to overall oxidative stress, induction of the MPT may not be required for initiation of superoxide production. Pretreatment with bongkrekic acid attenuates superoxide

production during the 45 min, 5 hrs, and 24 hrs 1,3-DNB exposure periods. Previous findings linking superoxide production and onset of MPT provide compelling evidence that net increases in superoxide anion production are sensitive to MPT inhibitors [8]. Since DNB-induced superoxide production is at least partially sensitive to the effects of bongkrekic acid, onset of MPT may account for the substantial increase in superoxide levels.

DNB induces persistent ROS production that increases the likelihood that protein carbonylation occurs in and around the mitochondria. Superoxide anion has a relatively long half-life that allows it to migrate from its site of production and interact with other molecules to form stronger oxidizing species [9]. Mitochondria contain an abundance of transition metals bound to various macromolecules, such as iron-sulfur clusters, which could degrade during the onset of cellular pathology and result in mitochondrial proteins being exposed to conditions favoring metal-catalyzed oxidations [9, 10]. On the other hand, the mitochondrion is also equipped with a variety of antioxidant defense mechanisms as is the cytosol and its component organelles [9]. Therefore, it is logical to ask whether or not in the face of a competent antioxidant system mitochondrial proteins that are acutely sensitive to oxidative modification trigger irreversible formation of the MPT. This study confirmed results from previous research showing that pretreatment with the iron-chelating antioxidant, deferoxamine, protects cells from 1, 3-DNB induced mitochondrial depolarization [1]. Since deferoxamine was more effective at inhibiting mitochondrial depolarization than trolox, it is possible that protecting against hydroxyl radical formation is more

important than inhibiting the formation of other ROS in order to prevent 1,3-DNB-induced mitochondrial dysfunction and that it is the formation of this highly reactive oxygen species that is the culprit in triggering the MPT.

Acknowledgments

This research was supported by grants from the NIEHS (NIH T32-ES07062) and the NIH (RO1-ES08846). We would like to thank Jen Fernandez for her assistance during the course of this study.

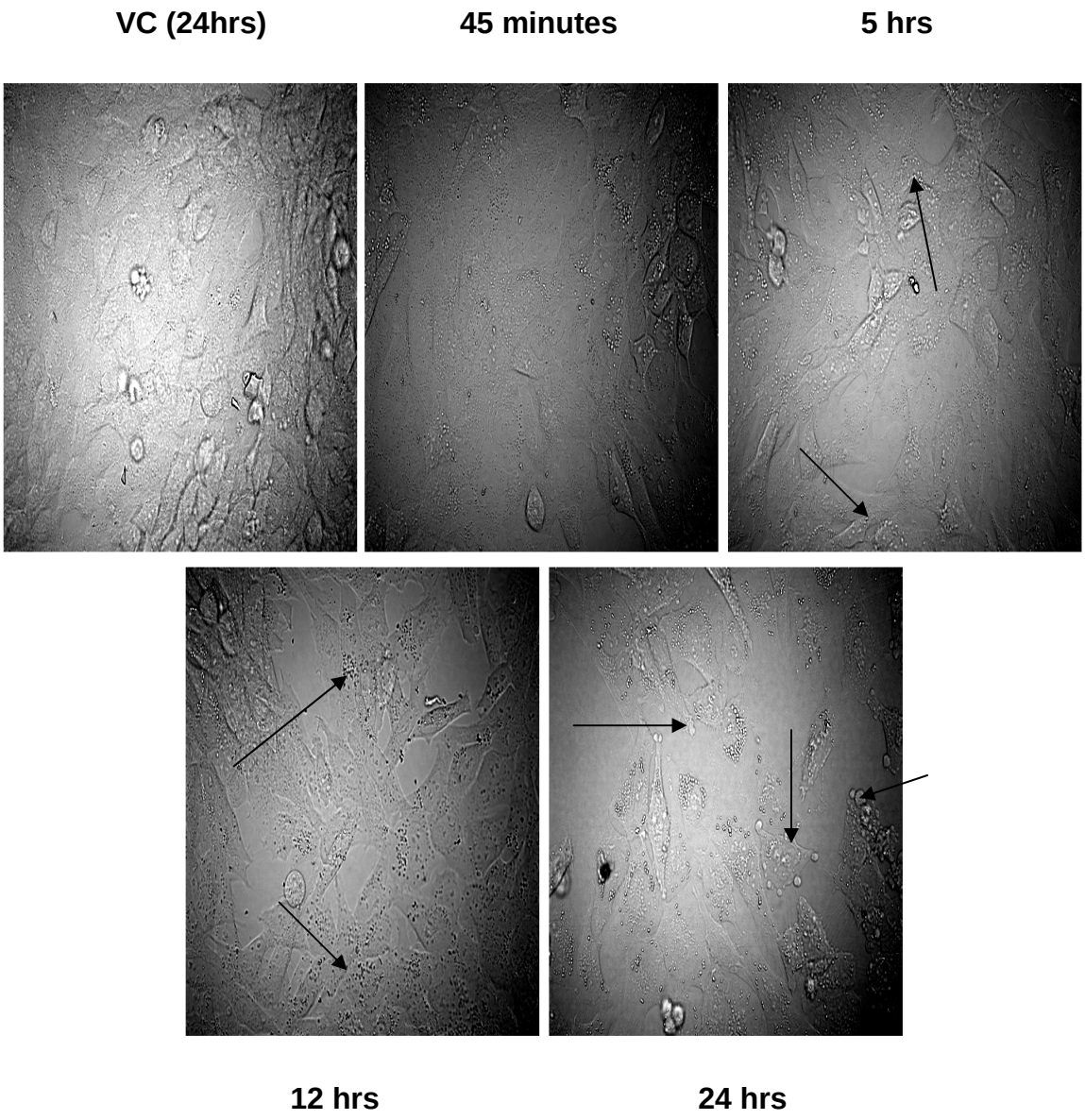

Figure 2.1. Differential interference contrast (DIC) images depicting time-dependent cytoxicity of DI TNC1 astrocytes exposed to 1mM 1,3-DNB. Black arrows indicate widespread vacuolization and formation of dark, punctuate bodies present 5 hrs and 12 hrs after initial 1,3-DNB exposure. Arrows indicate decreased cellular confluence, retracted processes, and membrane blebbing 24 hrs after commencement of 1,3-DNB exposure.

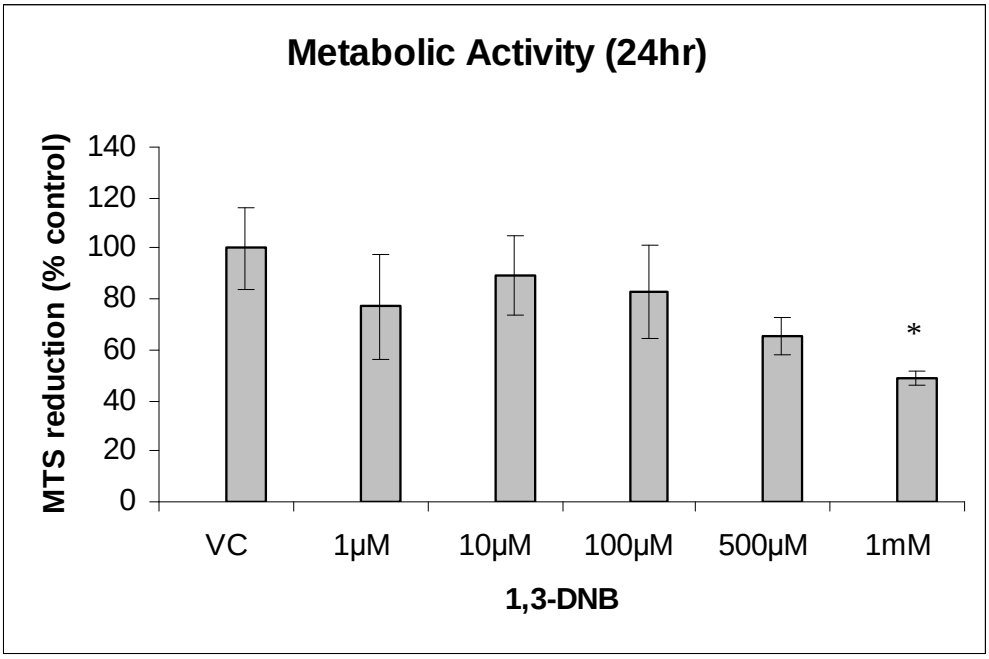

Figure 2.2. Concentration-dependent decrease in MTS reductive capability of DI TNC1 astrocytes exposed to 1,3-DNB over 24 hour period. Data is expressed as % DMSO control ± SEM with statistical significance (*****) if $p < 0.05$.

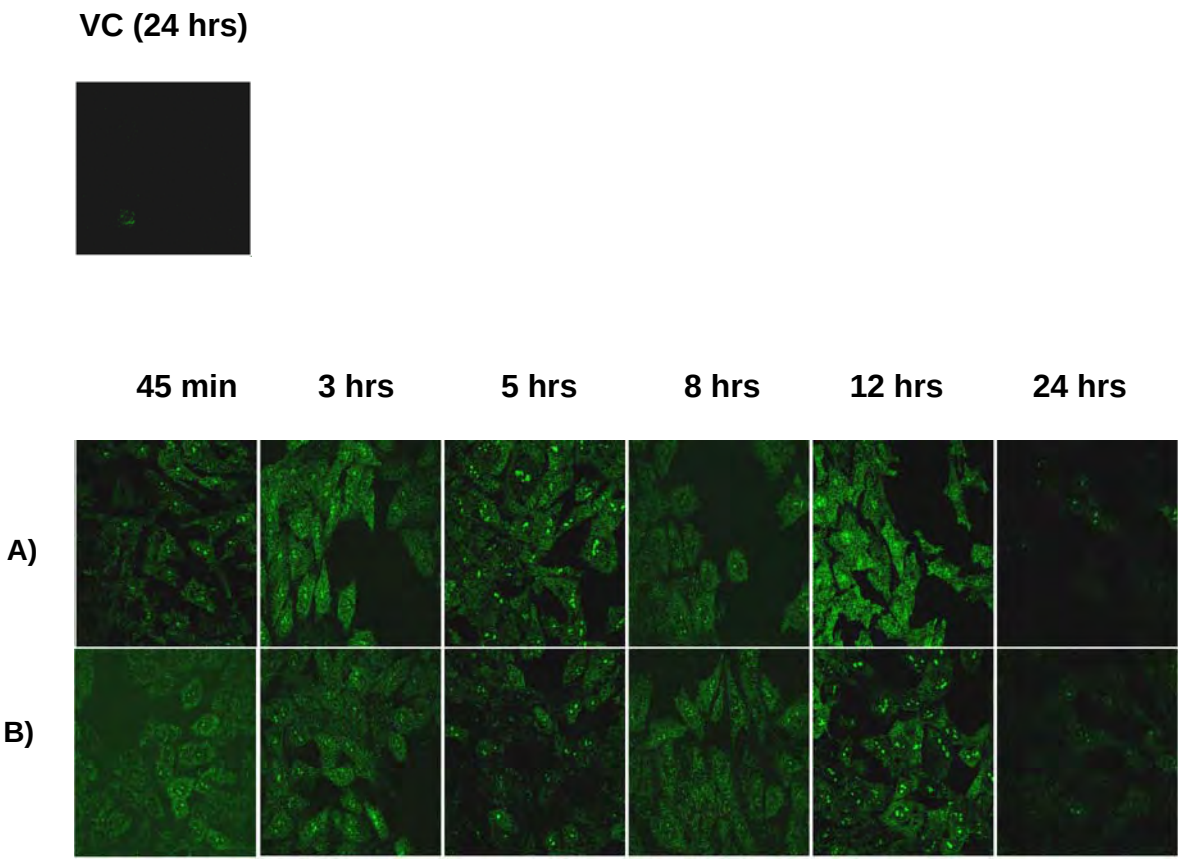

Figure 2.3. 1,3-DNB-induced production of mitochondrial superoxide anion in DI TNC1 cells measured using confocal microscopy. DI TNC1 cells were loaded with MitoSOX Red for 10 minutes after exposure to DMSO vehicle control or 1mM 1,3-DNB. Following pretreatment with 5μM BkA for 20 minutes, cells were exposed to 1mM 1,3-DNB and production of superoxide anion was measured.

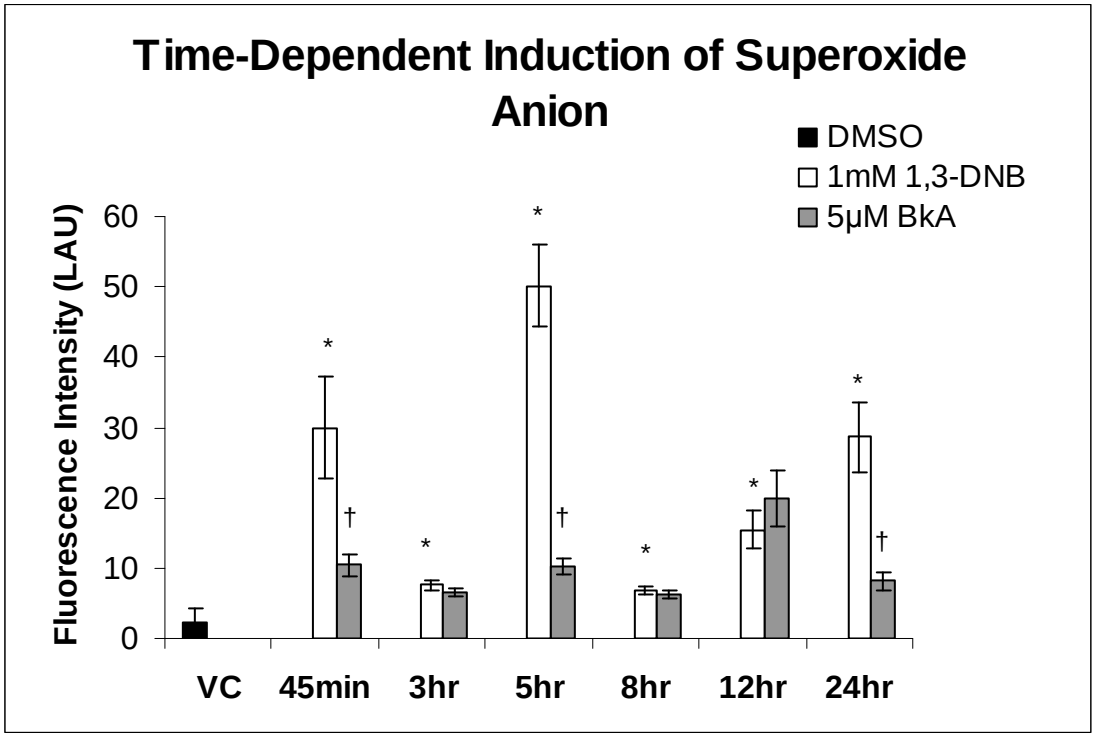

Figure 2.4. Changes in MitoSOX Red fluorescence were measured and graphed as linear arbitrary units (LAU) in 3 or 4 independent experiments (~7-10 cells per experiment). Values are expressed as mean ± SEM with statistical siginificance (*****) if $p < 0.001$ when compared to DMSO vehicle controls or (†) compared to 1,3-DNB treatment alone.

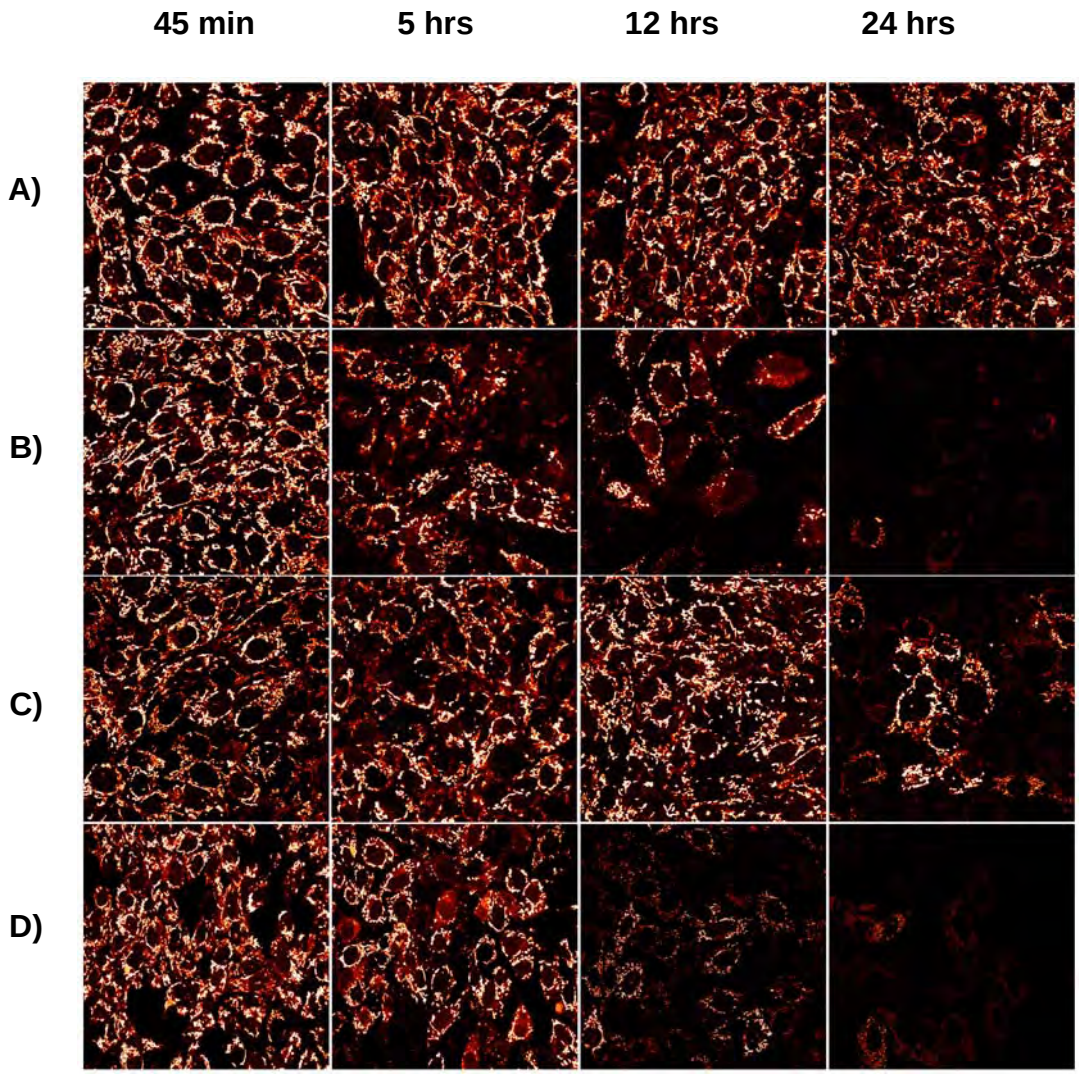

Figure 2.5. 1,3-DNB-induced loss of $\Delta\Psi_m$ in DI TNC1 cells measured using confocal microscopy. DI TNC1 cells were loaded with TMRM for 15 minutes after exposure to DMSO vehicle control (A) or 1mM 1,3-DNB (B). Following pretreatment with 600μM deferoxamine (C) or 100μM trolox (D) for 20 minutes, cells were exposed to 1mM 1,3-DNB and loss of $\Delta\Psi_m$ was measured.

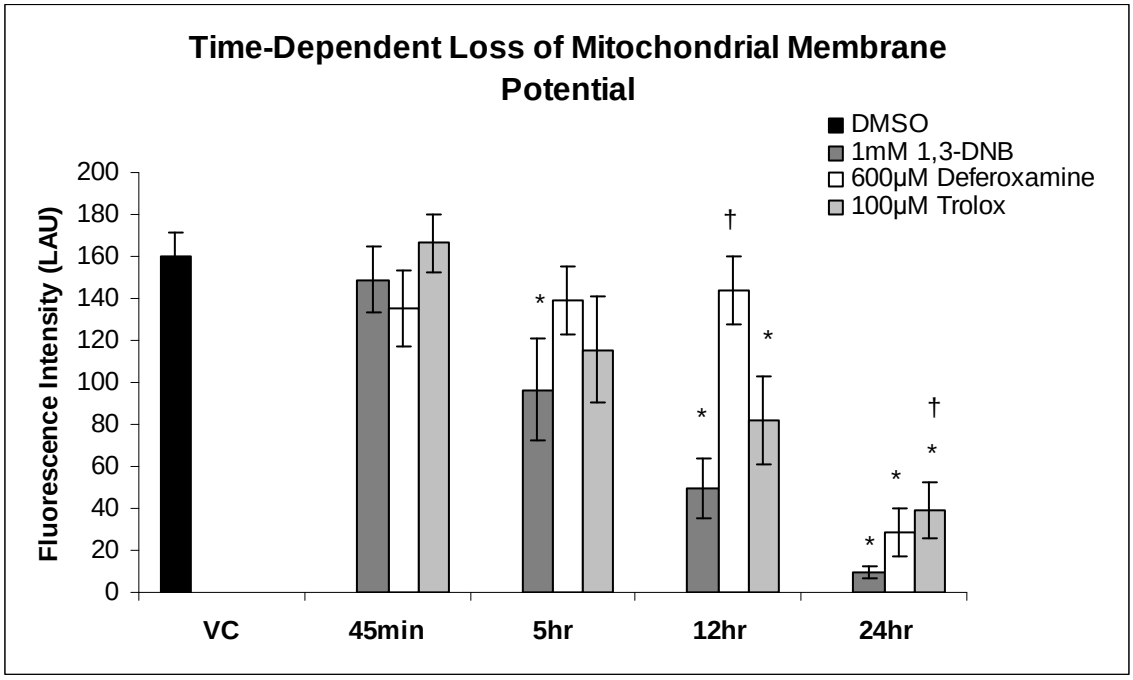

Figure 2.6. Changes in TMRM fluorescence were measured and graphed as linear arbitrary units (LAU) in 3 or 4 independent experiments (~7-10 cells per experiment). Values are expressed as mean ± SEM with statistical significance if $p < 0.001$ when compared to DMSO vehicle controls (*****) or compared to 1,3-DNB treatment alone (†).

References

1. Tjalkens, R. B.; Ewing, M. M.; Philbert, M. A. Differential cellular regulation of the mitochondrial permeability transition in an *in vitro* model of 1,3-dinitrobenzene-induced encephalopathy. *Brain Res.* **874**: 165-177; 2000.

2. Miller, T. J.; Phelka, A. D.; Tjalkens, R. B.; Dethloff, L. A.; Philbert, M. A. Cl-1010 induced opening of the mitochondrial permeability transition pore precedes oxidative stress and apoptosis in SY5Y neuroblastoma cells. *Brain Res.* **14**: 43-56; 2003.

3. Zorov, D. B.; Juhasova, M.; Sollott, S. J. Mitochondrial ROS-induced ROS release: An update and review. *Biochim. Biophys. Acta* **1757**: 509-517; 2006.

4. Philbert, M. A.; Nolan, C. C.; Cremer, J. E.; Tucker. D.; Brown, A. W. 1,3-dinitrobenzene-induced encephalopathy in rats. *Neuropathol. Appl. Neurobiol.* **13**: 371-389; 1987.

5. Romero, I. A.; Lister, T.; Richards, H. K.; Seville, M. P.; Wylie, S. P.; Ray, D. E. Early metabolic changes during *m*-dinitrobenzene neurotoxicity and the possible role of oxidative stress. *Free. Radic. Biol. Med.* **18**: 311-319; 1995.

6. Reeve, I. T.; Voss, J. C.; Miller, M. G. 1,3-dinitrobenzene metabolism and GSH depletion. *Chem. Res. Toxicol.* **15**: 361-366; 2002.

7. Romero, I. A.; Ray, D. E.; Chan, M. W. K.; Abbott, N. J. An *in vitro* study of *m*-dinitrobenzene toxicity on the cellular components of the blood-brain barrier, astrocytes and endothelial cells. *Toxicol. Appl. Pharmacol.* **139**: 94-101; 1996.

8. Tay, V. K. S.; Wang, A. S.; Leow, K. Y.; Ong, M.; Wong, K. P.; Boelsterli, U. A. Mitochondrial permeability transition as a source of superoxide anion induced by the nitroaromatic drug nimesulide *in vitro*. *Free Rad. Biol. Med*. **39**: 949-959; 2005.

9. Kohen, R.; Nyska, A. Oxidation of biological systems: oxidative stress phenomena, antioxidants, redox reactions, and methods for their quantification. *Toxicol. Pathol.* **30**: 620-650; 2002.

10. Tangeras, A.; Flatmark, T.; Backstrom, D.; Ehrenberg, A. Mitochondrial iron not bound in heme and iron-sulfur clusters. Estimation, compartmentation, and redox state. *Biophys. Acta* **589**: 162-175; 1980.

Chapter III

Determine whether or not 1,3-DNB-induced increases in ROS lead to oxidative modification of mPTP proteins

Introduction

Proteins are particularly susceptible to the effects of altered cellular redox states, i.e. increases in ROS. Proteins contain sulfhydryl groups that are highly reactive and can interact with ROS or other oxidizing agents. Oxidative stress can lead to various forms of oxidative modification including carbonylation, crosslinked thiol groups, as in the case of oxidized vicinal thiol groups, and thio-bonded adducts, as in the case of S-nitrosylated proteins. It has been shown that S-thiolation of proteins can occur within minutes after a burst of oxidative stress [1]. The mechanism of S-thiolation starts with the formation of partially oxidized sulfhydryl groups, thiyl radical or sulfenic acids, and without adequate glutathione reserves, can lead to the development irreversibly oxidized sulfinic and sulfonic acid groups. Modifying a critical sulfhydryl in this oxidative manner can alter the function of the protein(s) in question. For example, the redox state

of vicinal thiol groups in mPTP proteins affects the probability of whether or not the permeability transition pore exists in an open or closed state. Petronilli et al., (1994) showed that oxidized vicinal thiols within cysteinyl residues, alters the voltage sensing capability of the mPTP such that the gating potential of the pore increases, thus increasing the likelihood of pore opening [2]. This study also showed that pretreatment of mitochondria with low concentrations of the reducing agent, dithiothreitol (DTT), inhibits pore opening in the presence of oxidizing agents, like menadione. This implies that the mPTP proteins contain critical sulfhydryls whose oxidation states dictate the open or closed state of the mPTP. By triggering premature opening of the mPTP, oxidation of these critical protein residues can predispose other mitochondria to onset of the MPT through a positive feedback mechanism that exacerbates MPT-induced ROS production, leading to downstream oxidative damage of these otherwise unaffected mitochondria [3]. For example, increased protein carbonylation is known to occur in conjunction with increased mitochondrial ROS production [4, 5].

The origin of increased ROS generation in neural cell types exposed to 1,3-DNB is unknown, but it is plausible that this increase in ROS can result in downstream oxidative modification of mPTP proteins, predisposing the mitochondria of susceptible cell types to premature activation of MPT. Studies from our lab have shown that neural cell types susceptible to 1,3-DNB toxicity (i.e. brainstem astrocytes, SY5Y neuroblastoma cells) produce more ROS than resistant cell types (i.e. cortical astrocytes, C6 glioma cells) and also exhibit a lower threshold of MPT induction. This lower threshold of MPT induction

suggests that critical sulfhydryls within mPTP proteins may be oxidized due to significant increases in ROS as a result of 1,3-DNB exposure. This portion of the study will determine the extent to which significant increases in ROS may modify mPTP protein composition after exposure to 1,3-DNB.

Materials and Methods

Chemicals

Tissue culture media and materials were obtained from Gibco (Invitrogen, Carlsbad, CA). The Oxyblot immunodetection kit was obtained from Chemicon (Millipore, Billerica, MA). Primary antibodies for Western analysis of lipid peroxidation and protein nitrotyrosination were purchased from Abcam (Cambridge, MA). Secondary antibodies for immunoblot visualization, 2D Clean-Up kits, IPG buffer, and Destreak rehydration buffer were obtained from GE Healthcare (Piscataway, NJ). IPG Readystrips and 12% Tris-HCl Readygels were obtained from Bio-Rad (Hercules, CA). BCA protein quantification reagents were obtained from Pierce (Thermo Scientific, Rockford, IL). PVDF membranes were purchased from Millipore (Billerica, MA). All other reagents were of analytical grade and were obtained from Sigma-Aldrich (St. Louis, MO).

Cell Culture

DI TNC1 astrocytes, obtained from the American Type Culture Collection, were maintained in a humidified incubator at 37°C in an atmosphere of 5% CO_2 (13). Cells were grown in DMEM containing 4.5g/L D-glucose, L-glutamine, 10% fetal bovine serum, and 1% penicillin-streptomycin-glutamine mixture. Cells grown between passages 5 through 25 were used for all experiments.

Mitochondrial Protein Sample Preparation

Cells were grown to >90% confluence in 75 cm^2 flasks and exposed to 1µM and 1mM concentrations of 1,3-DNB for 45 minutes using 0.14% DMSO (v/v) as a vehicle control. After exposure, mitochondrial protein samples were isolated from each exposure group using a protocol based upon the MITOISO1 kit for soft tissue. Cells from 6 or 7 flasks per exposure group were homogenized in a teflon tissue grinder and glass pestle in 10 volumes of extraction buffer containing 2 mg/ml bovine serum albumin. The extraction buffer's composition consists of 220 mM mannitol, 70 mM sucrose, 0.5 mM EGTA, and 2 mM HEPES at a final pH of 7.4. The homogenate was transferred to a 15 mL conical tube and centrifuged at 500 x g for 5 minutes. The resulting supernatant was then removed, centrifuged at 11000 x g, and the pellet resuspended in extraction buffer. This step was repeated two more times in order to thoroughly wash the pellet. The mitochondrial protein pellet was resuspended in storage buffer containing 10 mM, HEPES, 250 mM sucrose, 1 mM ATP, 0.08 mM ADP, 5 mM sodium succinate, 2 mM K_2HPO_4, and 1mM DTT. A protease inhibitor cocktail

was added to each sample before protein concentrations were quantified or the samples placed in storage at -80°C. Protein concentrations were quantified using the BCA Protein Assay kit.

Two-dimensional (2D) gel electrophoresis

Aliquots of mitochondrial protein sample containing 70 µg of protein were prepared for SYPRO ruby staining and detection of protein carbonyls through Oxyblot analysis. Protein samples designated for Oxyblot analysis were derivatized for approximately 15 min at room temperature in a 1X dinitrophenylhydrazine (DNPH) solution provided for in an Oxyblot immunodetection kit. This reaction derivatizes carbonyl groups found on protein side chains to 2,4-dinitrophenylhydrazones that can be detected using Western blot analysis. Upon completion of the derivatization reaction, excess salts and other impurities were removed from each set of samples using a 2-D Clean-Up kit. Precipitates were incubated in wash buffer for at least an hour before centrifugation at 12,000 x g for 5 min. After the wash buffer was removed, 200 µl Destreak rehydration buffer containing 2.5 ul/ml IPG buffer (pH 3-10) was added to the protein pellet. A final centrifugation at 12,000 x g was required in order to remove any insoluble material that might hinder isoelectric focusing. Each sample was then added to a ReadyStrip IPG Strip 7 cm pH 3-10. The IPG strips were actively rehydrated overnight in the IEF focusing tray of the Protean IEF cell (Bio-Rad) using a current of 50 µA/IPG strip at 20°C. Isoelectric focusing was performed overnight at a voltage of 4000 V for a minimum of 20,000 Vh at 20°C.

Before separation in the second dimension, the IPG strips were equilibrated at room temperature using two separate buffer solutions. The IPG strips were first equilibrated for 20 min in 0.375 m Tris-HCl (pH 8.8) containing 6 M urea, 2% SDS, 20% glycerol, and 2% (w/v) dithiothreitol. The IPG strips were then equilibrated for 20 min in 0.375 M Tris-HCl (pH 8.8) containing 6 M urea, 2% SDS, 20% glycerol, and 2.5% (w/v) iodoacetamide. The IPG strips were then placed on ReadyGels 12% Tris-HCl in Mini-Protean III systems for electrophoresis. For the second dimension separation, the gels were run at a constant voltage of 100 V for approximately 1.45 h.

SYPRO Ruby staining

The gels were fixed in 50% methanol and 7% acetic acid twice, each for 30 min. Approximately 60 ml of SYPRO stain was added after the fixative was removed and the gels were stained overnight at room temperature. The gels were then washed in 10% methanol and 7% acetic acid and visualized in a Fujifilm FLA-5000 imaging system using Image Reader software.

Western Blot Analysis

Following separation in the second dimension, 2D gels designated for nitrotyrosination, 4-hydroxy-2-nonenal, or Oxyblot analysis were transferred to PVDF membranes. Membranes were incubated in blocking buffer for 1 hour at room temperature and then incubated overnight at 4°C in blocking buffer containing primary antibody targeting either 3-nitrotyrosines (1µg/ml) or 4-

hydroxy-2-nonenal (1µg/ml) were incubated in blocking buffer. The nitrocellulose membranes were exposed to blocking buffer for 1 hour and then incubated overnight at 4°C in rabbit primary antibody specific to 2,4-dinitrophenylhydrazone. An anti-rabbit, alkaline phophatase-labeled secondary, used for ECF-based immunodetection, was added following removal of the primary antibody and washing of the PVDF membranes. Images of carbonylated proteins were visualized using the Fujifilm FLA-5000 imaging system and Image Reader software. Densitometry measurements were conducted using Multi Gauge V2.2. Carbonylation index ratios representing percent change in carbonylation status were calculated using densitometric analysis of carbonylated protein targets normalized to the amount of protein detected in SYPRO Ruby-stained 2D gels.

Tandem Mass Spectrometry

LC/MS/MS analysis and protocol were provided by the Michigan Proteome Consortium (www.proteomeconsortium.org). Images of both the Coomassie-stained 2D gels and 2D Oxyblots were overlaid on one another and carbonylated proteins were matched with protein spots from the 2D gels for excision followed by mass spectrometric analysis. Bovine serum albumin was used as a reference marker for protein samples were digested with trypsin using the MassPrep robot. Target peptides were extracted from the gel plugs with 30µl of 2% acetonitrile 0.1% TFA. Five microliters of MALDI matrix was added to each extract and the extracts were dried using a Speed Vac. The peptides were dissolved in 5µl of

60% ACN 0.1% TFA. An aliquot of each sample was spotted onto a MALDI target for MS/MS analysis. Protein identification was accomplished by matching peptide sequences using the International Protein Index (IPI) database.

Statistical Analysis

Changes in carbonylation intensity between the index ratios of vehicle control and treatment groups were expressed as percentages ± SEM (n= 3 images/treatment, 6-10 pooled biological replicates) were compared using two-way ANOVA followed by post-hoc Dunnett's t-test, with $p < 0.05$ representing a significant difference between the means.

Results

Immunodetection of protein carbonyls

Confocal microscopic analysis of DI TNC1 astrocytes exposed to 1mM 1,3-DNB revealed that loss of $\Delta\Psi_m$ at 5 hrs is subsequent to significant production of superoxide anion. 2D Oxyblots were used to determine whether or not 1,3-DNB induced ROS altered the carbonylation status of mitochondrial proteins before loss of $\Delta\Psi_m$ was initially observed, specifically 45 min after exposure. The oxidation of specific proteins in the presence of increased ROS production during the early stages of toxicant exposure likely impair mitochondrial function downstream, as exhibited by significant loss of the $\Delta\Psi_m$ at 5 hrs. Carbonylation index ratios were measured by normalizing the intensities

of anti-DNP immunoreactivity observed in the 2D Oxyblots to the protein signatures in the 2D gels stained with Sypro Ruby in order to eliminate the possibility that any changes in carbonylation intensity would be due to changes in protein concentration.

The 2D Western analysis revealed that DI TNC1 astrocytes exposed to 500μM 1,3-DNB for 45 minutes did not induce the formation nitotyrosine or 4-hydroxy-2-nonenal adducts (Figure 3.1). The 2D Oxyblot analysis revealed that several proteins were sensitive to 1,3-DNB-induced carbonylation at 45 min as indicated by an intense pattern of immunoreactivity (Figure 3.3). The intensity of marked carbonylation is significantly less in 2D Oxyblots derived using mitochondrial protein isolated from DI TNC1 astrocytes exposed to only the DMSO control. Pre-incubation of DI TNC1 astrocytes with antioxidants, Trolox and deferoxamine, attenuated the intensity of protein carbonylation as compared to treatment with 1,3-DNB alone (Figure 3.4). The selectivity of proteins that appear to be targets of 1,3-DNB induced carbonylation remain consistent throughout each treatment group. In addition, comparing an Oxyblot to its corresponding 2D gel reveals that not all protein spots within a 2D gel exhibit carbonyl immunoreactivity. In order to determine if protein carbonylation is dose-dependent, DI TNC1 astrocytes were incubated with 1μM 1,3-DNB for 45 min (Figure 3.3). Exposing the cells to a lower concentration of 1,3-DNB results in fewer individual proteins carbonylated by 1,3-DNB induced oxidative stress. This data shows that carbonylation intensity and the number of proteins susceptible to

DNB-induced carbonylation increases when cells are exposed to higher concentrations of 1,3-DNB.

Tandem mass spectrometric identification of carbonylated proteins

Targets of 1,3-DNB induced protein carbonylation were identified using tandem mass spectrometry. Since the use of dinitrophenylhydrazine to derivatize protein carbonyls for immunodetection may interfere with mass spectrometric identification of proteins [6], non-DNPH exposed mitochondrial protein samples were separated on 2D gels and protein spots excised from these gels were designated for further identification. DNPH-treated and untreated protein samples were compared using SYPRO Ruby-stained 2D gels in order to show that DNPH-treatment has no effect on protein migration in either the first or second dimension (Figure 3.2). 2D Oxyblot images were matched with corresponding Coomassie-stained 2D gels containing mitochondrial proteins isolated from DI TNC1 astrocytes treated with 1mM 1,3-DNB for 45 min. Several proteins exhibited increased carbonyl immunoreactivity as indicated by the 2D Oxyblot analysis. Peptide sequences were generated using LC/MS/MS and then successfully matched using the Mascot search engine and the IPI database (Figure 3.5). Mitochondrial proteins identified include the F1-ATP synthase beta-chain, aconitate hydratase, two isoforms of aldehyde dehydrogenase, and mitochondrial Hsp70. The majority of these susceptible proteins have expected molecular weight values in the 50 kDa and 70 kDa range, while the pI values are between 4 and 7. The predicted values of the identified proteins are in

agreement with the observed position of these proteins in the 2D gels. The total ion score of each protein listed in Table 1 was identified with greater than 95% confidence. LC/MS/MS analysis was applied to mitochondrial proteins isolated from DI TNC1 astrocytes exposed to 1μM 1,3-DNB for 45 min (Figure 3.6). There were fewer carbonylated proteins observed during the 2D Oxyblot analysis of proteins isolated from cells treated with 1μM 1,3-DNB for the same amount of time. Carbonylated mitochondrial proteins identified in both the 1mM and 1μM 1,3-DNB treatment groups include the beta-chain of F1-ATP synthase beta-chain and mtHsp70. The carbonylation signal intensity ratios obtained for these particular mitochondrial proteins are listed in Figure 3.7. Each treatment group designated for LC/MS/MS analysis was repeated 3 times in order to confirm protein identification. Differential centrifugation was used to isolate mitochondrial proteins from DI TNC1 astrocytes. Previous studies report the difficulty in obtaining purified mitochondrial proteins using various methods, including differential centrifugation [7, 8, 9]. Some cytosolic proteins, nonetheless, were consistently identified in mitochondrial preparations from DITNC1 astrocytes exposed to 1mM and 1μM 1,3-DNB. A complete table displaying all mitochondrial, ER, and cytosolic proteins identified during the low concentration (1μM 1,3-DNB) and high concentration (1mM 1,3-DNB) treatments is presented in Figure 3.8. This finding suggests that cytoplasmic and endoplasmic reticular proteins are also targets of oxidative carbonylation following exposure to DNB.

Discussion

This study demonstrates the capability of 1,3-DNB to modify mitochondrial proteins through oxidative carbonylation in DI TNC1 astrocytes. Mitochondrial proteins were carbonylated within the first hour of 1,3-DNB exposure and pretreatment with antioxidants prior to 1,3-DNB exposure partially inhibited the formation of protein carbonyls. Protein carbonylation occurred before loss of the $\Delta\Psi_m$, but during DNB-induced production of superoxide anion. Fewer proteins were carbonylated when the cells were exposed to a lower concentration of 1,3-DNB, suggesting that DNB-induced protein carbonylation is dose-dependent and may be a function of the sensitivity of individual proteins to oxidation. These findings also imply that oxidative stress may be an important precursor to the onset of the mitochondrial permeability transition and that these fundamental alterations occur hours before mitochondrial dysfunction is observed. Whether or not these protein changes are required and/or sufficient for induction of the MPT remains to be determined. Nonetheless, the detection of a small and highly conserved number of proteins that are acutely sensitive to oxidation leads to the tantalizing conclusion that modification of these proteins may regulate, in some fashion, the function and fate of mitochondria in oxidative environments.

DNB induces persistent ROS production that increases the likelihood that protein carbonylation occurs in and around the mitochondria. Superoxide anion has a relatively long half-life that allows it to migrate from its site of production

and interact with other molecules to form stronger oxidizing species [10]. Mitochondria contain an abundance of transition metals packaged within various macromolecules, such as iron-sulfur clusters, which could degrade during the onset of cellular pathology and result in mitochondrial proteins being exposed to conditions favoring metal-catalyzed oxidations [10, 11]. On the other hand, the mitochondrion is also equipped with a variety of antioxidant defense mechanisms as is the cytosol and its component organelles [10]. Therefore, it is logical to ask whether or not in the face of a competent antioxidant system mitochondrial proteins that are acutely sensitive to carbonyl formation trigger irreversible formation of the MPT. This study confirmed results from previous research showing that pretreatment with the iron-chelating antioxidant, deferoxamine, protects cells from 1, 3-DNB induced mitochondrial depolarization [12]. Since deferoxamine was more effective at inhibiting mitochondrial depolarization than trolox, it is possible that protecting against hydroxyl radical formation is more important than inhibiting the formation of other ROS in order to prevent 1,3-DNB-induced mitochondrial dysfunction and that it is the formation of this highly reactive oxygen species that is the culprit in triggering the MPT. Future experiments are aimed at ascertaining the functionality of the mitochondrial proteins most sensitive to carbonylation.

The results presented in this study are the first to show that protein carbonylation accompanies the development of 1,3-DNB neurotoxicity. However, there exists a basal level of mitochondrial protein carbonylation in control cells. Therefore, carbonylation of mitochondrial proteins, aside from being an index of

oxidative stress, may have a primary role in physiological regulation of mitochondrial function in addition to signaling the need for proteolytic degradation of effete and severely damaged proteins [4, 13]. Excessive production of ROS may amplify the oxidative protein 'signal' in specific targets, shifting the function of carbonylation from cell signaling to a precursor of pathologic change.

Specifically, tandem mass spectrometry permitted identification of two carbonylated mitochondrial proteins present in samples isolated from cells exposed to both high and low dose concentrations of 1,3-DNB, namely, mtHsp70 and F1-ATP synthase beta-chain. Comparison of the carbonylation signal intensity ratios in Table 2 demonstrated that both concentrations of 1,3-DNB induced significant increases in carbonylation intensity of the F1-ATP synthase beta-chain as compared to control. DNB-induced carbonylation of the F1-ATP synthase beta-chain was reduced when cells were pretreated with deferoxamine and trolox. In contrast, basal levels of carbonylated mtHsp70 appeared to be high in control cells and were not significantly increased as a function of exposure to 1,3-DNB. The differential susceptibility of these two important mitochondrial proteins to oxidation lends credence to the idea that alterations in specific protein oxidation may mediate normal mitochondrial function and/or dysfunction. Both are exposed to a basal level of oxidative stress by virtue of their location in the mitochondrion [14]. However, the (patho) physiological significance of the lack of an increase in carbonylation of proteins that are constitutively oxidized is not clear.

The mitochondrial Hsp70 homolog, mtHsp70 (Hsp75/Grp75/Hspa9a), resides in the mitochondrial matrix and is thought to chaperone the proper folding of mitochondrial proteins. The activation of mtHsp70 is mediated by impaired assembly of mitochondrial proteins, including the multi-subunit mitochondrial complexes [15]. Protein oxidation can lead to the formation of potentially harmful, oxidized protein aggregates that are subject to chaperone-mediated proteolysis [16]. Protein-protein interactions between chaperone mediator and oxidized peptides, or direct interaction with ROS, can lead to carbonylation of the chaperone protein which explains how mtHsp70 becomes a target of oxidative carbonylation and has been linked to disease states such as ischemia [11, 16, 17, 18].

The major sources of mitochondrial ROS are the multi-subunit complexes responsible for aerobic respiration. Since these proteins are intimately involved with the production of ROS, it is no surprise that the subunits which comprise each complex are potential targets of oxidative damage. In particular, the alpha- and beta-chains of F1-ATP synthase (Complex V) are well established targets of oxidative carbonylation linked to various other pathologic mechanisms [19, 20, 21, 22]. Carbonylation of the F1-ATP synthase beta-chain may likely contribute to DNB–induced mitochondrial depolarization and ATP depletion in susceptible astrocytes. By modifying the structure of the F1 unit, ATP production may cease and unpaired electrons meant for the purpose of ATP production may instead interact with molecular oxygen to form superoxide anion.

In summary, this study provides important new insights into how oxidative damage may mediate the neurotoxicity of 1,3-DNB and other chemicals that target mitochondrial function. Several reports confirm the involvement of oxidative stress during the development of nitrocompound–induced neuropathology, however this study is the first to demonstrate the precise macromolecular targets of oxidative carbonylation. Future studies will need to address the role of these targets in promoting the loss of function in susceptible astrocyte following exposure to chemicals that induce acute energy deprivation syndromes.

Acknowledgments

This research was supported by grants from the NIEHS (NIH T32-ES07062) and the NIH (RO1-ES08846). We would like to thank Jen Fernandez, and the members of the Michigan Proteomics Consortium for their assistance during the course of this study.

4-hydroxy-2-nonenal **Nitrotyrosination**

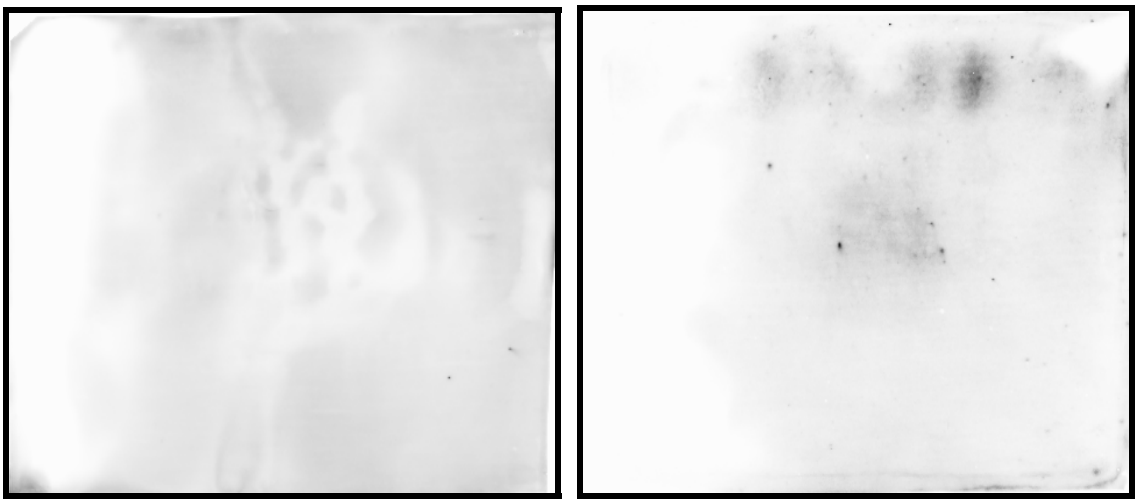

Figure 3.1. Two-dimensional Western blot analysis revealed no markers of lipid peroxidation and nitrotyrosination in mitochondrial proteins isolated from DI TNC1 astrocytes exposed to 500µM 1,3-DNB for 45 min.

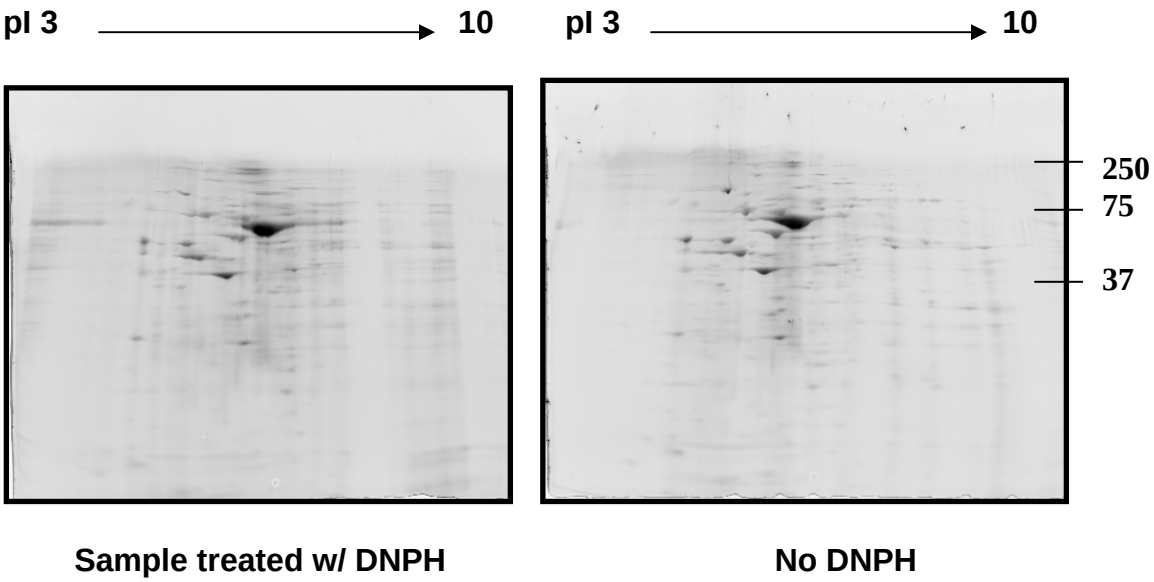

Figure 3.2. Two-dimensional gel electrophoresis of mitochondrial proteins isolated from DI TNC1 astrocytes after exposure to 1mM 1,3-DNB, for 45 minutes. Mitochondrial protein samples derivatized with DNPH prior to 2D Oxyblot analysis display no observable changes in migration according to isoelectric point or mass.

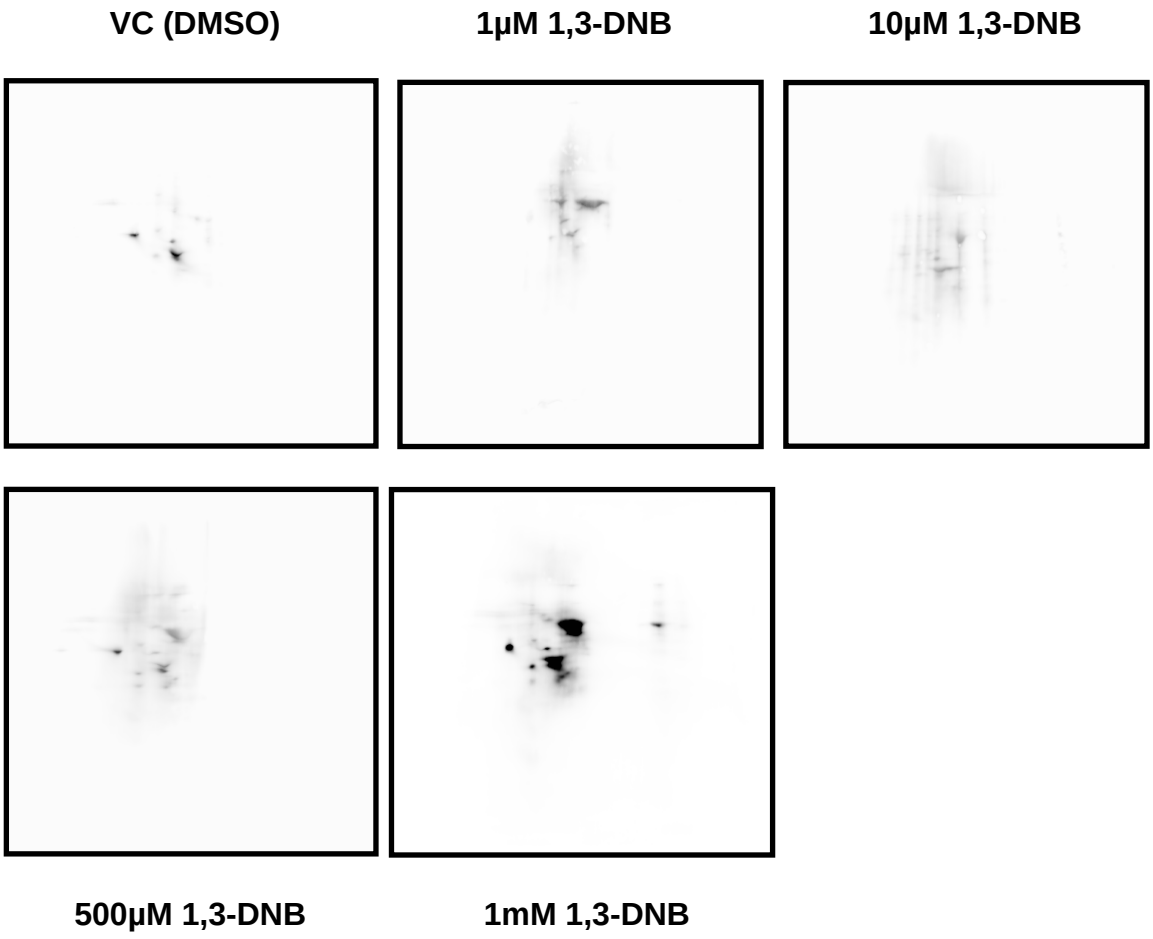

Figure 3.3. Concentration-dependent two-dimensional Oxyblot analysis of mitochondrial protein isolated from DI TNC1 astrocytes exposed to 1,3-DNB for 45 minutes.

600µM Deferoxamine **100µM Trolox**

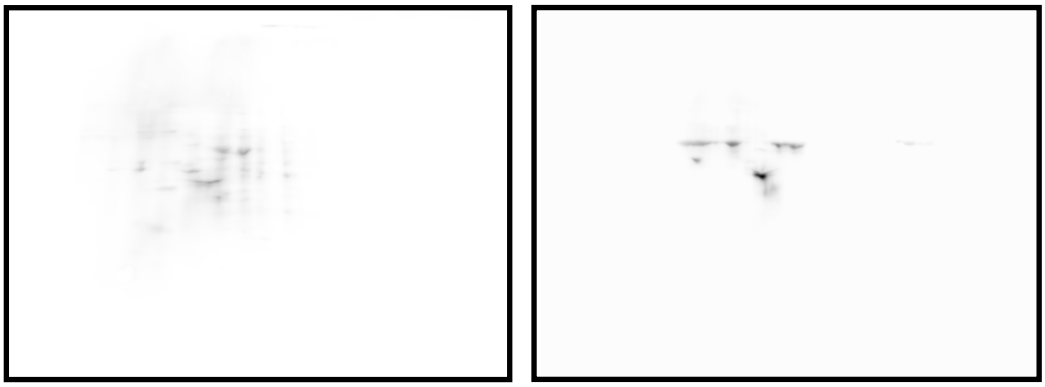

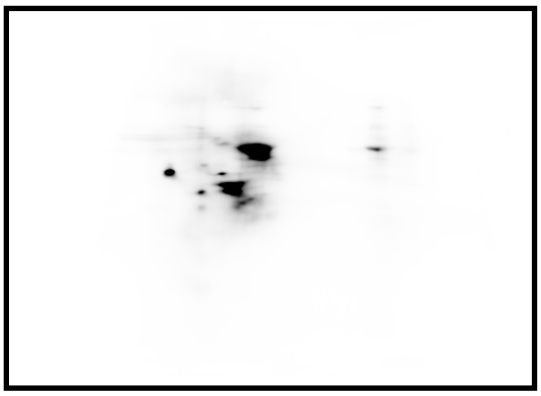

1mM 1,3-DNB (no antioxidant pretreatment)

Figure 3.4. Two-dimensional Oxyblot analysis of mitochondrial protein isolated from DI TNC1 astrocytes pretreated with 600µM deferoxamine or 100µM trolox prior to 45 minute treatment with 1mM 1,3-DNB exposure.

2D Oxyblot **2D gel**

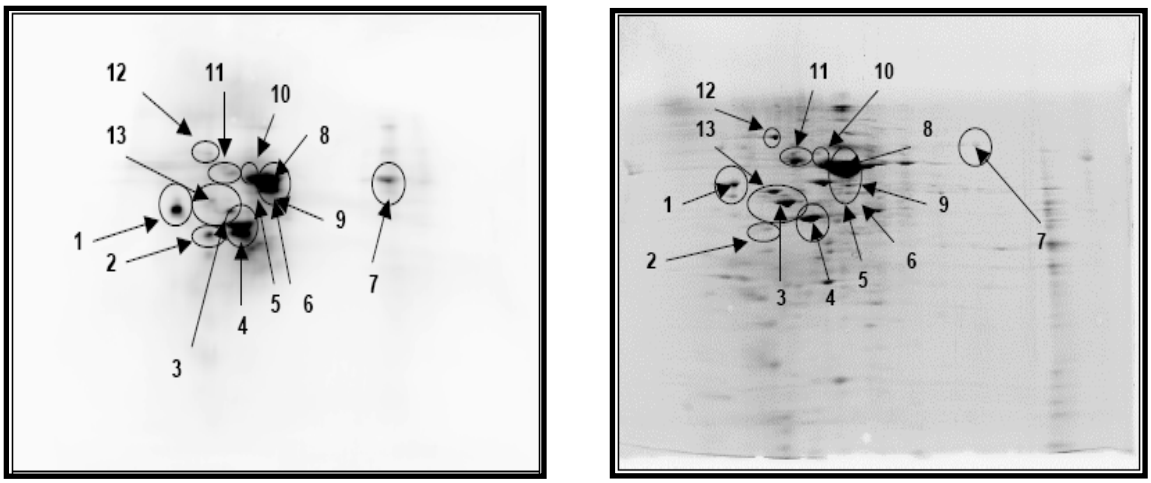

Spot Label	Protein Name	Protein MW	Protein PI
1	Calreticulin precursor	48137	4
2	Vimentin	53757.1	5.06
3	ATP synthase subunit beta, mitochondrial precursor	56318	5
4	Actin, cytoplasmic 2	75736	9
5	Aldehyde dehydrogenase, mitochondrial precursor	56966	7
6	Aldehyde dehydrogenase, mitochondrial precursor	56966	7
7	Aconitate hydratase, mitochondrial precursor	86121	8
8	Serum albumin precursor	70682	6
9	Protein disulfide-isomerase, A3 precursor	57499	6
10	mtHsp70, mitochondrial precursor	74097	5.97
11	Grp78 kDa glucose-regulated protein precursor	72473.5	5.07
12	Tumor rejection antigen gp96	74390	5
13	Protein disulfide-isomerase precursor	57314.8	4.82

Figure 3.5. Tandem mass spectrometric analysis of carbonylated mitochondrial proteins isolated from DI TNC1 astrocytes after exposure to 1mM 1,3-DNB for 45 minutes. Serum albumin (2 mg/ml) was added to the protein isolation in order to remove excess lipids from the isolate and act as a reference protein marker. Images of 2D Oxyblots were overlaid on corresponding 2D gel images stained with either SYPRO Ruby or Coomassie Blue. Carbonylated proteins were spot-picked from the 2D gel and identified using LC/MS/MS at the Michigan Proteome Consortium.

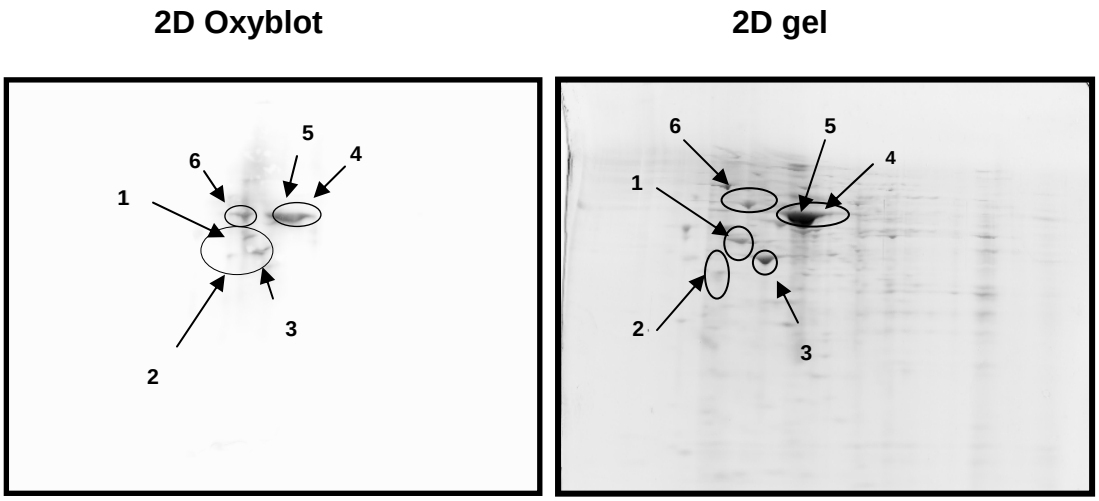

Spot Label	Protein Name	Protein MW	Protein PI
1	F1-ATP synthase subunit beta, mitochondrial precursor	56318	5
2	Vimentin	53757.1	5.06
3	Actin, cytoplasmic 2	75736	5.3
4	Serum albumin precursor	70682	6
5	mtHsp70, mitochondrial precursor	74097	5.97
6	Grp78 kDa glucose-regulated protein precursor	72473.5	5.07

Figure 3.6. Tandem mass spectrometric analysis of carbonylated mitochondrial proteins isolated from DI TNC1 astrocytes after exposure to 1µM 1,3-DNB for 45 minutes.

Protein	DMSO	1mM 1,3-DNB	600µM Deferoxamine	100µM Trolox	1µM 1,3-DNB
F1-ATP synthase beta-subunit	19.74 ± 0.09	* 45.93 ± 2.41	20.39 ± 3.71	12.59 ± 1.67	* 54.21 ± 6.28
mtHsp70, mitochondrial precursor	49.81 ± 6.22	46.28 ± 1.84	63.68 ± 0.95	29.41 ± 0.2	65.77 ± 2.67

Figure 3.7. Carbonylation intensity ratios of individual mitochondrial proteins identified during low concentration (1µM 1,3-DNB) and high concentration (1mM 1,3-DNB. Index ratios represent the percent change in carbonylation status using densitometric analysis of carbonylated protein targets normalized to densitometric intensity of total protein detected in SYPRO Ruby-stained 2D gels. Changes in carbonylation intensity between the index ratios of vehicle control and treatment groups were expressed as percentages ± SEM (n= 3 images/treatment, 6-10 pooled biological replicates) with $p < 0.05$ representing a significant difference (*****) between the means.

Protein Name	Peptide Ion Score	Peptide Ion Score C.I. %	Peptide Mass	Accession Number	Protein MW	Protein PI	Best Peptide Sequence	Match Error (Da)	Total Ion Score C.I. %	Total Ion Score
Calreticulin precursor	88.5	100	1784.85	IPI00191728	48137	4	IKDPDAAKPEDWDER	0.00	100.00	317.09
** Vimentin	82	100	1570.89	IPI00230941	53757.1	5.06	ISLPLPNFSSLNLR	-0.01	100.00	392.1322
** ATP synthase subunit beta, mitochondrial precursor	122.23	100	1435.76	IPI00551812	56318	5	FTQAGSEVSALLGR	0.01	100.00	540.07
** Actin, cytoplasmic	116.42	100	2215.08	IPI00764461	75736	9	DLYANTVLSGGTTMYPGIADR	0.01	100.00	506.18
Aldehyde dehydrogenase, mitochondrial precursor	74.52	100	1531.74	IPI00197770	56966	7	TIPIDGDFFSYTR	-0.01	100.00	269.68
Aldehyde dehydrogenase, mitochondrial precursor	60.98	100	1402.72	IPI00197770	56966	7	AAQAAFQLGSPWR	0.00	100.00	255.74
Aconitate hydratase, mitochondrial precursor	65.1	100	1601.79	IPI00421539	86121	8	NAVTQEFGPVPDTAR	0.00	100.00	311.02
** Serum albumin precursor	55.67	100	1749.68	IPI00191737	70682	6	ECCHGDLLECADDR	0.02	99.98	55.67
Protein disulfide-isomerase A3 precursor	51.78	100	2302.14	IPI00324741	57499	6	EYDDNGEGITIFRPLHLANK	0.00	100.00	189.56
** Mitochondrial heat shock protein 70, mitochondrial precursor	153	100	2055.95	IPI00363265	74097.0	5.97	STNGDTFLGGEDFDQALLR	-0.01	100.00	677.37891
** Grp78 kDa, glucose-regulated protein precursor	146	100	1933.99	IPI00206624	72473.5	5.07	DNHLLGTFDLTGIPPAPR	-0.02	100.00	972.08997
Tumor rejection antigen gp96	107.26	100	2250.04	IPI00734561	74390	5	FQSSHHSTDITSLDQYVER	0.00	100.00	382.54
Protein disulfide-isomerase precursor	121	100	1780.82	IPI00198887	57314.8	4.82	VDATEESDLAQQYGVR	-0.01	100	703.34003

Figure 3.8. Carbonylated proteins identified using LC/MS/MS in 1µM and 1mM 1,3-DNB, 45 min exposure. Double asterisks (**) before protein name indicate carbonylated proteins identified in 1µM 1,3-DNB, 45 min exposure group**.** Proteins were identified by the Michigan Proteome Consortium, using the International Protein Index database.

References

1. Biswas, S.; Chida, A. S.; Rahman, I. Redox modifications of protein-thiols: emerging roles in cell signaling. *Biochem. Pharmacol.* **71**: 551-564; 2005.

2. Petronilli, V.; Constantini, P.; Scorrano, L.; Colonna, R.; Passamonti, S.; Bernardi, P. The voltage sensor of the mitochondrial permeability transition pore is tuned by the oxidation-reduction state of vicinal thiols. Increase of the gating potential by oxidants and its reversal by reducing agents. *J. Biol. Chem.* **269**: 16638-16642; 1994.

3. Zorov, D. B.; Juhasova, M.; Sollott, S. J. Mitochondrial ROS-induced ROS release: An update and review. *Biochim. Biophys. Acta* **1757**: 509-517; 2006.

4. Nyström, T. Role of oxidative carbonylation in protein quality control and senescence. *Embo J.* **24**: 1311-1317; 2005.

5. Dalle-Donne, I.; Aldini, G.; Carini, M.; Colombo. R.; Rossi, R.; Milzani, A. Protein carbonylation, cellular dysfunction, and disease progression. *J. Cell. Mol. Med.* **10**: 389-406; 2006.

6. Castegna, A.; Aksenov, M.; Aksenova, M.; Thongboonkerd, V.; Klein, J. B.; Pierce, W. M.; Booze, R.; Markesbery, W. R.; Butterfield, D. A. Proteomic identification of oxidatively modified proteins in Alzheimer's disease brain. Part I: Creatine kinase BB, glutamine synthase, and ubiquitin carboxy-terminal hydrolase L-1. *Free. Rad. Biol. Med.* **33**: 562-571; 2002.

7. Scheffler, N. K.; Miller, S. W.; Carroll, A. K.; Anderson, C.; Davis, R. E.; Ghosh, S. S.; Gibson, B. W. Two-dimensional electrophoresis and mass spectrophotometric identification of mitochondrial proteins from an SH-SY5Y neuroblastoma cell line. *Mitochondrion* **1**: 161-179; 2001.

8. Goetz, J. G.; Nabi, I. R. Interaction of the smooth endoplasmic reticulum and mitochondria. *Biochem. Soc. Trans.* **34**: 370-373; 2006.

9. Walter, L.; Hajnóczky, G. Mitochondria and endoplasmic reticulum: the lethal interorganelle cross-talk. *J. Bioenerg. Biomembr.* **37**: 191-206; 2005.

10. Kohen, R.; Nyska, A. Oxidation of biological systems: oxidative stress phenomena, antioxidants, redox reactions, and methods for their quantification. *Toxicol. Pathol.* **30**: 620-650; 2002.

11. Tangeras, A.; Flatmark, T.; Backstrom, D.; Ehrenberg, A. Mitochondrial iron not bound in heme and iron-sulfur clusters. Estimation, compartmentation, and redox state. *Biophys. Acta* **589**: 162-175; 1980.

12. Tjalkens, R. B.; Ewing, M. M.; Philbert, M. A. Differential cellular regulation of the mitochondrial permeability transition in an *in vitro* model of 1,3-dinitrobenzene-induced encephalopathy. *Brain Res.* **874**: 165-177; 2000.

13. Wong, C. M.; Cheema, A. K.; Zhang, L.; Suzuki, Y. J. Protein carbonyaltion as a novel mechanism in redox signaling. *Circ. Res.* **102**: 310-318; 2008.

14. Magi, B.; Ettorre, A.; Liberatori, S.; Bini, L.; Andreassi, M.; Frosali, S.; Neri, P.; Pallini, V.; Di Stefano, A. Selectivity of protein carbonylation in the apoptotic response to oxidative stress associated with photodynamic therapy: a cell biochemical and proteomic investigation. *Cell Death Differ.* **11**: 842-852; 2004.

15. Yoneda, T.; Benedetti, C.; Urano, F.; Clark, S. G.; Harding, H. P.; Ron, D. Compartment-specific perturbation of protein handling activates genes encoding mitochondrial chaperones. *J. Cell Sci.* **117**: 4055-4066; 2004.

16. Costa, V.; Quintanilha, A.; Moradas-Ferreira, P. Protein oxidation, repair mechanisms, and proteolysis in *Saccharomyces cerevisiae*. *Life* **59**: 293-298; 2007.

17. Yaguchi, T.; Aida, S.; Kaul, S. C; Wadhwa, R. Involvement of mortalin in cellular senescence from the perspective of its mitochondrial import, chaperone, and oxidative stress management functions. *Ann. N .Y. Acad. Sci.* **1100**: 306-311; 2007.

18. Voloboueva, L. A.; Duan, M.; Ouyang, Y.; Emery, J. F.; Stoy, C.; Giffard, R. G. Overexpression of mitochondrial Hsp70/Hsp75 protects astrocytes against ischemic injury *in vitro*. *J. Cereb. Blood Flow Metab.* **28**: 1009-1016; 2008.

19. Prokai, L.; Yan, L-J.; Vera-Serrano, J. L.; Stevens Jr., S. M.; Forster, M. J. Mass spectrometry-based survey of age-associated protein carbonylation in rat brain mitochodria. *J. Mass. Spectrom.* **42**: 1583-1589; 2007.

20. Je, J. H.; Lee. T. H.; Kim, D. H.; Cho, Y. H.; Lee, J. H.; Kim, S. C.; Lee, S-K., Lee, J.; Lee, M-G. Mitochondrial ATP synthase is a target for TNBS-induced protein carbonylation in XS-106 dendritic cells. *Proteomics* **8**: 2384-2393; 2008.

21. Wen, J-J.; Garg, N. Oxidative modification of mitochondrial respiratory complexes in response to the stress of *Trypanosoma cruzi* infection. *Free Rad. Biol. Med.* **37**: 2072-2081; 2004.

22. Guerrieri, F.; Vendemiale, G.; Grattagliano, I.; Cocco, T.; Pellecchia, G.; Altomare, E. Mitochondrial oxidative alterations following partial hepatectomy. *Free Rad. Biol. Med.* **26**: 34-41; 1999.

Chapter IV

Determine whether or not 1,3-DNB-induced pattern of protein carbonylation is unique to 1,3-DNB exposure

Introduction

1, 3-Dinitrobenzene (1,3-DNB) serves as a model neurotoxicant for acute energy deprivation syndromes in the central nervous system. Exposure to 1, 3-DNB causes symmetrical, bilateral gliovascular lesions in the brainstem distinctive of the regions affected in other chemical-induced mitochondrial encephalopathies, Leigh's syndrome, and Wernicke's encephalopathy [1]. The regional distribution of lesions and the primary cellular targets of disease, the Type 1 astrocyte, suggest a cellular mechanism common to each encephalopathy. 1, 3-DNB induces significant perturbations in metabolic function and oxidative stress within susceptible brainstem nuclei [2, 3, 4, 5]. Even though the exact molecular pathway that leads to 1,3-DNB neurotoxicity is still unknown, previous research supports a mechanism that is mediated through the generation of ROS, which leads to DNB-induced mitochondrial dysfunction and onset of MPT [2]. A recent *in vitro* study from our laboratory links DNB-induced oxidative stress and mitochondrial dysfunction to the concentration-dependent oxidative

carbonylation of specific mitochondrial protein targets in DI TNC1 cells exposed to 1,3-DNB. This data suggests that the carbonylation of key proteins early in 1,3-DNB neurotoxicity may be indicators of downstream metabolic breakdown and the development of subsequent pathology.

Protein carbonylation alters protein function through irreversible, selective modification of amino acid residues [5,6]. Specific patterns of protein carbonylation associated with imbalance of the cellular redox state are known to occur in neurodegenerative pathology, including 1,3-DNB neurotoxicity [7, 8, 9]. In such cases of ROS-linked pathogenesis, oxidative stress increases the likelihood that susceptible proteins will become targets of carbonylation. In addition to amino acid sequence and increased ROS production, another factor that determines protein susceptibility to carbonylation is whether or not the cellular location places a protein at greater risk of exposure to damaging ROS. Proteins located in close proximity to ROS-generating mechanisms, such as the protein complexes that mediate aerobic respiration, are prone to oxidative damage when metabolic disturbances lead to increased mitochondrial ROS production [6,10]. DNB-induced mitochondrial superoxide anion is associated with carbonylation of the F1-ATP synthase beta-subunit prior to loss of the $\Delta\Psi_m$. This evidence suggests that a biochemical, oxidative threshold must be surpassed before molecular indications of cellular toxicity occur. However, it must be noted that DNB exposure induces a carbonylation pattern which includes not only mitochondrial proteins, but also proteins localized in the cytosol and the endoplasmic reticulum. The array of proteins oxidized during exposure

to 1,3-DNB demonstrate how neurotoxicity may develop through a pathway that includes, but is not limited to, oxidation of solely mitochondrial proteins.

The objective of this study was to determine whether or not 1,3-DNB induces a unique pattern of carbonylated proteins. Identifying specific patterns of protein carbonylation, among other examples of toxicant-induced mitochondrial dysfunction, may help elucidate the specific molecular mechanism underlying the development of 1,3-DNB-induced mitochondrial toxicity. This study was performed using other well-established mitochondrial and metabolic toxicants in a comparative analysis of mitochondrial dysfunction and protein carbonylation. The other toxicants included in this study were 3-chloropropanediol (3-CPD), 2,4-dinitrophenol (2,4-DNP), and 3-nitropropionic acid (3-NPA). 3-CPD is the active metabolite of α-chlorohydrin and, similar to 1,3-DNB, has been used as a model of chemical-induced energy deprivation syndromes [11,12]. 3-CPD targets type 1 brainstem astrocytes and disrupts metabolic function through inhibition of glyceraldehyde-3-phosphate dehydrogenase [13]. 2,4-DNP inhibits mitochondrial respiration by uncoupling proton transport down the inner mitochondrial membrane, resulting in increased ROS production and loss of the $\Delta\Psi_m$ [14,15]. 3-NPA disrupts oxidative phosphorylation through suicide inhibition of succinate dehydogenase and has been shown to induce protein carbonylation *in vivo* [16,17].

In this *in vitro* study, confocal microscopy and proteomic analysis were used to analyze time- and concentration-dependent mitochondrial dysfunction and protein carbonyl formation using toxicant concentrations that did not induce

gross morphological changes or significant metabolic dysfunction. Concentration- and time-dependent measurements of metabolic activity for each toxicant were obtained using MTS assays. Confocal microscopic analysis of mitochondrial function was performed using the fluorescent probe, TMRM. Two-dimensional gel electrophoresis followed by immunodetection was used to detect protein carbonylation in response to toxicant exposure. Carbonylated proteins were then identified using tandem mass spectrometry. The results of this study demonstrate that exposure to each toxicant resulted in a slightly conserved, yet different, pattern of carbonylated proteins. These data provides insight as to how exposure to different toxicants may lead to pathology through similar cellular targets, but how pathogenesis may occur through different molecular pathways.

Materials and Methods

Chemicals

Tissue culture media and materials were obtained from Gibco (Invitrogen, Carlsbad, CA). CellTiter 96 MTS assay solution was obtained from Promega (Madison, WI). The flurorescent probe, tetramethyl rhodamine methyl ester (TMRM), was obtained from Molecular Probes (Invitrogen Eugene, OR). The Oxyblot immunodetection kit was obtained from Chemicon (Millipore, Billerica, MA). Secondary antibodies for immunoblot visualization, 2D Clean-Up kits, and Destreak rehydration buffer were obtained from GE Healthcare (Piscataway, NJ). IPG Readystrips and 12% Tris-HCl Readygels were obtained from Bio-Rad

(Hercules, CA). BCA protein quantification reagents were obtained from Pierce (Thermo Scientific, Rockford, IL). PVDF membranes were purchased from Millipore (Billerica, MA). All other reagents were of analytical grade and were obtained from Sigma-Aldrich (St. Louis, MO).

Cell Culture

DITNC1 astrocytes, obtained from the American Type Culture Collection (ATCC), were maintained in a humidified incubator at 37°C in an atmosphere of 5% CO_2. Cells were grown in DMEM containing 4.5g/L D-glucose, L-glutamine, 10% fetal bovine serum, and 1% penicillin-streptomycin-glutamine mixture. Cells grown between passages 5 through 25 were used for all experiments.

MTS assay

The CellTiter 96 cell proliferation assay was used to measure concentration-dependent and time-dependent deficits in metabolic activity of DI TNC1 astrocytes exposed to concentrations of 1,3-DNB, 3-NPA, 2,4-DNP, and 3-CPD within 24 and 48 hr time periods. The CellTiter 96 solution contains a tetrazolium salt that is converted into formazan by cellular dehydrogenases within metabolically active cells. DI TNC1 cells were subcultured at a density of 5000 cells/well in a 96-well tissue culture plate. Cultures were allowed to proliferate for 24 hrs before addition of 1µM, 10µM, and 100µM concentrations of 1,3-DNB, 3-NPA, 2,4-DNP, and 3-CPD in DMEM containing 10% FBS and 1% PSG. After each 24 hr and 48 hr exposure period, the dosing media from each well was

removed and replaced with serum-free, phenol-free DMEM containing 20µL MTS/PMS solution/well. After 1.5 hrs of incubation, formazan production was measured at an absorbance of 490nm in a Gemini SpectraMax spectrophotometer (Molecular Devices, Sunnyvale, CA). Mean absorbance values from 4 independent experiments for each exposure group were graphed as percentages ± SEM of the DMSO control.

Laser Scanning Confocal Microscopy

Confocal microscopy was used to study the effect of 1,3-DNB, 3-NPA, 2,4-DNP, and 3-CPD on mitochondrial function. Cells were plated on 22 mm round, glass coverslips and treated with 1µM, 10µM, and 100µM of each chemical for 24 and 48 hrs, using 0.05% DMSO (v/v) as a vehicle control. Following each exposure, $\Delta\Psi_m$ was measured by incubating the cells in 20 mM HBSS/HEPES buffer containing 500 nM TMRM for 15 min at 37°C. To determine whether limiting oxidative stress could inhibit 1,3-DNB-induced loss of $\Delta\Psi_m$, cells were pretreated with 600 µM deferoxamine before incubation with each toxicant. After individual groups of treated cells were incubated in buffer solution containing each respective dye, the coverslips were placed in a heated stage for live-cell imaging analysis. Confocal analysis was conducted on using an Olympus Fluoview/FV300 combined with an inverted Olympus IX-70 microscope. The confocal microscope was equipped with a system of Argon and HeNe lasers (Melles Griot) with emission parameters for TMRM and MitoSox Red, each set at 543 nm. Images were obtained using an oil immersion 60X objective lens at an

exposure rate of 2.41s/scan in order to limit photobleaching of the dyes. About 2% of the maximum laser intensity was used for analyzing TMRM fluorescence. Mean fluorescence intensities from 3 or 4 independent experiments, ~7-10 cells per experiment, were measured using Adobe Photoshop and graphed using Microsoft Excel.

Mitochondrial Protein Sample Preparation

Cells were grown to >90% confluency in 75 cm^2 flasks and exposed to 100µM concentrations of 1,3-DNB, 3-NPA, 2,4-DNP, and 3-CPD for 48 hrs, using 0.1% DMSO as a vehicle control. After exposure, mitochondrial protein samples were isolated from each exposure group using a protocol based upon the MITOISO1 kit for soft tissue. Cells from 6 or 7 flasks per exposure group were homogenized in a teflon tissue grinder and glass pestle in 10 volumes of extraction buffer containing 2 mg/ml bovine serum albumin. The extraction buffer's composition consists of 220 mM mannitol, 70 mM sucrose, 0.5 mM EGTA, and 2 mM HEPES at a final pH of 7.4. The homogenate was transferred to a 15 ml conical tube and centrifuged at 500 x g for 5 minutes. The resulting supernatant was then removed, centrifuged at 11000 x g, and the pellet resuspended in extraction buffer. This step was repeated two more times in order to thoroughly wash the pellet. The mitochondrial protein pellet was resuspended in storage buffer containing 10 mM, HEPES, 250 mM sucrose, 1 mM ATP, 0.08 mM ADP, 5 mM sodium succinate, 2 mM K_2HPO_4, and 1mM DTT. A protease inhibitor cocktail was added to each sample before protein

concentrations were quantified or the samples placed in storage at -80°C. Protein concentrations were quantified using the BCA Protein Assay kit.

Two-dimensional (2D) gel electrophoresis

Aliquots of mitochondrial protein sample containing 70 µg of protein were prepared for SYPRO ruby staining and detection of protein carbonyls through Oxyblot analysis. Protein samples designated for Oxyblot analysis were derivatized for approximately 15 min at room temperature in a 1X DNPH solution provided for in an Oxyblot immunodetection kit. This reaction derivatizes carbonyl groups found on protein side chains to 2,4-dinitrophenylhydrazones that can be detected using Western blot analysis. Upon completion of the derivatization reaction, excess salts and other impurities were removed from each set of samples using a 2-D Clean-Up kit. Precipitates were incubated in wash buffer for at least an hour before centrifugation at 12,000 x g for 5 min. After the wash buffer was removed, 200 µl Destreak rehydration buffer containing 2.5 ul/ml IPG buffer (pH 3-10) was added to the protein pellet. A final centrifugation at 12,000 x g was required in order to remove any insoluble material that might hinder isoelectric focusing. Each sample was then added to a ReadyStrip IPG Strip 7 cm, pH 3-10. The IPG strips were actively rehydrated overnight in the IEF focusing tray of the Protean IEF cell using a current of 50 µA/IPG strip at 20°C. Isoelectric focusing was performed overnight at a voltage of 4000 V for a minimum of 20,000 Vh at 20°C. Before separation in the second dimension, the IPG strips were incubated at room temperature in equilibration

buffer for approximately 30 minutes. The equilibration buffer was comprised of 0.375 M Tris-HCl (pH 8.8) buffer containing 6 M urea, 2% SDS, 20% glycerol, and 2% (w/v) DTT. The IPG strips were then placed on ReadyGels 12% Tris-HCl in Mini-Protean III systems for electrophoresis. For the second dimension separation, the gels were run at a constant voltage of 100 V for approximately 1.45 h.

SYPRO Ruby staining

The gels were fixed in 50% methanol and 7% acetic acid twice, each for 30 min. Approximately 60 ml of SYPRO stain was added after the fixative was removed and the gels were stained overnight at room temperature. The gels were then washed in 10% methanol and 7% acetic acid and visualized in a Fujifilm FLA-5000 imaging system using Image Reader software.

Western Blot Analysis

Following separation in the second dimension, 2D gels designated for Oxyblot analysis were transferred to PVDF membranes. The nitrocellulose membranes were exposed to blocking buffer for 1 hour at room temperature and then incubated overnight at 4°C in rabbit primary antibody specific to 2,4-dinitrophenylhydrazone. An anti-rabbit, alkaline phophatase-labeled secondary, used for ECF-based immunodetection, was added following removal of the primary antibody and washing of the PVDF membranes. Images of carbonylated proteins were visualized using the Fujifilm FLA-5000 imaging system and Image

Reader software. Densitometry measurements were conducted using Multi Gauge V2.2.

Tandem Mass Spectrometry

LC/MS/MS analysis and protocol were provided by the Michigan Proteome Consortium (www.proteomeconsortium.org). Images of both the SYPRO Ruby stained 2D gels and 2D Oxyblots were overlaid on one another and carbonylated proteins were matched with protein spots from the 2D gels for excision followed by mass spectrometric analysis. Bovine serum albumin was used as a reference marker for protein samples were digested with trypsin using the MassPrep robot. Target peptides were extracted from the gel plugs with 30 µl of 2% acetonitrile 0.1% TFA. Five microliters of MALDI matrix was added to each extract and the extracts were dried using a Speed Vac. The peptides were dissolved in 5µl of 60% ACN 0.1% TFA. An aliquot of each sample was spotted onto a MALDI target for MS/MS analysis. Protein identification was accomplished by matching peptide sequences using the International Protein Index (IPI) database [REF).

Statistical Analysis

MTS reduction data was expressed as mean ±SEM % DMSO control and compared using a two-tailed Student's t-test, with $p < 0.05$ representing significance difference between treatment and control. Confocal microscopy data were expressed as the mean of the observed fluorescence intensity ±SEM.

Data from fluorescent images were compared using a two-tailed Student's t-test, with $p < 0.001$ representing a significant difference between the means.

Results

Concentration- and time-dependent analysis of metabolic activity in DI TNC1 astrocytes exposed to 1,3-DNB, 2,4-DNP, 3-NPA, and 3-CPD

Cellular metabolic activity was determined in DI TNC1 cells exposed to each toxicant for either 24 or 48 hours. During the 24 hr exposure period, 1mM concentrations of each toxicant caused significant deficits in MTS reduction, although signs of concentration-dependent loss in metabolic activity were observed in DI TNC1 cells exposed to lower concentrations of 1,3-DNB, 3-CPD, and 2,4-DNP (Figure 4.1 and Figure 4.2). Significant loss of metabolic activity in cells exposed to 2,4-DNP was initially observed in the 500 μM treatment group (~63% DMSO control). Interestingly, non-significant increases in metabolic activity occurred when DI TNC1 cells were exposed to 1μM, 100μM, and 500μM concentrations of 3-NPA, with a significant increase observed at 10μM concentration.

During the 48 hr exposure period, the patterns of metabolic activity in cells exposed to 1,3-DNB and 2,4-DNP remained similar to the trends observed during the 24 hr exposure period (Figure 4.3 and 4.4). Cells exposed to 1,3-DNB exhibited a concentration-dependent loss in metabolic activity. Cells exposed to 2,4-DNP experienced a slight, non-significant increase in metabolic activity

during exposure to 10μM and 100μM 2,4-DNP, only to result in significant loss of metabolic activity during exposure to 500μM and 1mM 2,4-DNP (~59% and 58% DMSO control, respectively). Although a concentration-dependent trend was not observed, some loss in metabolic activity occurred in DI TNC1 cells exposed to 10μM and 500μM 3-NPA with the first sign of significant loss occurring during the 1mM exposure (~78% DMSO control). Cells exposed to 3-CPD for 48 hours exhibited no change in metabolic activity.

Concentration- and time-dependent analysis of mitochondrial function in DI TNC1 astrocytes exposed to 1,3-DNB, 2,4-DNP, 3-NPA, and 3-CPD

Maintenance of the $\Delta\Psi_m$ in DI TNC1 astrocytes exposed to 1,3-DNB, 2,4-DNP, 3-NPA, and 3-CPD over 24 or 48 hour periods was assessed with the fluorescent dye, TMRM. Previous research demonstrated that DI TNC1 astrocytes are susceptible to time-dependent loss of $\Delta\Psi_m$ upon exposure to 1mM 1,3-DNB, with significant loss of $\Delta\Psi_m$ first occurring at 5hrs followed by almost complete loss of $\Delta\Psi_m$ at the end of a 24-hour exposure period. In order to study concentration-based thresholds of mitochondrial toxicity using lower toxicant concentrations, the concentration/time regimen applied in this portion of the analysis demonstrated an inability to induce statistically significant metabolic deficits (i.e. MTS reductive capability) and changes in cellular morphology (unpublished data). After 24- and 48-hours, exposure to 1μM, 10μM, and 100μM of each toxicant resulted in a concentration-dependent decrease of TMRM fluorescence (Figure 4.5 and Figure 4.8). Exposure to the DMSO vehicle control

alone had no effect on TMRM fluorescence. Partial loss of TMRM fluorescence occurred for treatment groups during the 24- and 48-hour exposure periods and each concentration-dependent decrease was statistically significant when compared to the DMSO control (Figure 4.7 and Figure 4.10). Pretreatment with 600μM deferoxamine before commencement of the 24 hr exposure period prevented significant concentration-dependent loss of $\Delta\Psi_m$ in DI TNC1 cells exposed to 2,4-DNP and 3-CPD (Figure 4.6). Although cells pretreated with deferoxamine prior to 1,3-DNB and 3-NPA still demonstrated significant concentration-dependent deficits, TMRM fluorescence intensity was higher than in cells not pretreated with the antioxidant indicating some degree of protection. Pretreatment with 600μM deferoxamine did not prevent significant concentration-dependent loss of TMRM fluorescence in any of the 48-hour exposure groups, except in cells exposed to 10μM 3-NPA (Figure 4.9). However, pretreatment with deferoxamine once again conveyed some protection in that TMRM fluorescence intensity was higher than in the cells exposed to the toxicants alone (Figure 4.10).

Closer inspection of the confocal images used to measure TMRM fluorescence revealed that exposure to 1,3-DNB, 2,4-DNP, 3-NPA, and 3-CPD lead to changes in mitochondrial morphology in addition to decreases in $\Delta\Psi_m$ (Figure 4.15). In the images of DI TNC1 astrocytes exposed to the DMSO control, mitochondria appeared as fibrillar, torpedo-shaped structures dispersed throughout the cytoplasm and surrounding the nucleus. Cells exposed to the toxicants presented mitochondria that appeared more compact. This

morphological effect was apparent in many cells visualized within the image area, indicating that this was likely not an effect localized in one or two cells. In several instances, TMRM fluorescence revealed that compacted mitochondria appeared to fluoresce just as brightly as normal, fibrillar-shaped mitochondria. Morphological analysis was performed only on a qualitative basis of observation and not through any form of quantitation.

Immunodetection and tandem mass spectrometric detection of protein carbonyls in DI TNC1 astrocytes exposed to 1,3-DNB, 2,4-DNP, 3-NPA and 3-CPD

Confocal microscopic analysis revealed that exposure to 1,3-DNB, 2,4-DNP, 3-NPA, and 3-CPD over 24 and 48 hours resulted in concentration-dependent loss of the $\Delta\Psi_m$. Previous research demonstrated that 1mM 1,3-DNB-induced oxidative stress resulted in protein carbonylation of specific DI TNC1 astrocyte proteins within the first hour of exposure, prior to loss of $\Delta\Psi_m$. This suggests that 1,3-DNB exposure may lead to mitochondrial dysfunction and subsequent toxicity through a molecular pathway mediated by the oxidation of specific proteins. If the 1,3-DNB-induced carbonylated protein fingerprint is unique to 1,3-DNB neurotoxicity, then exposure to each metabolic toxicant used in this study should result in a different pattern of protein carbonylation. 2D Oxyblot analysis followed by tandem mass spectrometry was used to identify targets of protein carbonylation in treated DI TNC1 astrocytes. The concentration and exposure period selected for each treatment group was 100μM of each toxicant for 48 hours since exposure to these particular

concentrations/time periods resulted in perturbation of mitochondrial function without complete loss of the $\Delta\Psi_m$ and no significant disruption in metabolic capacity.

2D Oxyblot analysis revealed that several proteins were sensitive to 1,3-DNB, 3-NPA, and 3-CPD-induced carbonylation after 48 hours of exposure as indicated by an intense pattern of immunoreactivity (Figure 4.11). In addition, Oxyblot analysis for each treatment group revealed that not all proteins within a 2D gel exhibit carbonyl immunoreactivity. The 2D gels used to separate protein samples from DI TNC1 cells treated with 2,4-DNP developed an anomalous streaking pattern across the gel, rendering subsequent Oxyblot analysis for individual proteins impossible. Carbonylation intensity is less in 2D Oxyblots derived using mitochondrial protein isolated from cells exposed only to the DMSO control. The selectivity of proteins that appear to be targets of 1,3-DNB, 3-NPA, and 3-CPD-induced carbonylation are consistent throughout each treatment group. The carbonylation patterns that resulted from exposure to each toxicant were similar to each other in terms of the region within which carbonylated proteins migrated. Most of the carbonylated proteins appeared within a PI range of approximately 4-7 and a mass range of 50-70 kDa. However, there were differences in the number of carbonylated proteins identified within each separate treatment. LC/MS/MS analysis revealed that the proteins identified during 3-CPD exposure (calreticulin precursor, vimentin, actin, and the serum albumin marker) were carbonylated in all three treatment groups (Figure 4.13). Carbonylated proteins identified in the 1,3-DNB exposure group

also included F1-ATP synthase beta-subunit and protein disulfide isomerase (Figure 4.12). Carbonylated proteins identified in the 3-NPA exposure group also included F1-ATP synthase beta-subunit, Grp78 glucose-regulated protein, tumor rejection antigen gp96, protein disulfide isomerase, and a member of the pumilio-family RNA binding domains, D19Bwg1357e (Figure 4.14). Each peptide sequence was matched using the Mascot search engine and the IPI database. The total ion scores represent proteins identified with greater than 95% confidence and the predicted mass values of each protein are in agreement with the observed position in each 2D gel.

Discussion

This study demonstrates that 1,3-DNB induces a pattern of oxidative carbonylation in DI TNC1 astrocytes that bears some similarity to the protein carbonylation that occurs in cells exposed to other metabolic/mitochondrial toxicants. DI TNC1 astrocytes exposed to 1,3-DNB, 2,4-DNP, 3-NPA, and 3-CPD exhibit concentration- dependent decreases in metabolic activity over 24 and 48 hour exposure periods. Cells exposed to each of these toxicants at concentrations below the levels that induced metabolic deficits exhibited concentration-dependent decreases in TMRM fluorescence, signifying partial loss of $\Delta\Psi_m$, during exposure periods of 24 and 48 hours. Deferoxamine pretreatment was effective at preventing significant loss of TMRM fluorescence in DI TNC1 cells exposed to 2,4-DNP and 3-CPD for 24 hours and partially, though

not significantly, effective at preventing decreases in fluorescence intensity in the other treatment groups. Protein carbonylation in DI TNC1 astrocytes exposed to 100μM of 1,3-DNB, 3-NPA, and 3-CPD for 48 hours coincided with partial loss of $\Delta\Psi_m$. Exposure to 1,3-DNB, 3-NPA, and 3-CPD resulted in a conserved pattern of protein carbonylation, suggesting that some proteins are inherently susceptible to certain types of oxidative modification regardless of the toxic insult. However, additional proteins carbonylated during exposure to 1,3-DNB and 3-NPA suggest that downstream mitochondrial dysfunction and cellular toxicity may develop through alternative, specific molecular pathways mediated by oxidative stress. Whether or not changes in the oxidation status of individual proteins dictate mitochondrial and metabolic dysfunction remains to be determined. These findings provide evidence supporting the notion that although chemical-induced toxicity may share a common cellular mechanism, cellular pathology is ultimately dependent upon key changes occurring at the molecular level, such as within the molecular structure of a protein.

The MTS reduction analysis indicated that DI TNC1 astrocytes are susceptible to concentration-dependent metabolic perturbation after a 24 hours of exposure to 1,3-DNB, 2,4-DNP, 3-NPA, and 3-CPD. Similar concentration-dependent decreases in metabolic activity were observed during the 48 hour exposure period. However, exposure to increasing concentrations of 3-CPD for 48 hours did not result in any loss of metabolic activity. Additionally, during the 24 hour period, cells exposed to 3-NPA lead to both significant and non-significant increases in metabolic activity prior to experiencing a drop in MTS

reduction at the 1mM concentration. In a study performed by Stair *et. al* 2005, cultured primary Type 1 astrocytes from F344 rats experienced similar increases in cellular metabolic activity upon exposure to 1,3-DNB [18]. It is possible that increased metabolic activity observed in both the DI TNC1 astrocytes and cultured astrocytes denote compensatory increases in metabolic output, in a cellular response stimulated by toxicant exposure. This is supported by previous research showing that metabolic activity increases in brain regions susceptible to 1,3-DNB as indicated by time-dependent increases in glucose consumption and lactate production [4].

Interestingly, the present study demonstrated that although metabolic activity in DI TNC1 astrocytes was disrupted upon exposure to higher concentrations of each toxicant, mitochondrial perturbation was induced using lower concentrations of each toxicant. 1,3-DNB, 2,4-DNP, 3-NPA, and 3-CPD were all capable of inducing significant loss of TMRM fluorescence in a concentration-dependent manner during 24 and 48 hour exposure periods. During the 24 hour exposure to 2,4-DNP and 3-CPD, deferoxamine pretreatment was successful in preventing significant loss of $\Delta\Psi_m$, even though antioxidant pretreatment was only moderately effective in the remaining the treatment groups. During the 48 hour treatment, deferoxamine pretreatment was partially effective at preventing loss of TMRM fluorescence, but significant loss of $\Delta\Psi_m$ still occurred. This data suggests that, at least during the 24 hour exposure, 2,4-DNP and 3-CPD-induced mitochondrial dysfunction can be attenuated with the use of certain antioxidants. Previous research described in Chapter II

demonstrated that antioxidant pretreatment was capable of delaying significant loss of the $\Delta\Psi_m$ in DI TNC1 astrocytes exposed to 1mM 1,3-DNB within a 24 hour period. However, it was also demonstrated that the cytoprotective effect of each antioxidant diminished by the end of the 24 hour exposure, represented by almost complete mitochondrial depolarization. Both the previously reported and current data suggest that antioxidant use attenuates the impact 1,3-DNB-induced oxidative stress has on mitochondrial function, but also that the cytoprotective effect of antioxidants diminishes over time. Once antioxidants are no longer effective in the presence of an oxidizing toxic insult, cellular defense mechanisms are overrun and oxidative damage of proteins ensues. It is possible that pretreating cells with deferoxamine will only provide sufficient protection against oxidative stress up to 24 hours after the initial toxicant exposure, and that by 48 hours, the cytoprotective effect mediated by deferoxamine has completely diminished.

The results presented in this study are the first to compare the 1,3-DNB-induced pattern of oxidative carbonylation with patterns of protein carbonylation resulting from exposure to other metabolic toxicants. The purpose of this study was to demonstrate whether or not exposure to different mitochondrial/metabolic toxicants, implicated as disruptors of redox status, lead to disturbances in cellular and mitochondrial function that develop through similar molecular pathways mediated by the oxidative modification of specific proteins. DI TNC1 astrocytes exposed to 1,3-DNB, 3-NPA, and 3-CPD resulted in the carbonylation of specific proteins. Certain proteins were identified as common targets of oxidative

carbonylation in each group of cells exposed to each toxicant. Calreticulin, vimentin, actin, and serum albumin were identified exclusively within the 3-CPD treatment group, but were also found among the carbonylation patterns induced by 1,3-DNB and 3-NPA. All four proteins are known to be substrates of oxidative carbonylation resulting from oxidations occurring in various pathology including Alzheimer's disease, metal-catalyzed oxidation, age-associated oxidation, and experimental autoimmune encephalomyelitis [19, 20, 21, 22]. This suggests that although these proteins are carbonylated as a result of toxicant exposure in this study, an as of yet unidentified characteristic about individual peptide structure bestows upon each protein an inherent level of shared susceptibility to oxidative carbonylation during various kinds of oxidative pathogenesis. The same can be said of each additional protein carbonylated during exposure to 1,3-DNB and 3-NPA (i.e. the F1-ATP synthase beta-subunit and protein disulfide isomerase). Exposure to 3-NPA also resulted in carbonylation of Grp78, tumor rejection antigen gp 96, and D19Bwg1357e. Although it is unknown as to whether or not specific patterns of oxidative modification dictate downstream pathology, this data offers an intriguing possibility in that specific carbonylated proteins identified during exposure to a certain toxicant may hold the key to understanding specific molecular mechanisms of cellular pathology.

All of the carbonylated proteins, with the exception of D19Bwg1357e, identified in this study were identified in a previous analysis of DNB-induced protein carbonylation described in Chapter III. The key difference between these two studies is that cellular exposure to 100μM 1,3-DNB for 48 hrs did not result in

the same number of proteins carbonylated as did DI TNC1 cells exposed to 1mM 1,3-DNB for 45 min. Protein carbonylation is an irreversible form of protein modification, so during a 48-hour exposure period, there exists the possibility that some oxidized targets of 1,3-DNB-induced carbonylation may have undergone proteolytic degradation [5,6]. Although the cellular mechanisms defining when proteolytic degradation occurs during 1,3-DNB exposure are unknown, exposure to low concentrations of 1,3-DNB over a long period of time may promote increased carbonylation among the most susceptible proteins along with increased protein degradation and disposal as opposed to an intense burst of ROS production induced by exposure to high concentrations of 1,3-DNB over a short period of time.

A particularly interesting observation made during the course of this study was how exposure to each metabolic toxicant resulted not only in partial depolarization of the inner mitochondrial membrane, but also rather dramatic morphological changes in mitochondrial shape. Mitochondria exposed to the DMSO control retained a normal, fibrillar shape which contrasted sharply when compared to the more compact mitochondria present after exposure to each toxicant. These morphological changes suggest that exposure to 1,3-DNB, 2,4-DNP, 3-NPA, and 3-CPD cause DI TNC1 mitochondria to undergo changes in aspect ratio, possibly through a common molecular mechanism. It is unknown whether such changes in mitochondrial shape precede or result from deficits in ATP production. Previous studies demonstrate that mitochondria are susceptible to structural events, such as fission, that develop as a part of a pathological

mechanism [23, 24]. Methodology for analyzing changes in mitochondrial architecture, such as measuring aspect ratio, counting number of misshapen mitochondria, and calculating $\Delta\Psi_m$ using TMRM are well-known [25], but were not applied to the current study. An additional dilemma that arises from an attempted evaluation of mitochondrial morphology during this analysis is that mitochondria are actually three-dimensional objects. Confocal microscopy, as it was applied for this study, was suitable for measuring loss of TMRM fluorescence, but not for a thorough analysis of three-dimensional morphological changes based upon the capture of two-dimensional images. It is tempting to suggest that carbonylation of key proteins lead to the changes in mitochondrial morphology observed in this study, even though a molecular basis for this event is yet undetermined. Future experimentation aimed at linking protein carbonylation with changes in mitochondrial morphology, using the appropriate methods, would help in determining if any connection truly exists.

In summary, this study provides important new insights into how protein carbonylation may mediate the neurotoxicity of 1,3-DNB and other metabolic toxicants that target mitochondrial function. Several reports confirm the presence of oxidized proteins during the development of various neuropathologic mechanisms, however this report is the first to demonstrate the similarities and differences between macromolecular targets of oxidative carbonylation among chemical-induced toxicity. Future studies will need to address the role of these individual proteins in promoting metabolic dysfunction in susceptible astrocyte

populations following exposure to chemicals that induce acute energy deprivation syndromes.

Acknowledgments

This research was supported by grants from the NIEHS (NIH T32-ES07062) and the NIH (RO1-ES08846). We would like to thank Jen Fernandez, Brad Martin, Evan Milton, and the members of the Michigan Proteomics Consortium for their assistance during the course of this study.

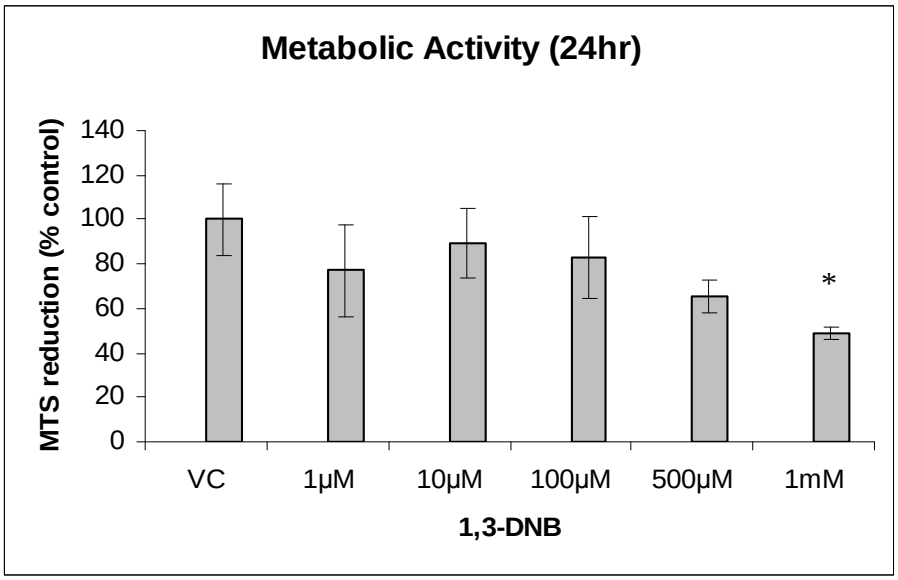

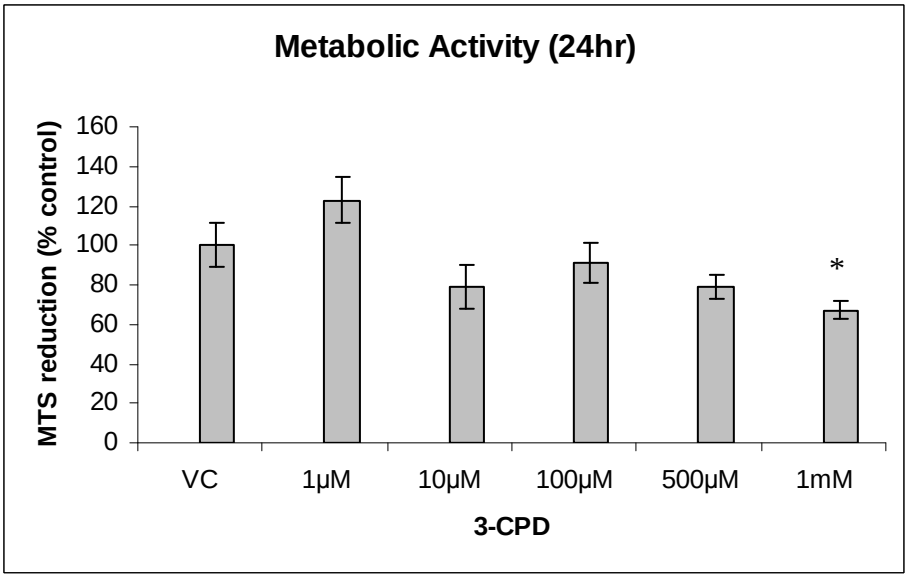

Figure 4.1. Concentration-dependent decrease in MTS reductive capability of DI TNC1 astrocytes exposed to 1,3-DNB or 3-CPD over 24 hour period. Data is expressed as % DMSO control ± SEM (n= 4) with statistical significance (*****) if $p < 0.05$.

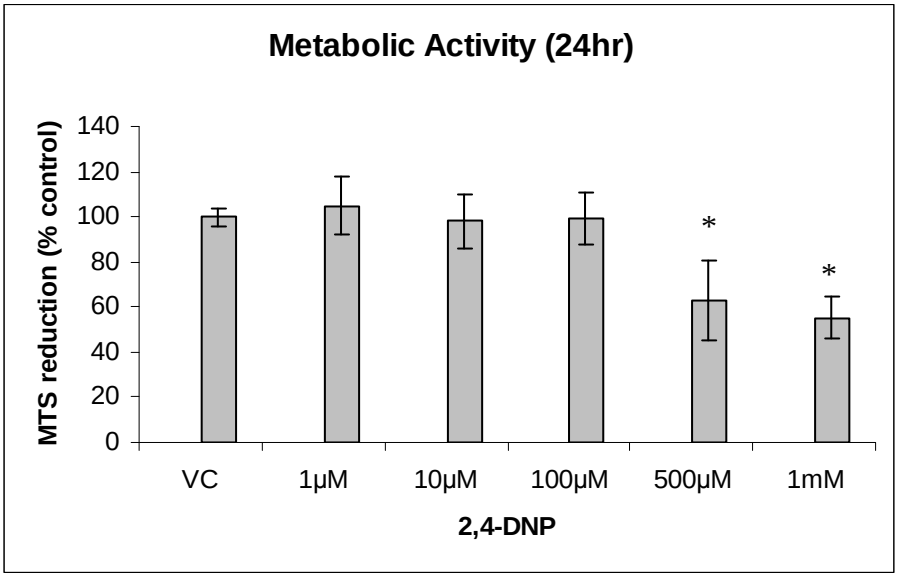

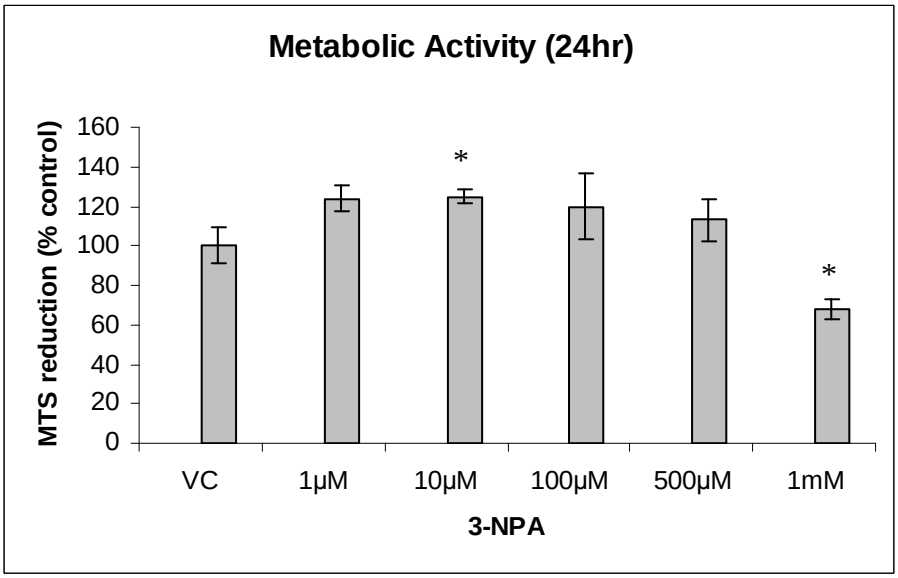

Figure 4.2. Concentration-dependent decrease in MTS reductive capability of DI TNC1 astrocytes exposed to 2,4-DNP or 3-NPA over 24 hour period. Data is expressed as % DMSO control ± SEM (n=4) with statistical significance (*****) if $p < 0.05$.

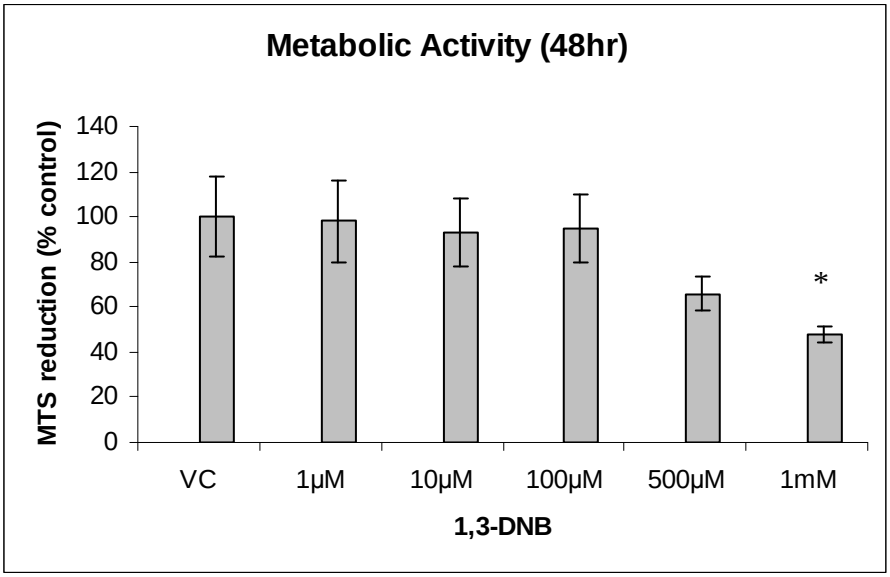

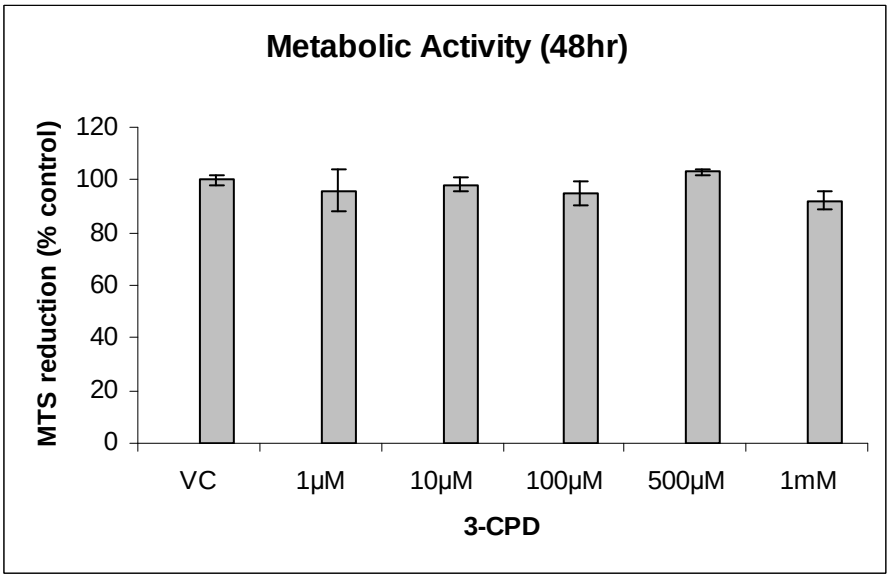

Figure 4.3. Concentration-dependent decrease in MTS reductive capability of DI TNC1 astrocytes exposed to 1,3-DNB or 3-CPD over 48 hour period. Data is expressed as % DMSO control ± SEM (n=4) with statistical significance (*****) if $p < 0.05$.

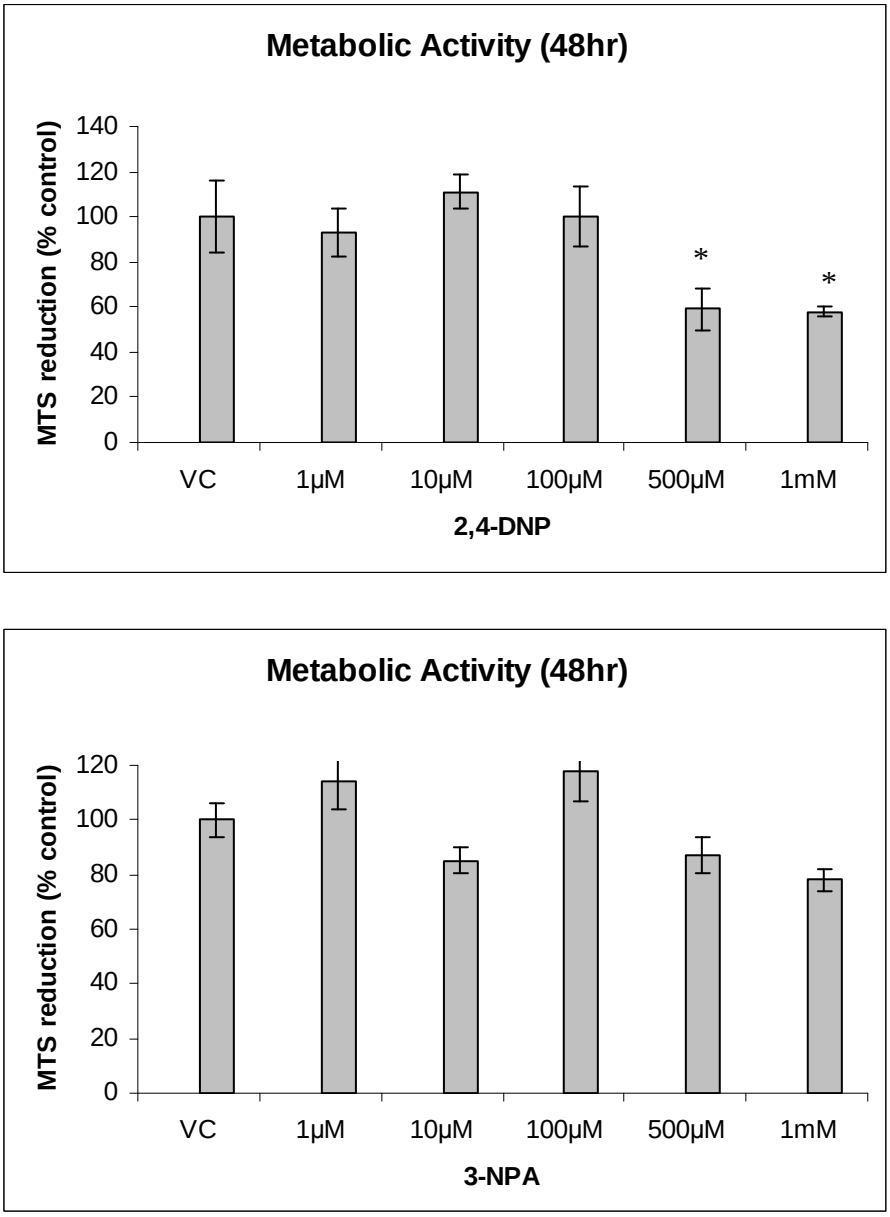

Figure 4.4. Concentration-dependent decrease in MTS reductive capability of DI TNC1 astrocytes exposed to 2,4-DNP or 3-NPA over 48 hour period. Data is expressed as % DMSO control ± SEM (n=4) with statistical significance (*****) if $p < 0.05$.

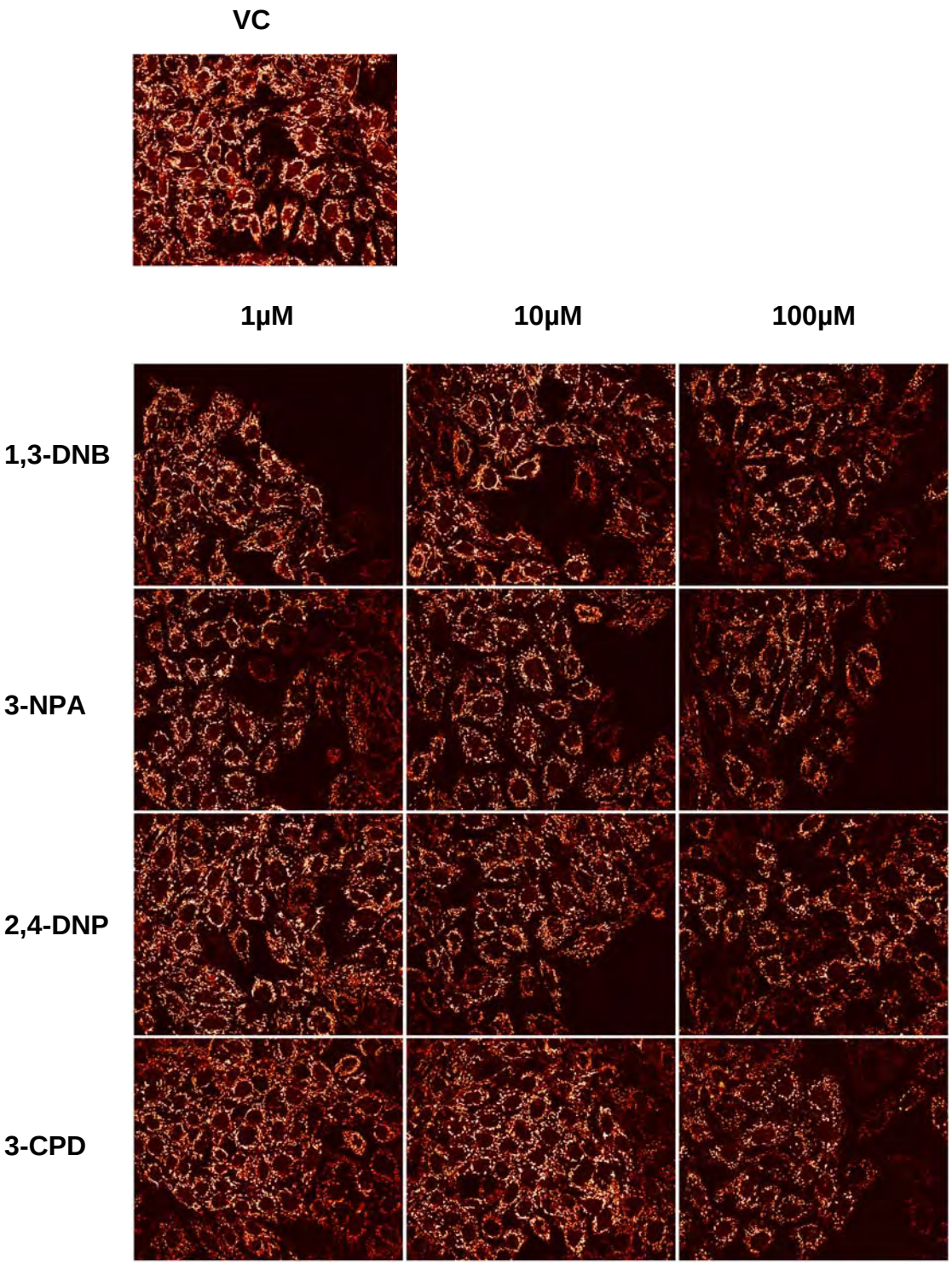

Figure 4.5. Concentration-dependent loss of $\Delta\Psi_m$ in DI TNC1 astrocytes measured over a 24-hour period using confocal microscopy. DI TNC1 cells were loaded with TMRM for 15 minutes after exposure to DMSO vehicle control, 100µM 1,3-DNB, 100µM 3-NPA, 100µM 2,4-DNP, or 100µM 3-CPD.

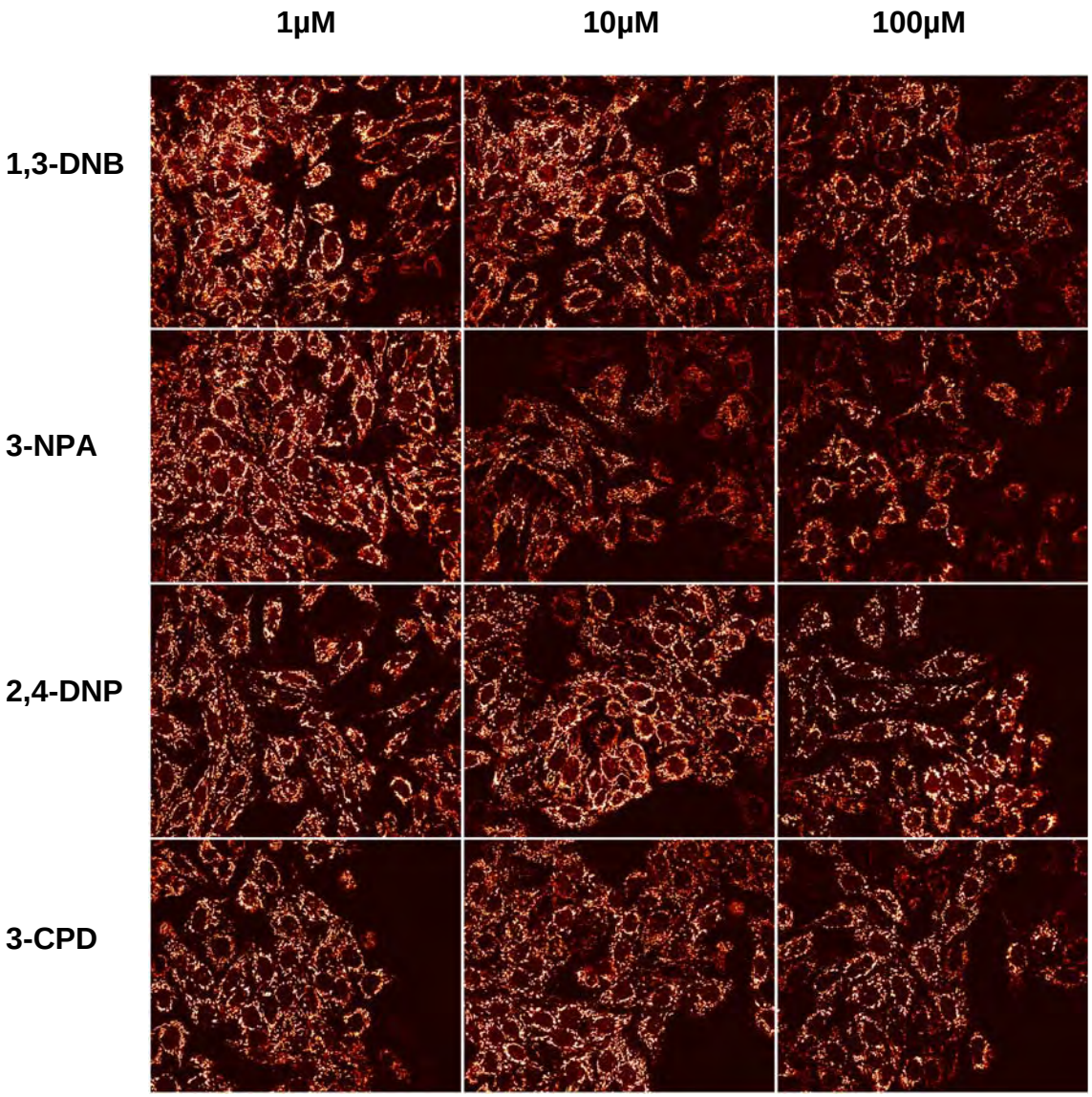

Figure 4.6. Concentration-dependent loss of $\Delta\Psi_m$ in DI TNC1 astrocytes pretreated with 600µM deferoxamine measured over a 24-hour period using confocal microscopy. DI TNC1 cells were loaded with TMRM for 15 minutes after exposure to 100µM 1,3-DNB, 100µM 3-NPA, 100µM 2,4-DNP, or 100µM 3-CPD.

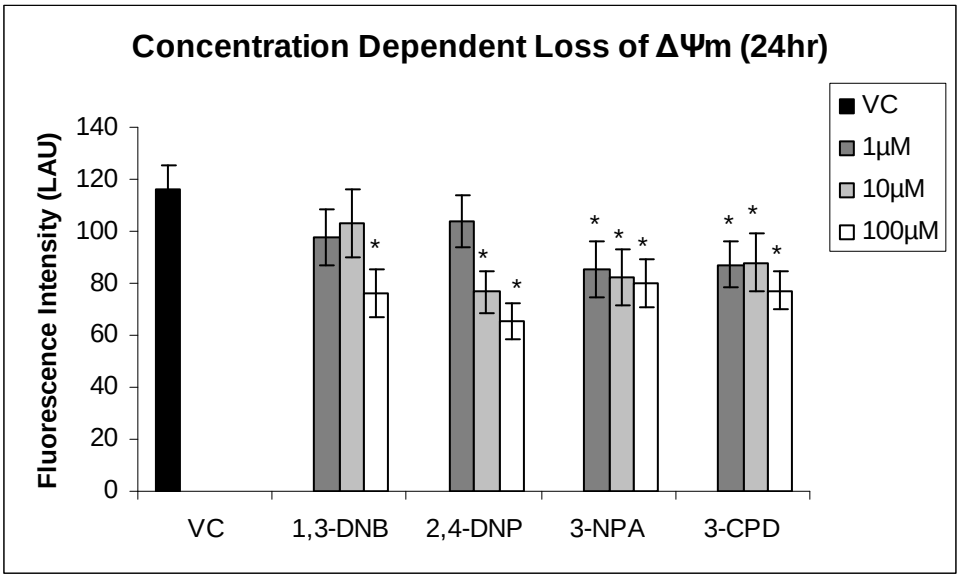

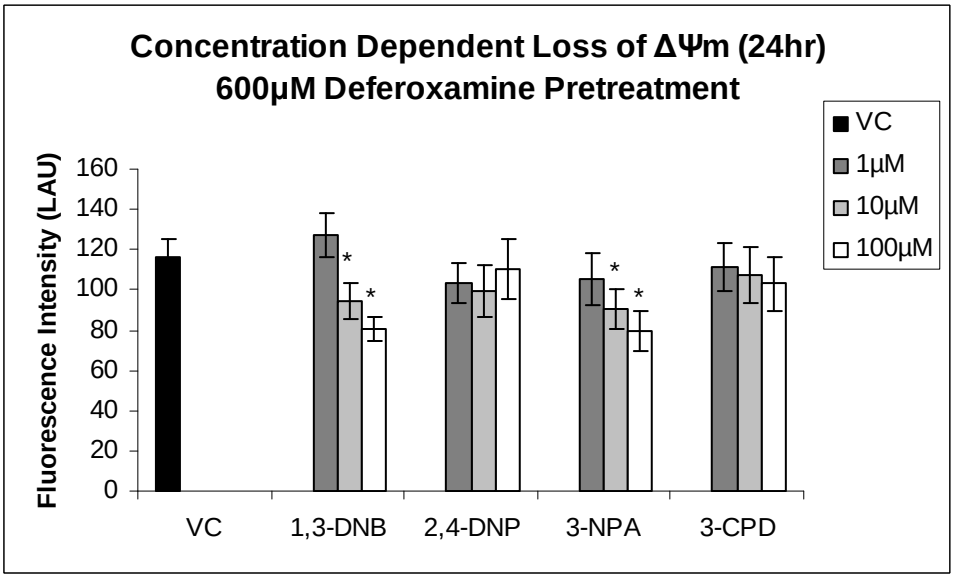

Figure 4.7. Changes in TMRM fluorescence were measured and graphed as linear arbitrary units (LAU) in 3-4 independent experiments (7-10 cells per experiment). Values are expressed as mean ± SEM with statistical significance if $p < 0.001$ when compared to DMSO vehicle controls (*****).

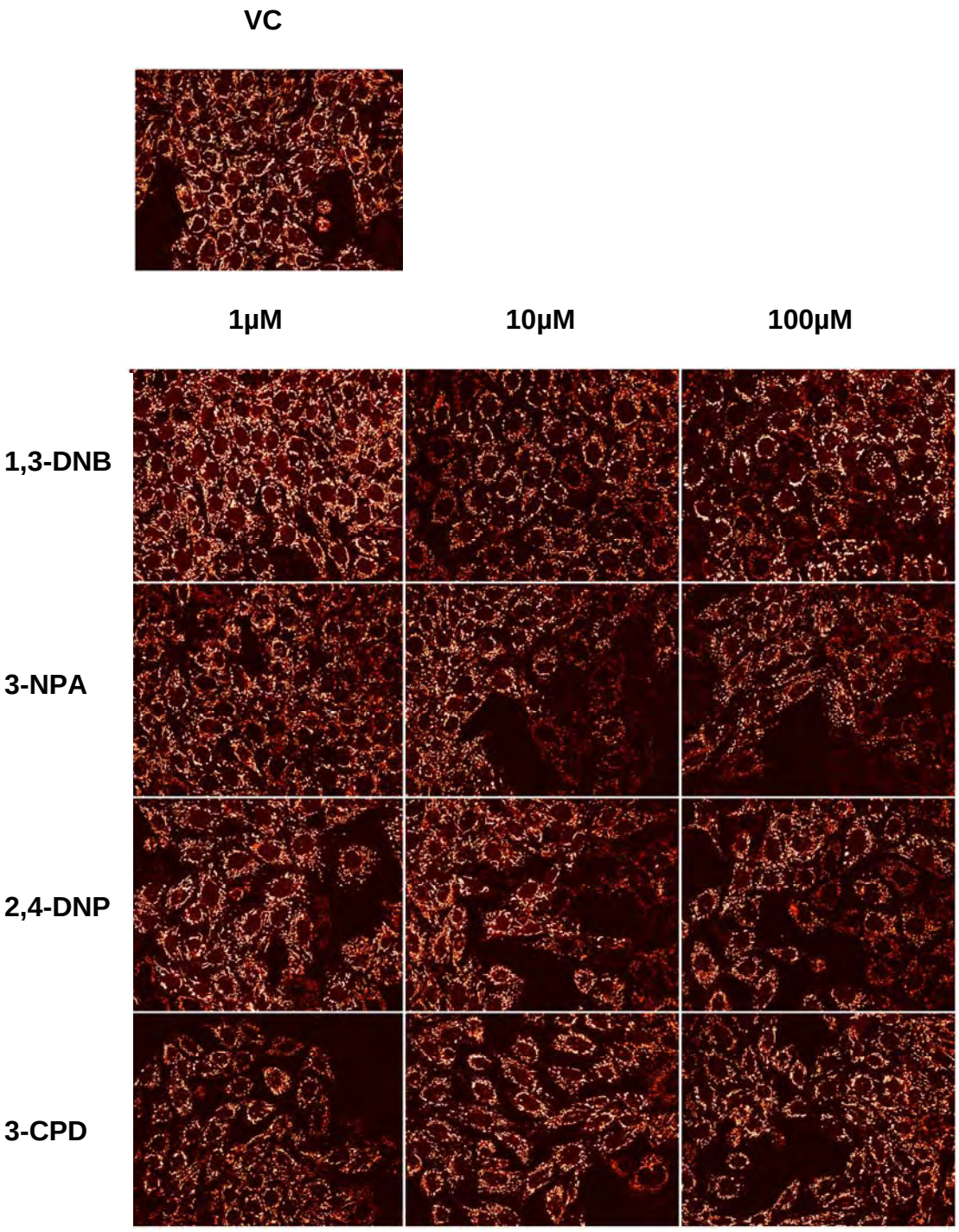

Figure 4.8. Concentration-dependent loss of $\Delta\Psi_m$ in DI TNC1 astrocytes measured over a 48-hour period using confocal microscopy. DI TNC1 cells were loaded with TMRM for 15 minutes after exposure to DMSO vehicle control, 100μM 1,3-DNB, 100μM 3-NPA, 100μM 2,4-DNP, or 100μM 3-CPD.

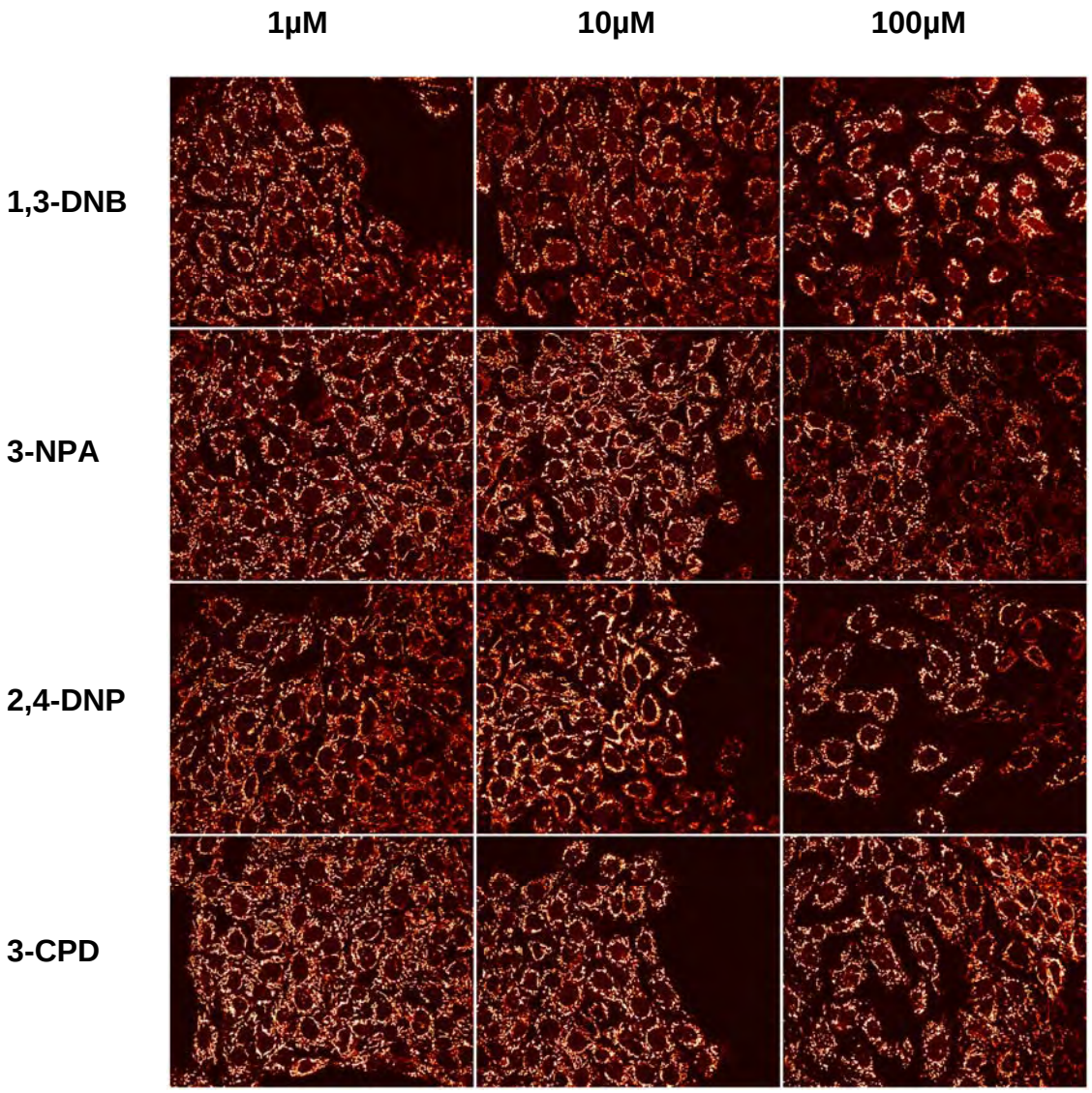

Figure 4.9. Concentration-dependent loss of $\Delta\Psi_m$ in DI TNC1 astrocytes pretreated with 600µM deferoxamine measured over a 48-hour period using confocal microscopy. DI TNC1 cells were loaded with TMRM for 15 minutes after exposure to 100µM 1,3-DNB, 100µM 3-NPA, 100µM 2,4-DNP, or 100µM 3-CPD.

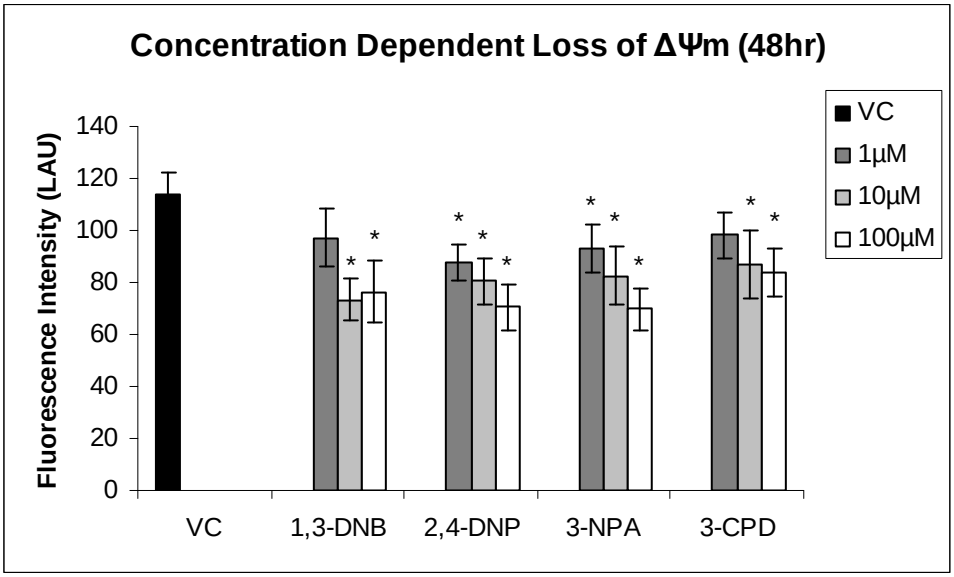

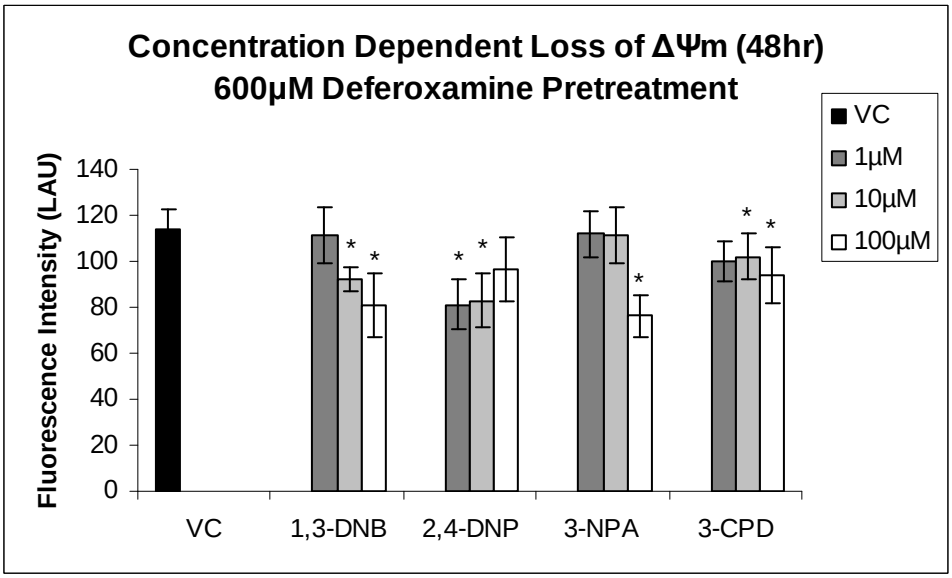

Figure 4.10. Changes in TMRM fluorescence were measured and graphed as linear arbitrary units (LAU) in 3-4 independent experiments (7-10 cells per experiment). Values are expressed as mean ± SEM with statistical significance if $p < 0.001$ when compared to DMSO vehicle controls (*****).

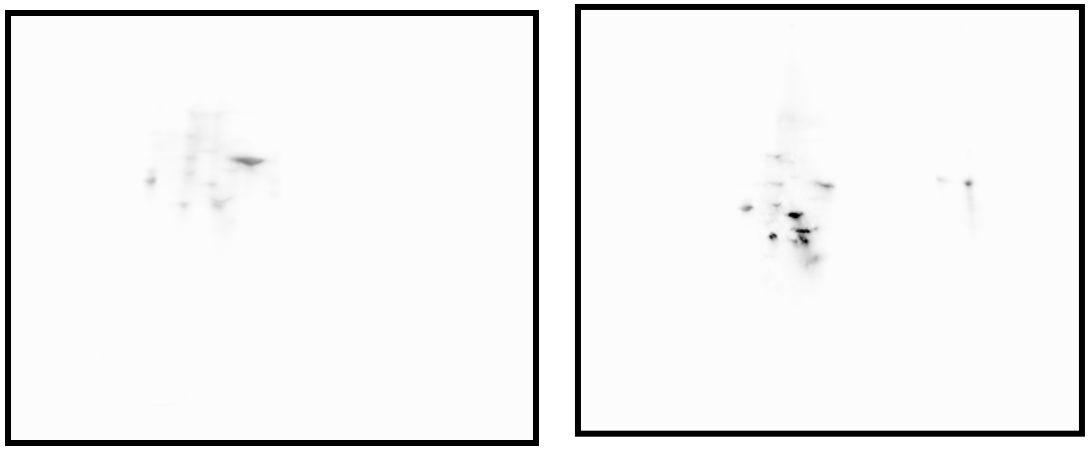

VC (DMSO) **100µM 3-NPA**

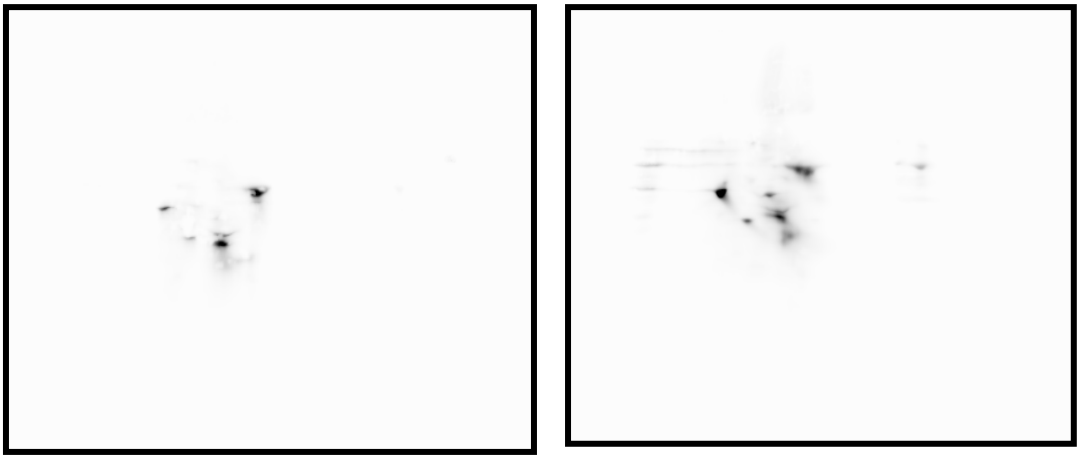

100µM 3-CPD **100µM 1,3-DNB**

Figure 4.11. Two-dimensional Oxyblot analysis of mitochondrial protein isolated from DI TNC1 astrocytes exposed to 100µM 1,3-DNB, 100µM 3-NPA, or 100µM 3-CPD for 48 hours.

Figure 4.12. Tandem mass spectrometric analysis of carbonylated mitochondrial proteins isolated from DI TNC1 astrocytes after exposure to 100µM 1,3-DNB for 48 hours. Serum albumin (2 mg/ml) was added to the protein isolation in order to remove excess lipids from the isolate and act as a reference protein marker. Images of 2D Oxyblots were overlaid on corresponding 2D gel images stained with either SYPRO Ruby or Coomassie Blue. Carbonylated proteins were spot-picked from the 2D gel and identified using LC/MS/MS at the Michigan Proteome Consortium.

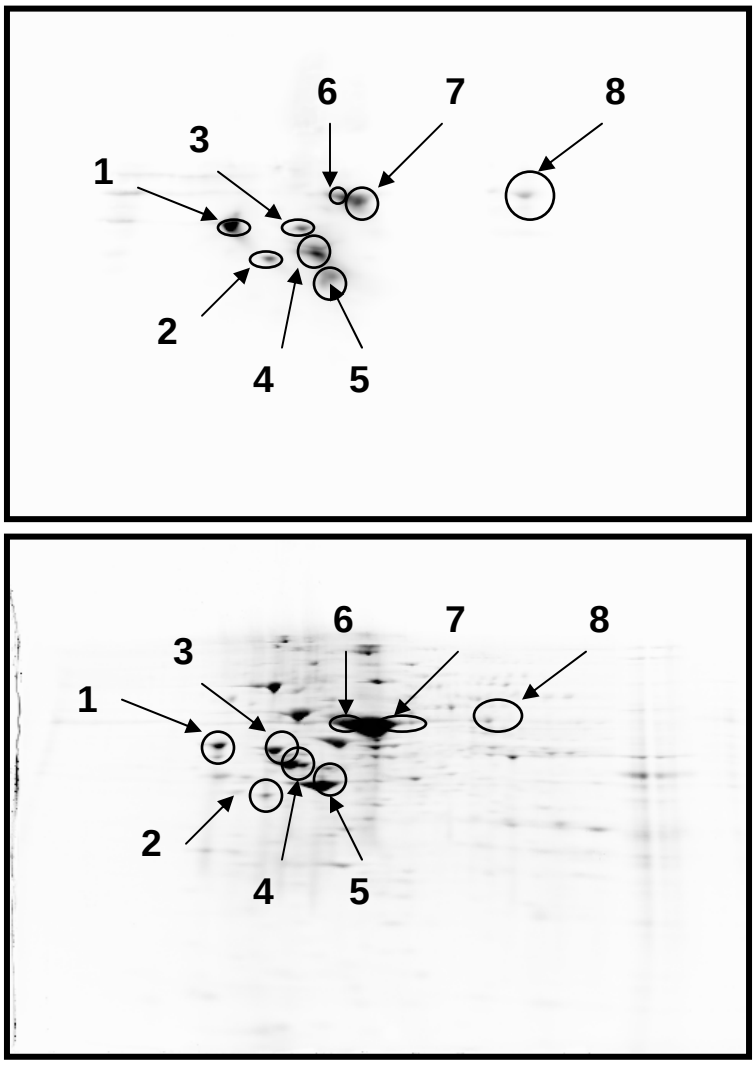

Spot Label	Protein Name
1	Calreticulin precursor
2	Vimentin
3	Protein disulfide isomerase precursor
4	F1 ATP synthase beta-subunit, mitochondrial precursor
5	Actin, cytoplasmic 2
6	Serum albumin precursor
7	Serum albumin precursor
8	Low abundance peak

Figure 4.13. Tandem mass spectrometric analysis of carbonylated mitochondrial proteins isolated from DI TNC1 astrocytes after exposure to 100µM 3-CPD for 48 hours.

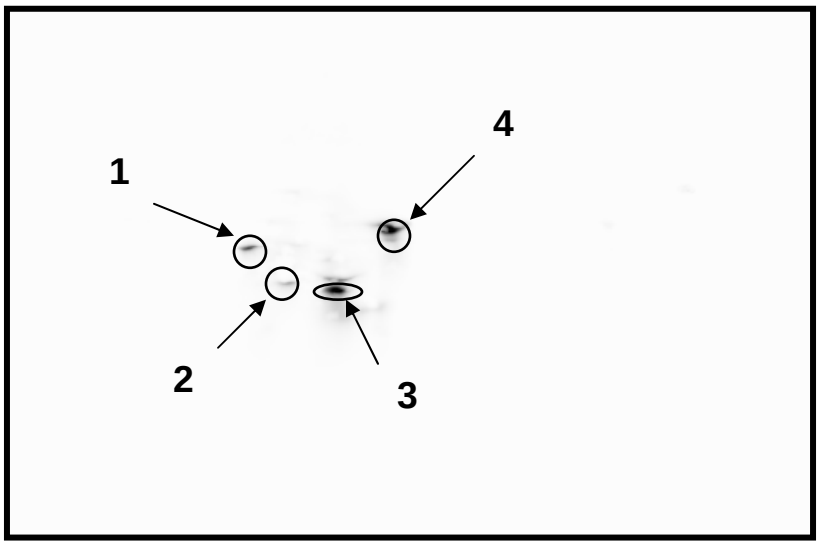

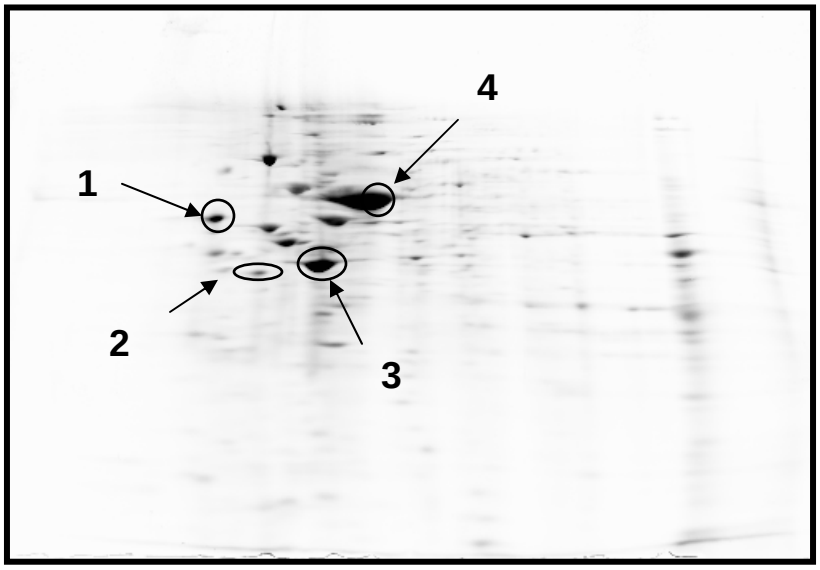

Spot Label	Protein Name
1	Calreticulin precursor
2	Vimentin
3	Actin, cytoplasmic 2
4	Serum albumin precursor

Figure 4.14. Tandem mass spectrometric analysis of carbonylated mitochondrial proteins isolated from DI TNC1 astrocytes after exposure to 100μM 3-NPA for 48 hours.

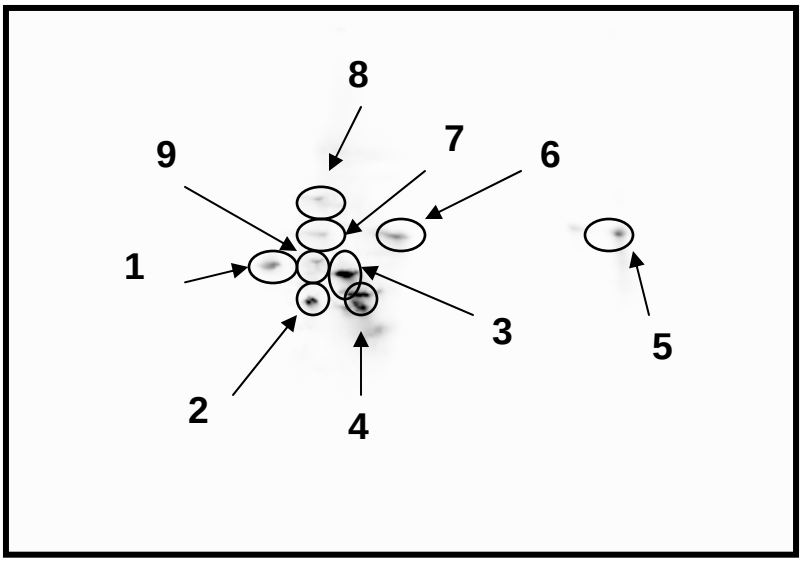

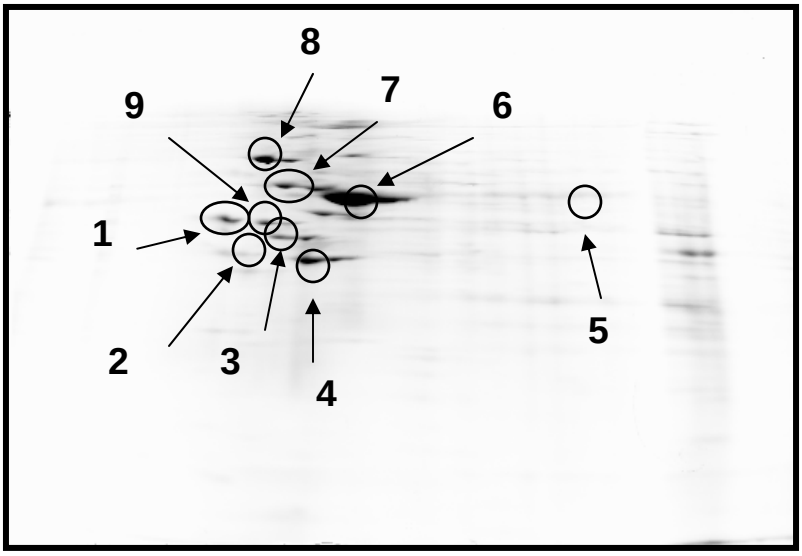

Spot Label	Protein Name
1	Calreticulin precursor
2	Vimentin
3	F1 ATP synthase beta subunit, mitochondrial precursor
4	Actin, cytoplasmic 2
5	D19Bwg1357e protein
6	Serum albumin precursor
7	Grp78 kDa glucose-regulated protein precursor
8	Tumor rejection antigen gp96
9	Protein disulfide-isomerase, A3 precursor

Figure 4.15. Fluorescent images of DI TNC1 astrocytes demonstrating changes in mitochondrial morphology. DI TNC1 cells were incubated with TMRM for 15 minutes after exposure to A) DMSO vehicle control B) 100µM 1,3-DNB C) 600 µM deferoxamine pretreatment prior to 100µM 1,3-DNB.

A)

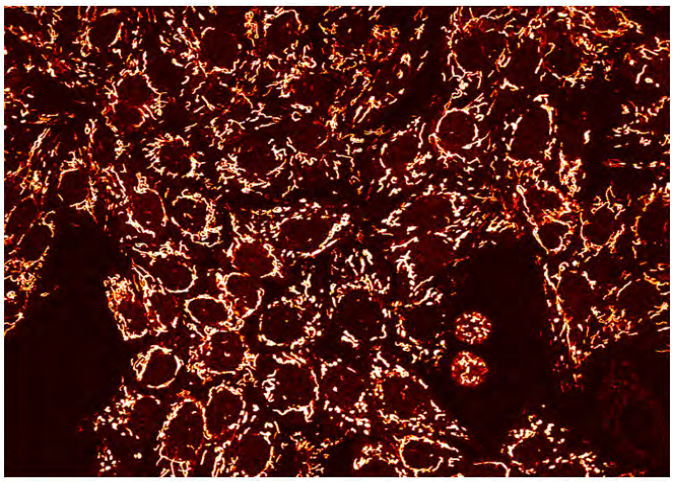

B)

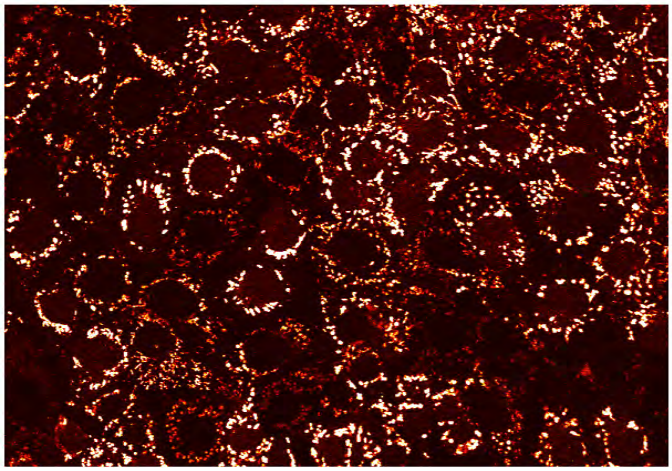

C)

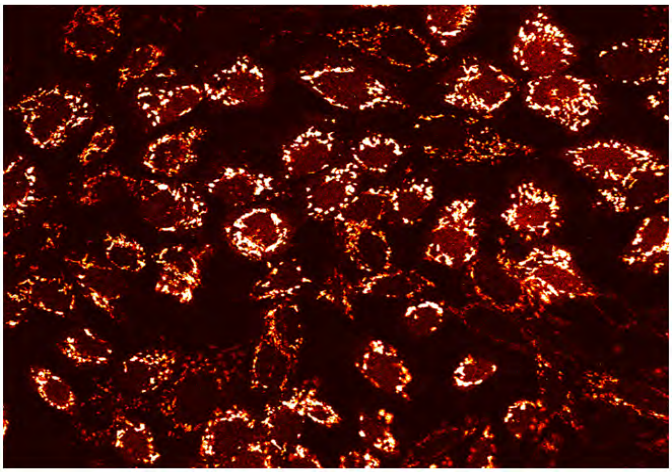

References

1. Philbert, M. A.; Nolan, C. C.; Cremer, J. E.; Tucker. D.; Brown, A. W. 1,3-dinitrobenzene-induced encephalopathy in rats. *Neuropathol. Appl. Neurobiol.* **13**: 371-389; 1987.

2. Tjalkens, R. B.; Ewing, M. M.; Philbert, M. A. Differential cellular regulation of the mitochondrial permeability transition in an *in vitro* model of 1,3-dinitrobenzene-induced encephalopathy. *Brain Res.* **874**: 165-177; 2000.

3. Romero, I. A.; Ray, D. E.; Chan, M. W. K.; Abbott, N. J. An *in vitro* study of *m*-dinitrobenzene toxicity on the cellular components of the blood-brain barrier, astrocytes and endothelial cells. *Toxicol. Appl. Pharmacol.* **139**: 94-101; 1996.

4. Romero, I. A.; Lister, T.; Richards, H. K.; Seville, M. P.; Wylie, S. P.; Ray, D. E. Early metabolic changes during *m*-dinitrobenzene neurotoxicity and the possible role of oxidative stress. *Free. Radic. Biol. Med.* **18**: 311-319; 1995.

5. Nyström, T. Role of oxidative carbonylation in protein quality control and senescence. *Embo J.* **24**: 1311-1317; 2005.

6. Dalle-Donne, I.; Aldini, G.; Carini, M.; Colombo. R.; Rossi, R.; Milzani, A. Protein carbonylation, cellular dysfunction, and disease progression. *J. Cell. Mol. Med.* **10**: 389-406; 2006.

7. Smith, M. A.; Sayre, L. M.; Anderson, V. E.; Harris, P. L. R.; Beal, M., F.; Kowall, N.; Perry, G. Cytochemical demonstration of oxidative damage in Alzheimer disease by immunochemical enhancement of the carbonyl reaction with 2,4-Dinitrophenylhydrazine. *J. Histochem. Cytochem.* **46**: 731-735; 1998.

8. Aksenov, M. Y.; Aksenova, M. V.; Butterfield, D. A.; Geddes, J. W.; Markesbery, W. R. Protein oxidation in the brain in Alzheimer's disease. *Neuroscience.* **103**: 373-383; 2001.

9. Castegna, A.; Aksenov, M.; Aksenova, M.; Thongboonkerd, V.; Klein, J. B.; Pierce, W. M.; Booze, R.; Markesbery, W. R.; Butterfield, D. A. Proteomic identification of oxidatively modified proteins in Alzheimer's disease brain. Part I: Creatine kinase BB, glutamine synthase, and ubiquitin carboxy-terminal hydrolase L-1. *Free. Rad. Biol. Med.* **33**: 562-571; 2002.

10. Prokai, L.; Yan, L-J.; Vera-Serrano, J. L.; Stevens Jr., S. M.; Forster, M. J. Mass spectrometry-based survey of age-associated protein carbonylation in rat brain mitochodria. *J. Mass. Spectrom.* **42**: 1583-1589; 2007.

11. Cavanagh, J.B.; Nolan, C.C. The neurotoxicity of alpha-chlorohydrin in rats and mice: II. Lesion topography and factors in selective vulnerability in acute energy deprivation syndromes. *Neuropathol Appl Neurobiol.* **19**: 471-479; 1993.

12. Willis, C.L.; Nolan, C. C.; Reith, S. N.; Lister, T.; Prior, M. J. W.; Guerin, C. J.; Mavroudis, G.; Ray, D. E. Focal astrocyte loss is followed by microvascular damage, with subsequent repair of the blood-brain barrier in the apparent absence of direct astrocyte contact. *Glia* **45**: 325-337; 2004.

13. Skamarauskas, J.; Carter, W.; Fowler, M.; Madjd, A.; Lister, T.; Mavroudis, G.; Ray, D. E. The selective neurotoxicity produced by 3-chloropropanediol in the rat is not a result of energy deprivation. *Toxicology* **232**: 268-276; 2007.

14. Han, Y. H.; Kim, S. W.; Kim, S. H.; Kim, S. Z.; Park, W. H. 2,4-dinitrophenol induces G1 phase arrest and apoptosis in human pulmonary adenocarcinoma Calu-6 cells. *Toxicol. In Vitro* **22**: 659-670; 2008.

15. Futakawa, N.; Kondoh, M.; Ueda, S.; Higashimoto, M.; Takiguchi, M.; Suzuki, S.; Sato, M. Involvement of oxidative stress in the synthesis of metallothionein induced by mitochondrial inhibitors. *Biol. Pharm Bull.* **29**: 2016-2020; 2006.

16. Huang, L.; Sun, G.; Cobessi, D.; Wang, A. C.; Shen, J. T.; Tung, E. Y.; Anderson, V. E.; Berry, E. A. 3-nitropropionic acid is a suicide inhibitor of mitochondrial respiration that, upon oxidation by complex II, forms a covalent adduct with a catalytic base arginine in the active site of the enzyme. *J. Biol. Chem.* **281**: 5965-5972; 2006.

17. La Fontaine, M. A.; Geddes, J. W.; Banks, A.; Butterfield, D. A. 3-nitropropionic acid induced in vivo protein oxidation in striatal and cortical synaptosomes: insights into Huntington's disease. *Brain Res.* **858**: 356-362; 2000.

18. Stair, E. L.; Reddy, G.; Ritchey, J. W.; Saliki, J. T.; Qualis Jr., C. W. Effects of 1,3,5-trinitrobenzene on cytotoxicity and metabolic activity of type I astrocytes in rats. *Int. J. Toxicol.* **24**:51-57; 2005.

19. Smerjac, S. M.; Bizzozero, O. A. Cytoskeletal protein carbonylation and degradation in experimental autoimmune encephalomyelitis. *J. Neurochem.* **105**: 763-772; 2008.

20. Rabek, J. P.; Boylston III, W. H.; Papaconstantinou, J. Carbonylation of ER chaperone proteins in aged mouse liver. *Biochem. Biophys. Res. Com.* **305**: 566-572; 2003.

21. Temple, A.; Yen, T.; Gronert, S. Identification of specific protein carbonylation sites in model oxidations of human serum albumin. *J. Am. Soc. Mass Spectrom.* **17**: 1172-1180; 2006.

22. Choi, J.; Malakowsky, C. A.; Talent, J. M.; Conrad, C. C.; Carroll, C. A.; Weintraub, S. T.; Gracy, R. W. Anti-apoptotic proteins are oxidized by $A\beta_{25-35}$ in Alzheimer's fibroblasts. *Biochim. Biophys. Acta* **1637**: 135-141; 2003.

23. Bossy-Wetzel, E.; Barsoum, M. J.; Godzik, A.; Schwarzenbacher, R.; Lipton, S. A. Mitochondrial fission in apoptosis, neurodegeneration and aging. *Curr. Opin. Cell Biol.* **15**: 706-716; 2003.

24. Leinninger, G. M.; Backus, C.; Sastry, A. M.; Yi, Y-B.; Wang, C-W.; Feldman, E. L. Mitochondria in DRG neurons undergo hyperglycemic mediated injury through Bim, Bax and the fission protein Drp1. *Neurobiol. Dis.* **23**: 11-22; 2006.

25. Koopman, W. J. H.; Distelmaier, F.; Esseling, J. J.; Smeitink, J. A. M.; Willems, P. H. J. M. Computer-assisted live cell analysis of mitochondrial membrane potential, morphology, and calcium handling. *Methods* **46**: 304-311; 2008.

Chapter V

In vivo 1,3-DNB exposure leads to protein carbonylation in F344 rat brainstem tissue

Introduction

Protein carbonylation is a post-translational form of oxidative modification involved in various pathophysiological mechanisms including protein quality control, age-dependent oxidative damage, and chemical-induced oxidation [1, 2, 3]. This dissertation provides novel experimental evidence identifying specific proteins within DI TNC1 astrocytes as susceptible targets of 1,3-DNB-induced protein carbonylation prior to development of downstream pathological markers, including mitochondrial and metabolic dysfunction. Rat models of neurologic protein oxidation support *in vitro* data presented within this study in that specific proteins, such as F1-ATP synthase and aconitate hydratase, are identified as *in vivo* targets of protein carbonylation [4]. Exposure to 1,3-DNB resulted in the carbonylation of ER proteins calreticulin, protein disulfide isomerase, and Grp78, which are established targets of age-associated oxidative carbonylation *in vivo*

[5]. *In vivo* studies like these established a precedent that confirmed proteins carbonylated during 1,3-DNB exposure as susceptible targets of oxidation.

Protein carbonylation clearly has a role in 1,3-DNB neurotoxicity as demonstrated by the findings in this *in vitro* study. This purpose of this analysis is to provide evidence of 1,3-DNB-induced protein carbonylation occurring in rat models used to study 1,3-DNB neurotoxicity *in vivo*. 2D gel electrophoresis followed by western blot analysis was used to detect protein carbonylation in brainstem protein samples obtained from in vivo exposure of 1,3-DNB. Preliminary results from this experiment demonstrate that 1,3-DNB exposure does, in fact, lead to marked carbonylation of brainstem tissue in susceptible rat models.

Materials and Methods

Chemicals

The Oxyblot immunodetection kit was obtained from Chemicon (Millipore, Billerica, MA). Secondary antibodies for immunoblot visualization, 2D Clean-Up kits, and Destreak rehydration buffer were obtained from GE Healthcare (Piscataway, NJ). IPG Readystrips and 12% Tris-HCl Readygels were obtained from Bio-Rad (Hercules, CA). BCA protein quantification reagents were obtained from Pierce (Thermo Scientific, Rockford, IL). PVDF membranes were purchased from Millipore (Billerica, MA). All other reagents were of analytical grade and were obtained from Sigma-Aldrich (St. Louis, MO).

Mitochondrial Protein Sample Preparation

Male F344 rats aged between 8-10 weeks, mean weight 280g, were separated into three animals/exposure group. Animals were administered 3 individual i.p. doses of 10 mg/kg DMSO (vehicle control) or 1,3-DNB. Animals were killed by decapitation 6 hrs, 12 hrs, or 24 hrs after the third and final 10 mg/kg dose. The vehicle control exposure group was killed 24 hrs after the final dose. Rat brainstems were quickly removed and placed into ice-cold PBS. Mitochondrial protein samples were isolated from each exposure group using the MITOISO1 kit for soft tissue produced by Sigma. Brainstem tissue was homogenized in a teflon tissue grinder and glass pestle in 10 volumes of extraction buffer containing 2 mg/ml bovine serum albumin. The extraction buffer's composition consists of 220 mM mannitol, 70 mM sucrose, 0.5 mM EGTA, and 2 mM HEPES at a final pH of 7.4. The homogenate was transferred to a 15 ml conical tube and centrifuged at 500 x g for 5 minutes. The resulting supernatant was then removed, centrifuged at 11000 x g, and the pellet resuspended in extraction buffer. This step was repeated two more times in order to thoroughly wash the pellet. The mitochondrial protein pellet was resuspended in storage buffer containing 10 mM, HEPES, 250 mM sucrose, 1 mM ATP, 0.08 mM ADP, 5 mM sodium succinate, 2 mM K_2HPO_4, and 1mM DTT. A protease inhibitor cocktail was added to each sample before protein

concentrations were quantified or the samples placed in storage at -80°C. Protein concentrations were quantified using the BCA Protein Assay kit.

Two-dimensional (2D) gel electrophoresis

Aliquots of mitochondrial protein sample containing 70 µg of protein were prepared for SYPRO ruby staining and detection of protein carbonyls through Oxyblot analysis. Protein samples designated for Oxyblot analysis were derivatized for approximately 15 min at room temperature in a 1X DNPH solution provided for in an Oxyblot immunodetection kit. This reaction derivatizes carbonyl groups found on protein side chains to 2,4-dinitrophenylhydrazones that can be detected using Western blot analysis. Upon completion of the derivatization reaction, excess salts and other impurities were removed from each set of samples using a 2-D Clean-Up kit. Precipitates were incubated in wash buffer for at least an hour before centrifugation at 12,000 x g for 5 min. After the wash buffer was removed, 200 µl Destreak rehydration buffer containing 2.5 ul/ml IPG buffer (pH 3-10) was added to the protein pellet. A final centrifugation at 12,000 x g was required in order to remove any insoluble material that might hinder isoelectric focusing. Each sample was then added to a ReadyStrip IPG Strip 7 cm, pH 3-10. The IPG strips were actively rehydrated overnight in the IEF focusing tray of the Protean IEF cell using a current of 50 µA/IPG strip at 20°C. Isoelectric focusing was performed overnight at a voltage of 4000 V for a minimum of 20,000 Vh at 20°C. Before separation in the second dimension, the IPG strips were equilibrated at room temperature using two

separate buffer solutions, the recipes of which were derived from Bio-Rad. The IPG strips were equilibrated for approximately 30 min in 0.375 m Tris-HCl (pH 8.8) buffer containing 6 M urea, 2% SDS, 20% glycerol, and 2% (w/v) DTT. The IPG strips were then placed on ReadyGels 12% Tris-HCl in Mini-Protean III systems for electrophoresis. For the second dimension separation, the gels were run at a constant voltage of 100 V for approximately 1.45 h.

Western Blot Analysis

Following separation in the second dimension, 2D gels designated for Oxyblot analysis were transferred to PVDF membranes. The nitrocellulose membranes were exposed to blocking buffer for 45 min and then incubated overnight at 4°C in rabbit primary antibody specific to 2,4-dinitrophenylhydrazone. An anti-rabbit, alkaline phophatase-labeled secondary, used for ECF-based immunodetection, was added following removal of the primary antibody and washing of the PVDF membranes. Images of carbonylated proteins were visualized using the Fujifilm FLA-5000 imaging system and Image Reader software.

Results

In vivo 1,3-DNB exposure causes protein carbonylation in F344 rat brainstem tissue

All three treated animals in the 24 hour 1,3-DNB exposure group developed characteristic symptoms of 1,3-DNB neurotoxicity including light-bluish changes in the color of their extremities indicative of methemoglobinemia and visible signs of ataxia, characterized by an unstable gait when attempting to move from one location to another. Brainstem mitochondrial proteins were isolated from each animal upon sacrifice and analyzed using 2D Oxyblots. Marked protein carbonylation was present in protein isolated from all of the animals treated with 1,3-DNB. A basal level of carbonylation was present in mitochondrial proteins isolated from animals dosed only with DMSO, but the intensity of the carbonylation signal appears to be much less when compared to brainstem proteins isolated from animals exposed to 1,3-DNB. Comparison of the 6 hr, 12 hr, and 24 hr 1,3-DNB exposure groups revealed an apparent time-dependent increase in the number of proteins carbonylated. Interestingly, increased protein carbonylation appeared as early as 6 hours after the final 10 mg/kg 1,3-DNB was administered, but the first symptoms of 1,3-DNB toxicity were not observed until 24 hours after the final 1,3-DNB dose.

Discussion

Preliminary results from this study indicate that 1,3-DNB exposure leads to the formation of protein carbonyls *in vivo*. Although 1,3-DNB-dependent increases in carbonylation were not statistically quantified for individual proteins, it appears that 1,3-DNB exposure leads to a time-dependent, overall increase in

the number of proteins carbonylated. Even though protein carbonylation was identified in brainstem tissue isolated from 1,3-DNB-exposed animals 6 hours after sacrifice, indications of 1,3-DNB toxicity (i.e. methemoglobinemia, ataxia) were not apparent until 24 hours following the final dose. These data corroborate the pharmacokinetics of 1,3-DNB induced lesion development as a function of concentration-time thresholds. Xu et al., (1999) demonstrated that low steady-state blood concentrations of 1,3-DNB, maintained at 2μM or above from a total infused dose of 30 mg/kg, for more than 18.8 hours are capable of inducing brain damage [6]. Reciprocally, higher steady-state concentrations of 1,3-DNB maintained in the blood for less than 18 hours would induce no brain damage. Hence, 1,3-DNB-induced symptoms of brain damage would not be expected for exposure periods less than 24 hours. One problem concerning the study of protein carbonylation *in vivo* is that protein samples were obtained from a heterogeneous mixture of cell types from the brainstem. It is likely that the protein samples used for Oxyblot analysis were derived from various types of glial and neuronal cells, thereby making it virtually impossible to reliably determine which oxidized proteins derived from type 1 astrocytes. This *in vivo* analysis emphasizes the importance of analyzing 1,3-DNB neurotoxicity in a susceptible, immortalized cell line in that specific molecular mechanisms of toxicity in be clarified in a single type of cell.

It is tempting to suggest that 1,3-DNB-induced protein carbonylation occurs prior to development of both lesions and symptoms of 1,3-DNB toxicity. In order to determine if 1,3-DNB oxidative stress mediates the molecular

mechanism of concentration- and time-dependent pathology through protein carbonylation, further *in vivo* analysis should determine if antioxidant use attenuates protein carbonylation and formation of brainstem lesions. This hypothesis could be tested using immunohistochemical analysis of brainstem slices from rats exposed to 1,3-DNB, in order to determine whether or not carbonylated proteins accumulate within brainstem lesion. Additionally, further analysis will require identification of individual carbonylated proteins isolated from brainstem tissue during the early phase of 1,3-DNB exposure. In order to avoid the problem of cellular heterogeneity, the experiments delineated in the preceding data chapters can be replicated in primary cultured type 1 brainstem astrocytes. Once each carbonylated protein is identified, experiments determining the extent of protein carbonylation and subsequent functional deficits caused by oxidative modification will provide more information about the potential mechanistic role individual proteins have during *in vivo* 1,3-DNB neuropathogenesis.

Acknowledgments

This research was supported by grants from the NIEHS (NIH T32-ES07062) and the NIH (RO1-ES08846). We would like to thank Jen Fernandez, Brad Martin, Evan Milton, and the members of the Michigan Proteomics Consortium for their assistance during the course of this study.

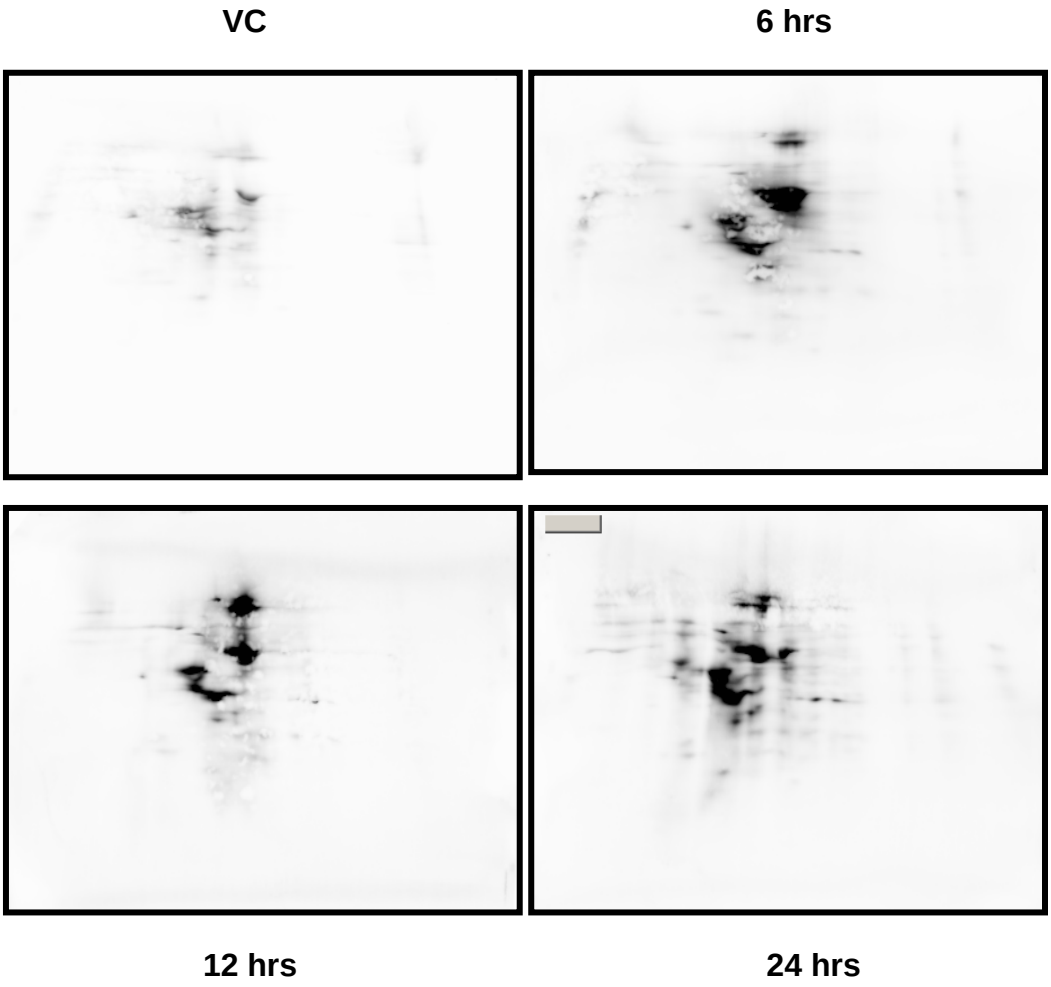

Figure 5.1. Time-dependent two-dimensional Oxyblot analysis of brainstem, mitochondrial protein isolated from F344 rats dosed with 10mg/kg 1,3-DNB or DMSO control (24 hrs) for 6 hrs, 12hrs, or 24 hrs.

References

1. Nyström, T. Role of oxidative carbonylation in protein quality control and senescence. *Embo J.* **24**: 1311-1317; 2005.

2. Humphries, K. M.; Szweda, P. A.; Szweda, L. I. Aging: a shift from redox regulation to oxidative damage. *Free Rad. Res.* **40**: 1239-1243; 2006.

3. Kaur, P.; Radotra, B.; Minz, R. W.; Gill, K. D. Impaired mitocondrial energy metabolismo and neuronal apoptotic cell death alter chronic dichlorvos (OP) exposure in rat brain. *Neurotoxicology* **28**: 1208-1219; 2007.

4. Prokai, L.; Yan, L-J.; Vera-Serrano, J. L.; Stevens Jr., S. M.; Forster, M. J. Mass spectrometry-based survey of age-associated protein carbonylation in rat brain mitochodria. *J. Mass. Spectrom.* **42**: 1583-1589; 2007.

5. Rabek, J. P.; Boylston III, W. H.; Papaconstantinou, J. Carbonylation of ER chaperone proteins in aged mouse liver. *Biochem. Biophys. Res. Com.* **305**: 566-572; 2003.

6. Xu, J.; Nolan, C. C.; Lister, T.; Purcell, W. M.; Ray, D. E. Pharmacokinetic factors and concentration-time threshold in m-dinitrobenzene-induced neurotoxicity. *Toxicol. Appl. Pharmacol.* **161**: 267-273; 1999.

Chapter VI

Conclusions and Future Work

Various kinds of neuropathologic mechanisms are known to develop through alterations in cellular redox state mediated by the production of oxidative stress [1, 2, 3, 4, 5, 6]. Unchecked production of ROS can lead to irreversible damage of various macromolecules including nucleic acids, lipids, and proteins [7]. Oxidative modification of susceptible proteins can cause changes in protein structure that may eventually disrupt protein and cellular function, leading to downstream pathology. The accumulation of proteins or enzymes damaged by oxidative modification often result from the severity of the oxidizing insult [8]. Several nitrocompounds are known to induce oxidative stress in susceptible tissue types, including the nervous system [9, 10]. The mechanism by which 1,3-DNB exposure leads to increased ROS production and subsequent toxicity develop is still a matter of much debate. The analysis described throughout this dissertation provided insight into how chemical-induced oxidative stress may lead to energy deprivation and metabolic disruption through protein oxidation. This study demonstrated that 1,3-DNB exposure not only leads to oxidative stress-

linked mitochondrial dysfunction, but that the molecular mechanism of cellular injury may occur through the oxidative carbonylation of specific proteins.

Metabolism of 1,3-DNB results in increased production of ROS that can lead to an imbalance in the cellular redox state [11]. Increased generation of ROS is known to occur in multiple cellular models of 1,3-DNB neurotoxicity [12, 13]. The research described in this dissertation demonstrates that DI TNC1 astrocytes are susceptible to the toxic effects of 1,3-DNB, and as such, act as a suitable *in vitro* model for the primary cellular target of 1,3-DNB, the type 1 brainstem astrocyte. The results presented in Chapter II demonstrate that DI TNC1 cells exposed to 1mM 1,3-DNB induce time-dependent increases in mitochondrial superoxide anion production, starting at 45 minutes and reaching maximum production at 5 hrs (~ 25-fold increase vs. DMSO control). Previous findings linking superoxide production and onset of MPT provide evidence that net increases in superoxide anion production are sensitive to MPT inhibitors [14]. Superoxide anion production was sensitive to pretreatment with MPT inhibitor, BkA, indicating that at least some ROS production occurs through opening of the mPTP.

Onset of MPT is normally considered a catastrophic event that leads to eventual apoptotic cellular death in as little as an hour after triggering the MPT [15]. Considering that most of the DI TNC1 cells in each culture exposed to 1mM 1,3-DNB did not die until 24 hours after initial exposure, it is likely that BkA-sensitive increases in superoxide anion present as early as 45 minutes after 1,3-DNB exposure represented transient opening of the mPTP. Previous research

describes how transient opening of the mPTP and release of ROS during ischemic preconditioning mediates protection against the damage caused by myocardial infarct which suggests that onset of MPT is not always a terminal event [16]. However, to imply that transient opening of the mPTP is not harmful to a cell would be misleading. Analysis of 1,3-DNB-induced time-dependent mitochondrial depolarization demonstrated that initial significant loss of $\Delta\Psi_m$ (~40% decrease TMRM fluorescence) occurred 5 hours after exposure. Loss of $\Delta\Psi_m$ coincided with peak superoxide anion production at 5 hours even though significant superoxide anion production (~ 15-fold increase vs. DMSO control) was detected as early as 45 minutes after 1,3-DNB exposure. This early phase of ROS production may act as the trigger that promotes downstream mitochondrial dysfunction. The production of superoxide anion continues after onset of mitochondrial depolarization suggesting that while uncoupling of mitochondrial electron transport may contribute significantly to overall oxidative stress, induction of the MPT may not be required for initiation of superoxide production. Zorov et al. (2006) described a phenomenon known as "mitochondrial ROS-induced ROS release" during which early generation of ROS reaches a threshold level that induces a gradual increasing cascade of MPT and mitochondrial depolarization across groups of mitochondria, stimulating further increases in ROS production and downstream pathology [17]. This phenomenon is initiated by surpassing a threshold level dependent on the severity of the initial ROS-inducing toxic insult. 1,3-DNB induced mitochondrial depolarization seems to follow a pattern similar to this, at least in the early stages, as loss of the $\Delta\Psi_m$

can be mitigated through the use of antioxidants. The decided course of action was to focus on the question of how 1,3-DNB-induced oxidative stress caused mitochondrial dysfunction. The potential answer is through the oxidative modification of key mitochondrial proteins.

This study was the first to show that 1,3-DNB exposure leads to the oxidative modification of specific mitochondrial proteins through carbonylation. Other mechanisms of protein modification were studied, including nitrotyrosination and 4-hydroxy-2-nonenal, but yielded negative results. 1,3-DNB induces persistent superoxide anion production that increases the likelihood that protein carbonylation occurs in and around the mitochondria. Superoxide anion has a relatively long half-life that allows it to migrate from its site of production and interact with other molecules, producing more reactive oxidizing species (such as hydroxyl radical) that are more capable of mediating protein carbonylation reactions [8]. Mitochondria contain an abundance of transition metals bound within various macromolecules, such as iron-sulfur clusters within proteins, which could degrade in the presence of ROS and result in mitochondrial proteins being exposed to conditions favoring metal-catalyzed oxidations requiring superoxide anion as a reactant [8, 18]. On the other hand, the mitochondrion is also equipped with a variety of antioxidant defense mechanisms as is the cytosol and its component organelles [8]. Therefore, it is logical to ask whether or not in the face of a competent antioxidant system mitochondrial proteins that are acutely sensitive to carbonyl formation contribute to the triggering of irreversible formation of the MPT. This study confirmed results from

previous research showing that pretreatment with the iron-chelating antioxidant, deferoxamine, protects cells from 1, 3-DNB induced mitochondrial depolarization [13]. This study also demonstrated that pretreatment with deferoxamine and trolox attenuated 1,3-DNB-induced protein carbonylation of specific mitochondrial proteins. However, since deferoxamine was more effective at inhibiting mitochondrial depolarization than trolox, it is possible that protecting against hydroxyl radical formation is more important than inhibiting the formation of other ROS in order to prevent 1,3-DNB-induced mitochondrial dysfunction and that it is the formation of this highly reactive oxygen species that eventually mediates onset of the MPT.

2D Oxyblots derived from cells exposed to 1,3-DNB exhibited marked changes in signal intensity, compared to the DMSO control, indicating increased protein carbonylation. However, as demonstrated by the control, there exists a basal level of specific protein carbonylation which suggests that protein carbonylation may have an important role in redox signaling as a method of regulating the need for protein turnover and proteolytic degradation of severely damaged proteins [19, 20]. The presence of increased ROS may increase the occurrence of protein carbonylation, altering the modification from “redox signal” to marker of oxidative stress. In this manner, increased ROS may shift from the carbonylation of a few specific targets to more complete, widespread modification of additional proteins. The results from Chapter III indicate that during the burst of 1,3-DNB-induced superoxide anion production detected at 45 minutes, 1mM 1,3-DNB exposure lead to carbonylation (or increased carbonylation) of at least

thirteen proteins. During the same time frame, 1µM 1,3-DNB exposure resulted in carbonylation of at least six proteins. Not only are the same six proteins carbonylated during the high-concentration exposure, but additional proteins become susceptible targets of protein modification indicating that the number of proteins oxidized may be dependent on the concentration of 1,3-DNB (i.e. the severity of the oxidizing insult). Further analysis should determine: 1) whether some innate structural characteristic within each protein increases its susceptibility to protein oxidation (i.e. iron sulfur clusters within aconitate hydratase) or 2) whether a combination of increased ROS and innate susceptibility results in protein carbonylation. However, protein carbonylation is irreversible, so any protein reaching a particular threshold of carbonylative damage is susceptible to rapid disposal. Hence, proteolytic degradation can effectively reduce the number of carbonylated proteins actually modified by 1,3-DNB exposure, prior to detection. However, if certain proteins are *too* severely carbonylated, then protein aggregates can form and escape degradation because the resultant protein aggregates tend to be poor substrates for the proteasome machinery [19]. It is possible, in this scenario, that 1,3-DNB exposure hypercarbonylates proteins in such a manner that target proteins become more prone to detection if they escape degradation through aggregate formation.

Densitometry was used to estimate carbonylation intensity ratios for two mitochondrial proteins identified in the high-concentration and low-concentration exposure groups: F1-ATP synthase beta-subunit and mtHsp70. Exposure to

both high and low concentrations of 1,3-DNB exposure resulted in significantly increased carbonylation of the F1-ATP synthase beta-subunit. Pretreating DI TNC1 cells with deferoxamine or trolox protected against 1,3-DNB-induced increases in F1-ATP synthase beta-subunit. However, unlike the F1-ATP synthase beta-subunit, mtHsp70 maintained a non-significant, basal level of carbonylation throughout each treatment of antioxidants or 1,3-DNB. These results highlight the differential susceptibility certain proteins exhibit toward protein carbonylation during 1,3-DNB exposure. Although F1-ATP synthase beta-subunit is presumably exposed to the same 1,3-DNB-dependent increases in ROS as mtHsp70, certain factors predispose the F1-ATP synthase beta-subunit to carbonylation in situations that do not dramatically alter the carbonylation status of mtHsp70. The differential susceptibility of these two important mitochondrial proteins to oxidation lends credence to the idea that alterations in specific protein oxidation may mediate normal mitochondrial function and/or dysfunction. Based upon the DMSO carbonylation indices, mtHsp70 is more carbonylated than F1-ATP synthase beta-subunit in a cellular environment unperturbed by 1,3-DNB exposure. In fact, mtHsp70 appears to be more carbonylated than F1-ATP synthase beta-subunit in every treatment group. Though the comparison is limited by the carbonylation indices of only two proteins, this data suggests that mtHsp70 is capable of withstanding more oxidative modifications to its structure compared to other functionally dissimilar proteins. This corresponds to previous reports that suggest chaperone proteins,

such as mtHsp70, act as redox shields that protect other proteins against oxidative damage [21, 22].

Previous research has already established that the alpha- and beta-subunits of the F1-ATP synthase enzyme complex are sensitive to different oxidizing insults including menadione, hydrogen peroxide, and Fe^{2+} -catalyzed oxidative carbonylation (23, 24, 25). This research is the first to observe that exposure to 1,3-DNB induces carbonylation of the F1 ATP-synthase beta-subunit in DI TNC1 astrocytes and that antioxidant pretreatment attenuated the degree to which this subunit was carbonylated. It must also be emphasized that beta-subunit is particularly susceptible to 1,3-DNB, as significant carbonylation occurred at both high (1mM) and low (1µM) concentrations of 1,3-DNB. Carbonylation of the F1-ATP synthase beta-chain may contribute to DNB–induced mitochondrial depolarization and ATP depletion in susceptible astrocytes. By modifying the structure of the F1 unit, ATP production may cease and unpaired electrons meant for the purpose of ATP production may instead interact with molecular oxygen to form superoxide anion. Tamarit et al. (1998) reported that high carbonyl content measured in the catalytic beta-subunit induced by exposure to menadione or paraquat, correlated with data indicating that oxidative damage lead to ATP depletion and F1F0-ATP synthase inactivation [23]. Given that deferoxamine was substantially more effective than trolox in preventing mitochondrial depolarization, it is tempting to suggest that 1,3-DNB exposure leads to Fenton oxidations that are responsible for carbonylating the beta-subunit of the F1-ATP synthase resulting in ATP depletion

and onset of the MPT. Whether or not 1,3-DNB induces catalytic dysfunction of the F1F0-ATP synthase and that dysfunction can be connected with the oxidative carbonylation of specific subunits is for future analysis to determine.

The data presented thus far indicate a potential relationship between the pattern of specific protein carbonylation and mitochondrial dysfunction in 1,3-DNB neurotoxicity. Unlike the initial study described in Chapters II and III, the purpose of this analysis was to study mitochondrial dysfunction and protein carbonylation without inducing changes in metabolic activity and cellular morphology associated with toxicity. In order to study the specificity of 1,3-DNB-induced carbonylation occurring on individual proteins during 1,3-DNB neurotoxicity, a comparative analysis of protein carbonylation was conducted using other well-established mitochondrial and metabolic toxicants known to induce oxidative stress within susceptible cell types. The toxicants included in this portion of the study included 1,3-DNB, 2,4-DNP, 3-NPA, and 3-CPD, with a complete analysis of the results discussed in Chapter IV. The specific mechanism of toxicity and relationship to mitochondrial dysfunction of each toxicant was reviewed in the introduction to this dissertation. DI TNC1 astrocytes exposed to each toxicant exhibited concentration-dependent deficits in metabolic function during exposure periods of 24 or 48 hours. In addition, when mitochondrial depolarization was measured, each toxicant induced significant concentration-dependent decreases in TMRM fluorescence. Significant loss of TMRM fluorescence (~34-44% loss of fluorescence) during this experimental analysis represented partial loss of the $\Delta\Psi_m$. During the 24 hour exposure to

2,4-DNP and 3-CPD, deferoxamine pretreatment was successful in preventing significant loss of $\Delta\Psi_m$, even though antioxidant pretreatment was only moderately effective in the remaining treatment groups. During the 48 hour treatment, deferoxamine pretreatment was partially effective at preventing loss of TMRM fluorescence during exposure to each toxicant, but significant loss of $\Delta\Psi_m$ still occurred. It is possible that pretreating cells with deferoxamine will only provide sufficient protection against oxidative stress up to 24 hours after the initial toxicant exposure, and that by 48 hours, the cytoprotective effect mediated by deferoxamine is completely diminished. This portion of the analysis was quite informative because the application of a concentration-response analysis of metabolic activity and mitochondrial depolarization clarified the necessary toxicant concentrations capable of inducing mitochondrial dysfunction without generating overt cellular toxicity.

MTS reduction and TMRM fluorescence analysis are established methods used to study general aspects of metabolic and mitochondrial function after exposure to a toxic insult. These particular methods are used to provide general cellular indications of toxicity and not specifics about the molecular mechanism underlying the mechanism. With this in mind, it is not surprising to note that a comparative analysis of DI TNC1 astrocytes upon exposure to 1,3-DNB, 2,4-DNP, 3-NPA, and 3-CPD caused similar concentration-dependent deficits in metabolic activity and mitochondrial depolarization. Specific information about the potential molecular mechanism of each toxicant became apparent when 2D Oxyblots and tandem mass spectrometry were used to identify carbonylation

patterns in mitochondrial proteins isolated from DI TNC1 astrocytes exposed to each toxicant. Each treatment group was exposed to 100µM of either 1,3-DNB, 2,4-DNP, 3-NPA, and 3-CPD for 48 hours. 1,3-DNB induced a carbonylation pattern much like what was observed after exposing cells to 1mM 1,3-DNB for 45 minutes. Fewer proteins were carbonylated during the exposure to 100µM 1,3-DNB for 48 hours. However, each protein identified during this experiment was identified as a target of protein carbonylation during the 1mM 1,3-DNB exposure. The proteins identified after the 100µM 1,3-DNB treatment include: calreticulin, vimentin, actin, serum albumin, F1-ATP synthase beta-subunit and protein disulfide isomerase. Exposure to 100µM 3-NPA and 100µM 3-CPD for 48 hours resulted in similar, conserved patterns of oxidized proteins with a few additionally identified or missing proteins from the group identified during the 1,3-DNB exposure. The carbonylated proteins identified after exposure to 3-NPA include: calreticulin, vimentin, actin, serum albumin, F1-ATP synthase beta-subunit, protein disulfide isomerase, Grp78, tumor rejection antigen gp 96, and D19Bwg1357e. The carbonylated proteins identified after exposure to 3-CPD include: calreticulin, vimentin, actin, and serum albumin.

The conserved patterns of protein oxidation suggest that each toxicant may initiate conserved molecular mechanisms that lead to similar pathologic indices, such as metabolic and mitochondrial dysfunction. On the other hand, because each carbonylation pattern differed by only a few proteins, it is possible that the molecular mechanisms progress through a pathway mediated by oxidation of identified proteins specific to each individual toxicant exposure. For

example, 3-NPA-induced metabolic and mitochondrial dysfunction may occur through oxidation of Grp78, tumor rejection antigen gp 96, and D19Bwg1357e. These particular proteins were not identified in the 100µM 1,3-DNB or 3-CPD treatment groups. Oxidation of one or some combination of these proteins may lead to the development of downstream toxicity. However, as mentioned in the discussion of Chapter IV, Grp78 was identified as a target of 1mM 1,3-DNB-induced carbonylation. Since it has already been established that toxicant concentration is a determinant with respect to the number of proteins carbonylated (Chapter III), it is possible that 100µM 1,3-DNB did not induce as much of an oxidizing insult as 1mM 1,3-DNB. An important difference between these two studies is that cellular exposure to 100µM 1,3-DNB for 48 hrs did not result in the same number of proteins carbonylated as did DI TNC1 cells exposed to 1mM 1,3-DNB for 45 min. Although the cellular mechanisms defining when proteolytic degradation occurs during 1,3-DNB exposure are unknown, oxidized proteins more likely undergo proteolytic degradation over a 48-hour exposure period as opposed to a 45 minute exposure period [2,19]. It is arguable that some oxidized proteins identified after one exposure period may be missing after a longer exposure period due to 1,3-DNB-induced activation of proteolysis.

1,3-DNB-induced protein carbonylation in DI TNC1 astrocytes occurred not only in mitochondrial proteins, but also proteins found within the ER and the cytosol. In addition, comparative analysis using other metabolic toxicants demonstrated that multiple proteins originating from different subcellular regions were also prone to oxidative carbonylation. As discussed earlier, carbonylation

of the F1-ATP synthase beta-subunit may be the candidate linking 1,3-DNB exposure with mitochondrial dysfunction. However, one cannot dismiss the notion that carbonylation of certain endoplasmic reticulum or cytosolic proteins may also lead to mitochondrial dysfunction and downstream pathology. Cross-talk between the endoplasmic reticulum and mitochondria mediated through direct contact, through mitochondrial-associated membranes or through cytosolic signaling pathways is known to control normal cellular functions including protein-folding, calcium homeostasis, and apoptosis [26, 27, 28]. Vimentin, protein disulfide isomerase, Grp78 and calreticulin were identified as targets of 1,3-DNB-induced carbonylation in this dissertation and as targets of carbonylation in previous research focusing on oxidative stress (29, 30). This data establishes a foundation upon which future experimentation can be used to determine whether or not protein carbonylation of ER and/or cytosolic proteins contribute to the molecular mechanism of 1,3-DNB neurotoxicity. Unpublished data from our laboratory demonstrated that 1,3-DNB induced time-dependent increases in Grp78 expression in primary culture type 1 astrocytes. It is tempting to hypothesize that astrocytes upregulating Grp78 expression are attempting to compensate for functional deficits that result from Grp78 proteins affected by 1,3-DNB-induced carbonylation. Increased carbonylation of Grp78 and the other targeted ER chaperones, PDI and calreticulin, could result in impaired protein assembly that disrupts ER function leading to dysfunctional calcium homoeostasis. Carbonylation of calreticulin alone may disrupt its ability to modulate calcium binding, increasing the intracellular calcium concentrations that

could feasibly lead to mitochondrial calcium overload and onset of the MPT. Vimentin is an intermediate filament protein that colocalizes with various organelles, including mitochondria [31]. Caspase-dependent cleavage of vimentin occurs during the cytoskeletal restructuring phase of apoptosis and is thought to be a precipitating event in the execution of the apoptotic signaling cascade [32]. Carbonylation of vimentin during 1,3-DNB exposure may predispose susceptible cells to apoptosis by causing premature proteolysis of vimentin filaments and initiation of the apoptotic cascade.

As described above, protein carbonylation of specific protein targets may lead to 1,3-DNB-induced mitochondrial dysfunction and cellular pathology through one or a combination of several mechanisms. This dissertation presents, for the first time, how 1,3-DNB-induced oxidative stress leads to the oxidative carbonylation of multiple protein targets within different subcellular regions. Future work aimed at understanding how 1,3-DNB exposure leads to mitochondrial dysfunction in susceptible cells should thoroughly investigate the relationship between the oxidative modification of specific protein targets and how these modifications lead to potential alterations in protein function. This work should not just include the study of mitochondrial proteins carbonylated as a result of 1,3-DNB exposure, but also proteins found in the cytosol and the ER. The initial aim of this study was to determine how modification of mitochondrial proteins alone could lead to 1,3-DNB-induced mitochondrial dysfunction. It was realized, during the course of this research, that by focusing on a particular group of proteins alone, one can erroneously ignore the complicated interplay of

mechanisms involving multiple subcellular regions that drive the development of pathogenesis.

The use of TMRM is considered a standard method of monitoring the presence of a functional $\Delta\Psi_m$ during live-cell analysis. Research conducted in this study confirms the use of TMRM as a method for analyzing 1,3-DNB-induced mitochondrial depolarization using two-dimensional digital images acquired through laser scanning confocal microscopy. Interpreting 1,3-DNB-induced mitochondrial depolarization could be a taken a step further if one could quantitatively measure 1,3-DNB-induced loss of $\Delta\Psi_m$ beyond measuring loss of TMRM fluorescence. A modified version of the Nernst equation $\Delta\Psi_m = -60^{10}$ $\log(7.6 \cdot F_{mit}/F_{nuc})$ was developed for use during live cell imaging analysis and tested in cultured fibroblasts [33]. This study demonstrated that ratiometric calculations of $\Delta\Psi_m$ can be made using mitochondrial (F_{mit}) and nuclear (F_{nuc}) TMRM fluorescence using a correction factor of 7.6, in order to account for fluorescence contributions made by regions outside the small mitochondrial compartments that dilute fluorescence intensity (known as the point spread function). Recent studies incorporate this revised version of the Nernst equation with dual-wavelength ratiometric confocal imaging in order to calculate increased mitochondrial depolarization [34]. In this study, mitochondrial depolarization was ratiometrically measured using both TMRM and a transfected mitochondrial-targeted green fluorescent protein (mitoAcGFP1). The reason for using a second fluorophore is that as the $\Delta\Psi_m$ depolarizes, the difference between cytosolic (background) and mitochondrial TMRM fluorescence decreases to such an

extent that background TMRM fluorescence intermingles with mitochondrial TMRM fluorescence. One can no longer reliably calculate the Nernst $\Delta\Psi_m$ using the binary picture/image based upon TMRM fluorescence alone.

In Chapter IV, a comparative analysis of multiple metabolic toxicants with 1,3-DNB revealed similarities between toxicant-induced metabolic- and mitochondrial dysfunction, along with differences in specific targets of protein carbonylation. Interestingly, confocal imaging during this portion of the study also revealed that certain concentrations of specific toxicants, especially 1,3-DNB, resulted in mitochondrial morphological changes that accompanied mitochondrial depolarization. Changes in mitochondrial morphology, such as mitochondrial fusion or fission, are known to occur in various forms of pathology associated with ATP production [34, 35, 36]. Mitochondrial fission is an event that occurs during inhibition of electron transport, ATP depletion, and apoptosis [37, 38]. Several mitochondria exposed to 100μM 1,3-DNB, for example, appeared to take on more compact shape, suggesting that a change occurred in mitochondrial aspect ratio denoting a possible fission event. Without any quantitative assessment, it is impossible to determine whether or not these morphological changes are related to 1,3-DNB-induced mitochondrial dysfunction. There are likely other molecular mechanisms involved in the events that dictate mitochondrial morphology, such as mitochondrial interactions with microtubules, that are induced upon exposure to 1,3-DNB. Future work in this regard should be focused on determining whether or not the morphological changes are dependent on 1,3-DNB exposure by quantifying indices such as

aspect ratio, number of mitochondria undergoing morphological changes, etc. using analytical devices that are computationally and statistically appropriate.

References

1. Romero, I. A.; Lister, T.; Richards, H. K.; Seville, M. P.; Wylie, S. P.; Ray, D. E. Early metabolic changes during *m*-dinitrobenzene neurotoxicity and the possible role of oxidative stress. *Free. Radic. Biol. Med.* **18**: 311-319; 1995.

2. Dalle-Donne, I.; Aldini, G.; Carini, M.; Colombo. R.; Rossi, R.; Milzani, A. Protein carbonylation, cellular dysfunction, and disease progression. *J. Cell. Mol. Med.* **10**: 389-406; 2006.

3. Smith, M. A.; Sayre, L. M.; Anderson, V. E.; Harris, P. L. R.; Beal, M., F.; Kowall, N.; Perry, G. Cytochemical demonstration of oxidative damage in Alzheimer disease by immunochemical enhancement of the carbonyl reaction with 2,4-Dinitrophenylhydrazine. *J. Histochem. Cytochem.* **46**: 731-735; 1998.

4. Aksenov, M. Y.; Aksenova, M. V.; Butterfield, D. A.; Geddes, J. W.; Markesbery, W. R. Protein oxidation in the brain in Alzheimer's disease. *Neuroscience.* **103**: 373-383; 2001.

5. Castegna, A.; Aksenov, M.; Aksenova, M.; Thongboonkerd, V.; Klein, J. B.; Pierce, W. M.; Booze, R.; Markesbery, W. R.; Butterfield, D. A. Proteomic identification of oxidatively modified proteins in Alzheimer's disease brain. Part I: Creatine kinase BB, glutamine synthase, and ubiquitin carboxy-terminal hydrolase L-1. *Free. Rad. Biol. Med.* **33**: 562-571; 2002.

6. La Fontaine, M. A.; Geddes, J. W.; Banks, A.; Butterfield, D. A. 3-nitropropionic acid induced in vivo protein oxidation in striatal and cortical synaptosomes: insights into Huntington's disease. *Brain Res.* **858**: 356-362; 2000.

7. Stadtman, E. R.; Berlett, B. S. Fenton chemistry. Amino acid oxidation. *J. Biol. Chem.* **266**: 17201-17211; 1991.

8. Kohen, R.; Nyska, A. Oxidation of biological systems: oxidative stress phenomena, antioxidants, redox reactions, and methods for their quantification. *Toxicol. Pathol.* **30**: 620-650; 2002.

9. Mason, R. P.; Josephy, P. D. An electron spin resonance investigation of the iron-catalyzed reaction of metronidazole with cysteine. *J. Inorg. Biochem.* **24**: 161-165; 1985.

10. Philbert, M. A.; Nolan, C. C.; Cremer, J. E.; Tucker. D.; Brown, A. W. 1,3-dinitrobenzene-induced encephalopathy in rats. *Neuropathol. Appl. Neurobiol.* **13**: 371-389; 1987.

11. Romero, I. A.; Lister, T.; Richards, H. K.; Seville, M. P.; Wylie, S. P.; Ray, D. E. Early metabolic changes during *m*-dinitrobenzene neurotoxicity and the possible role of oxidative stress. *Free. Radic. Biol. Med.* **18**: 311-319; 1995.

12. Romero, I. A.; Ray, D. E.; Chan, M. W. K.; Abbott, N. J. An in vitro study of m-dinitrobenzene toxicity on the cellular components of the blood-brain barrier, astrocytes and endothelial. *Toxicol. Appl. Pharmacol.* **139**: 94-101; 1996.

13. Tjalkens, R. B.; Ewing, M. M.; Philbert, M. A. Differential cellular regulation of the mitochondrial permeability transition in an *in vitro* model of 1,3-dinitrobenzene-induced encephalopathy. *Brain Res.* **874**: 165-177; 2000.

14. Tay, V. K. S.; Wang, A. S.; Leow, K. Y.; Ong, M.; Wong, K. P.; Boelsterli, U. A. Mitochondrial permeability transition as a source of superoxide anion induced by the nitroaromatic drug nimesulide *in vitro*. *Free Rad. Biol. Med*. **39**: 949-959; 2005.

15. Ding, W-X.; Shen, H-M.; Ong, C-N. Critical role of reactive oxygen species and mitochondrial permeability transition in microcystin-induced rapid apoptosis in rat heptatocytes. *Hepatology* **32**: 547-555; 2000.

16. Hausenloy, D.; Wynne, A.; Duchen, M.; Yellon, D. Transient mitochondrial permeability transition pore opening mediates preconditioning-induced protection. *Circulation* **109**: 1714-1717; 2004.

17. Zorov, D. B.; Juhasova, M.; Sollott, S. J. Mitochondrial ROS-induced ROS release: An update and review. *Biochim. Biophys. Acta* **1757**: 509-517; 2006.

18. Tangeras, A.; Flatmark, T.; Backstrom, D.; Ehrenberg, A. Mitochondrial iron not bound in heme and iron-sulfur clusters. Estimation, compartmentation, and redox state. *Biophys. Acta* **589**: 162-175; 1980.

19. Nyström, T. Role of oxidative carbonylation in protein quality control and senescence. *Embo J.* **24**: 1311-1317; 2005.

20. Wong, C. M.; Cheema, A. K.; Zhang, L.; Suzuki, Y. J. Protein carbonyaltion as a novel mechanism in redox signaling. *Circ. Res.* **102**: 310-318; 2008.

21. Magi, B.; Ettorre, A.; Liberatori, S.; Bini, L.; Andreassi, M.; Frosali, S.; Neri, P.; Pallini, V.; Di Stefano, A. Selectivity of protein carbonylation in the apoptotic response to oxidative stress associated with photodynamic therapy: a cell biochemical and proteomic investigation. *Cell Death Differ.* **11**: 842-852; 2004.

22. Cabiscol, E.; Piulats, E.; Echave, P.; Herrero, E.; Ros, J. Oxidative stress promotes specific protein damage in *Saccharomyces cerevisiae*. J. Biol. Chem. 275: 27393-27398; 2000.

23. Tamarit, J.; Cabiscol, E.; Ros, J. Identification of the major oxidatively damaged proteins in *Escherichia coli* cells exposed to oxidative stress. *J. Biol. Chem.* **273**: 3027-3032; 1998.

24. Prokai, L.; Yan, L-J.; Vera-Serrano, J. L.; Stevens Jr., S. M.; Forster, M. J. Mass spectrometry-based survey of age-associated protein carbonylation in rat brain mitochodria. *J. Mass. Spectrom.* **42**: 1583-1589; 2007.

25. Belogrudov, G. I. Mitochondrial ATP synthase: Fe^{2+}-catalyzed fragmentation of the soluble F_1-ATPase. Arch. Biochem. Biophys. 335: 131-138; 1996.

26. Walter, L.; Hajnóczky, G. Mitochondria and endoplasmic reticulum: the lethal interorganelle cross-talk. *J. Bioenerg. Biomembr.* **37**: 191-206; 2005.

27. Goetz, J. G.; Nabi, I. R. Interaction of the smooth endoplasmic reticulum and mitochondria. *Biochem. Soc. Trans.* **34**: 370-373; 2006.

28. Yoneda, T.; Benedetti, C.; Urano, F.; Clark, S. G.; Harding, H. P.; Ron, D. Compartment-specific perturbation of protein handling activates genes encoding mitochondrial chaperones. *J. Cell Sci.* **117**: 4055-4066; 2004.

29. Choi, J.; Malakowsky, C. A.; Talent, J. M.; Conrad, C. C.; Carroll, C. A.; Weintraub, S. T.; Gracy, R. W. Anti-apoptotic proteins are oxidized by $A\beta_{25-35}$ in Alzheimer's fibroblasts. *Biochim. Biophys. Acta* **1637**: 135-141; 2003.

30. Rabek, J. P.; Boylston III, W. H.; Papaconstantinou, J. Carbonylation of ER chaperone proteins in aged mouse liver. *Biochem. Biophys. Res. Com.* **305**: 566-572; 2003.

31. Katsumoto, T.; Mitsushima, A.; Kurimura, T. The role of the vimentin intermediate filaments in rat 3Y1 cells eluidated by immunoelecton microscopy and computer graphic reconstruction. *Biol. Cell* **68**: 139-146; 1990.

32. Byun, Y.; Chen, F.; Chang, R.; Trivedi, M.; Green, K. J.; Cryns, V. L. Caspase cleavage of vimentin disrupts intermediate filaments and promotes apoptosis. *Cell Death Differ.* **8**: 443-450.

33. Fink C.; Morgan, F.; Loew, L. M. Intracellular fluorescent probe concentrations by confocal microscopy. *Biophys. J.* **75**: 1648-1658; 1998.

34. Koopman, W. J. H.; Distelmaier, F.; Esseling, J. J.; Smeitink, J. A. M.; Willems, P. H. J. M. Computer-assisted live cell analysis of mitochondrial membrane potential, morphology, and calcium handling. *Methods* **46**: 304-311; 2008.

35. Paumard, P.; Vaillier, J.; Coulary, B.; Schaeffer, J.; Soubannier, V.; Mueller, D. M.; Brèthes, D.; di Rago, J-P.; Velours, J. The ATP synthase is involved in generating mitochondrial cristae morphology. *EMBO J.* **21**: 221-230; 2002.

36. Koopman, W. J. H.; Visch, H-J.; Smeitink, J. A. M.; Willems, P. H. G. M. Simultaneous quantitative measurement and automated analysis of mitochondrial morphology, mass, potential, and motility in living human skin fibroblasts. *ISAC* **69A**: 1-12; 2005.

37. Leinninger, G. M.; Backus, C.; Sastry, A. M.; Yi, Y-B.; Wang, C-W.; Feldman, E. L. Mitochondria in DRG neurons undergo hyperglycemic mediated injury through Bim, Bax and the fission protein Drp1. *Neurobiol. Dis.* **23**: 11-22; 2006.

38. De Vos, K. J.; Allan, V. J.; Grierson, A. J.; Sheetz, M. P. Mitochondrial function and actin regulate dynamin-related protein 1-dependent mitocondrial fission. *Curr. Biol.* **15**: 678-683; 2005.